

Dual NADPH oxidase 2 – the NAADP forming enzyme in T cells

Dissertation

Zur Erlangung der Würde des Doktors der Naturwissenschaften des Fachbereichs
Biologie der Fakultät für Mathematik, Informatik und Naturwissenschaften der
Universität Hamburg

vorgelegt von

Feng Gu

aus Lanzhou, China

Hamburg, 2022

Folgende Gutachter empfehlen die Annahme der Dissertation:

Prof. Dr. rer. nat. Dr. med. habil. Andreas H. Guse

Prof. Dr. rer. nat. Christian Lohr

Prüfungskommission:

Prof. Dr. rer. nat. Christian Lohr, Vorsitz

PD Dr. rer. nat. Hartwig Lüthen, stellv. Vorsitz

Prof. Dr. rer. nat. Dr. med. habil. Andreas H. Guse

Prof. Dr. rer. nat. Sabine Windhorst

Datum der Disputation: 09.06.2022

Content

List of figures	IV
List of tables	V
Abbreviations.....	VI
Abstract	IX
Zusammenfassung.....	XI
1. Introduction	1
1.1. T cells in immunity	1
1.2. Ca²⁺ signaling upon T cell activation	2
1.3. NAADP-induced Ca²⁺ signaling in CD4⁺ T cells	5
1.4. NAADP synthases and hydrolases <i>in vitro</i>	6
1.4.1. NAADP synthesis and degradation by CD38	7
1.4.2. NAADP synthesis by SARM1.....	10
1.4.3. NAADP degradation by AP	10
1.4.4. NAADP reduction by Glu-6-P-DH	11
1.4.5. NAADP synthesis by NOX5	11
1.5. Overview of NOX/DUOX family.....	12
1.5.1. NOX1	13
1.5.2. NOX2.....	14
1.5.3. NOX3.....	15
1.5.4. NOX4.....	15
1.5.5. NOX5.....	16
1.5.6. DUOX1 and DUOX2.....	16
1.5.7. Pharmacological inhibitors of NOX/DUOX family.....	17
2. Study aims	19
3. Methods and materials	20
3.1. Materials	20
3.2. Solutions	22

Content

3.3.	Mediums	23
3.4.	Mouse models	24
3.5.	Isolation of primary murine T cells	24
3.6.	DUOX1 and DUOX2 single knockouts in rat effector T cells	24
3.7.	Imaging of initial Ca ²⁺ microdomains and analysis	25
3.8.	Imaging of global Ca ²⁺ signals and analysis	26
3.9.	Cell culture of Jurkat T cells	27
3.10.	Determination of H ₂ O ₂ using HyPer7 sensor	27
3.11.	NAADPH production	28
3.12.	Enzyme assay in a cell-free system and HPLC conditions	29
4.	Results	30
4.1.	Role of CD38 in Ca ²⁺ signaling upon TCR/CD3 ligation	30
4.2.	Role of NADPH oxidases in Ca ²⁺ signaling upon T cell activation	33
4.2.1.	Role of NOX1 in Ca ²⁺ signaling upon TCR/CD3 ligation	33
4.2.2.	Role of NOX2 in Ca ²⁺ signaling upon TCR/CD3 ligation	35
4.2.3.	The role of DUOX isozymes	38
4.2.3.1.	DUOX1 and DUOX2 oxidize NAADPH to NAADP in cell-free system ..	38
4.2.3.2.	DUOX1 and DUOX2 affect Ca ²⁺ microdomain formation differently ...	40
4.2.3.3.	DUOX1 and DUOX2 affect global Ca ²⁺ signaling differently	44
4.2.3.4.	Role of H ₂ O ₂ , the byproduct of DUOX forming NAADP	47
4.2.3.4.1.	Catalase has no effect on Ca ²⁺ signaling	47
4.2.3.4.2.	Aquaporin3 inhibitor has no effect on Ca ²⁺ microdomain formation ..	49
4.2.3.4.3.	BHA has no effect on Ca ²⁺ microdomain formation	51
4.2.3.4.4.	Exogenous H ₂ O ₂ has no effect on Ca ²⁺ microdomain formation	53
4.2.3.4.5.	No detectable H ₂ O ₂ production within 15 s post TCR/CD3 ligation	55
5.	Discussion	57
5.1.	Key findings in this study	57
5.1.1.	Understanding the role of CD38 upon TCR stimulation	58
5.1.2.	DUOX2, the major NAADP forming enzyme in CD4 ⁺ T cells	59
5.2.	Limitations of this study	62
5.3.	H ₂ O ₂ in the early phase of T cell activation	64

Content

5.4.	Outlook	67
5.4.1.	Usage of different substrates	67
5.4.2.	Endogenous NAADPH pool in T cells.....	68
5.4.3.	NOX/DUOX as NAADP forming enzyme in other cell types.....	68
6.	References.....	70
	Eidesstattliche Versicherung	89
	Acknowledgements	90
	Publications and presentations	91

List of figures

Fig. 1: Ca ²⁺ signaling in the early phase of T cell activation.	4
Fig. 2: NAADP generation (arrows in red) and metabolism (arrows in blue) <i>in vitro</i>	7
Fig. 3: Structure of isozymes in NADPH oxidase family.	13
Fig. 4: Lack of CD38 has no effect on Ca ²⁺ microdomain formation or global Ca ²⁺ signals in response to TCR stimulation.	31
Fig. 5: Absence of NOX1 affects neither Ca ²⁺ microdomain formation nor the global Ca ²⁺ signals upon TCR stimulation.	34
Fig. 6: Lack of NOX2 affects neither the Ca ²⁺ microdomains nor the overall Ca ²⁺ signals after TCR stimulation.	36
Fig. 7: Synthesis of NAADP from its reduced form NAADPH <i>in vitro</i> by DUOX1 and DUOX2.	39
Fig. 8: Single knockouts of DUOX1 and DUOX2 in CD4 ⁺ effector rat T cells reduce Ca ²⁺ microdomain formation in the first 15 s.	41
Fig. 9: DUOX2 is essential for initial NAADP formation	43
Fig. 10: Single knockouts of DUOX1 and DUOX2 in CD4 ⁺ effector rat T cells influence global Ca ²⁺ signaling differently.	45
Fig. 11: H ₂ O ₂ -consuming catalase in extracellular buffer affects neither Ca ²⁺ microdomain formation nor the global Ca ²⁺ signals in primary T cells upon TCR stimulation.	48
Fig. 12: DFP00173, an AQP3 inhibitor, has no effect on the formation of Ca ²⁺ microdomains in primary T cells after TCR activation.	50
Fig. 13: Membrane-permeable ROS scavenger BHA does not affect Ca ²⁺ microdomain formation in primary T cells upon TCR stimulation.	52
Fig. 14: Exogenous H ₂ O ₂ at 80 nM does not increase Ca ²⁺ microdomains in primary T cells without bead stimulation.	54
Fig. 15: No measurable H ₂ O ₂ generation after TCR/CD3 stimulation by using ultrasensitive H ₂ O ₂ indicator HyPer7.	56
Fig. 16: Ca ²⁺ signaling upon TCR stimulation and key findings in this thesis.	57
Fig. 17: Kinetics of production of Ca ²⁺ releasing second messengers and ROS in the first 12 min upon TCR/CD3 ligation.	64

List of tables

Table 1: CD4+ effector T cell subsets.....	1
Table 2: List of compounds and devices used for Ca ²⁺ imaging.....	20
Table 3: List of adenine nucleotides standards used for HPLC assay	21
Table 4: List of compounds and devices used for enzyme assay	21
Table 5: List of other compounds used for buffer solution and medium	22
Table 6: Number of Ca ²⁺ microdomains per frame (mean ± SEM) in WT versus CD38-deficient T cells shown in Fig. 4 B and C.....	32
Table 7: Number of Ca ²⁺ microdomains per frame (mean ± SEM) in WT versus NOX1-deficient T cells shown in Fig. 5 B and C.	35
Table 8: Number of Ca ²⁺ microdomains per frame (mean ± SEM) in WT versus NOX2-deficient T cells shown in Fig. 6 B and C.	37
Table 9: Number of Ca ²⁺ microdomains per frame (mean ± SEM) in WT versus DUOX1- or DUOX2-single knockout T cells in the first 15 s and in 5 s periods.....	42
Table 10: Parameters (mean ± SEM) of global Ca ²⁺ signals in WT versus DUOX1- or DUOX2-single knockout T cells shown in Fig. 10.....	47
Table 11: Number of Ca ²⁺ microdomains per frame (mean ± SEM) in WT T cells with and without catalase shown in Fig. 11 B and C.....	49
Table 12: Number of Ca ²⁺ microdomains per frame (mean ± SEM) in WT T cells with and without AQP3 inhibitor DFP00173 shown in Fig. 12 B and C.....	51
Table 13: Number of Ca ²⁺ microdomains per frame (mean ± SEM) in WT T cells with and without ROS scavenger BHA shown in Fig. 13 B and C.	53
Table 14: Number of Ca ²⁺ microdomains per frame (mean ± SEM) and percentage of responding cells in WT T cells with 80 nM exogenous H ₂ O ₂ shown in Fig. 14 A and C.	55
Table 15: Slope of HyPer7 signals (mean ± SEM) shown in Fig. 15B.....	56

Abbreviations

[Ca ²⁺] _i	free cytosolic Ca ²⁺ concentration
ADPR	adenosine diphosphate ribose
ADPRP	2'-phospho-adenosine diphosphate ribose
AP	alkaline phosphatase
APC	antigen presenting cell
AQP	aquaporin
ATP	adenosine triphosphate
BHA	butylated hydroxy anisole
BSA	bovine serum albumin
Ca ²⁺	calcium ion
cADPR	cyclic adenosine diphosphate ribose
cADPRP	2'-phospho-cyclic adenosine diphosphate ribose
CAMKII	calcium/calmodulin-dependent kinase II
cAMP	cyclic adenosine monophosphate
CCK	cholecystokinin
CD	cluster of differentiation
CGD	chronic granulomatous disease
CICR	Ca ²⁺ induced Ca ²⁺ release
CNS	central nervous system
Cos-7 cells	fibroblast-like cell line derived from monkey kidney tissue
CRAC	Ca ²⁺ release-activated Ca ²⁺ channel
DCFDA	2',7'-dichlorodihydrofluorescein diacetate
DHE	dihydroethidium
DMSO	dimethyl sulfoxide
DPI	diphenyleneiodonium
DUOX	dual NADPH oxidase
DUOXA	dual NADPH oxidase activator, maturation factor of DUOX
EAE	experimental autoimmune encephalomyelitis
EDTA	ethylenediaminetetraacetic acid
EF hand motif	a helix–loop–helix structural domain or motif found in a large family of calcium-binding proteins
EGTA	ethylene glycol-bis (β-aminoethyl ether)-N,N,N',N'-tetra acetic acid
ER	endoplasmic reticulum
FAD	flavin adenine dinucleotide
FBS	phosphate-buffered saline
FCS/FBS	fetal calf serum/fetal bovine serum
GFP	green fluorescent protein
Glu-6-P-DH	glucose 6-phosphate dehydrogenase
GTP	guanosine-5'-triphosphate
H ₂ O ₂	hydrogen peroxide
HEK293 cells	human embryonic kidney 293 cells
HeLa cells	an immortal cell line derived from human cervical cancer cells

Abbreviations

HEPES	4-(2-hydroxyethyl)-1-piperazineethanesulfonic acid
HL60 cells	a human leukemia cell line
HN1L/JPT2	hematological and neurological expressed 1-like protein/Jupiter microtubule-associated homolog 2
IFN	interferon
IL	interleukin
InsP ₃	D- <i>myo</i> -inositol 1,4,5-trisphosphate
InsP ₃ R	D- <i>myo</i> -inositol 1,4,5-trisphosphate receptor
Jurkat T cells	an immortalized line of a human T lymphocyte
Kd	dissociation constant
kDa	kilodalton
LAK cells	lymphokine activated killer cells
LP-1 cells	a human myeloma cell line
MHC	major histocompatibility complex
NAAD	nicotinic acid adenine dinucleotide
NAADP	nicotinic acid adenine dinucleotide phosphate
NAADPH	reduced form of NAADP
NAD	nicotinamide adenine dinucleotide
NADH	reduced form of NAD
NADP	nicotinamide adenine dinucleotide phosphate
NADPH	reduced form of NADP
NCS	newborn calf serum
ND	neurodegenerative diseases
NFAT	nuclear factor of activated T cells
NOX	NADPH oxidase
NOXA1	NOX1 activator 1
NOXO1	NOX1 organizer 1
NTA	nitrilotriacetic acid
O ₂	oxygen
OKT3	anti-human CD3 monoclonal antibody
ORAI1	calcium release-activated calcium channel protein 1
P2X receptor	ATP-gated P2X purinoreceptor cation channel
PBS	phosphate-buffered salt solution
PenStrep	penicillin-streptomycin
PHL-domain	pleckstrin homology-like domain
PKA	protein kinase A
PKC	protein kinase C
PKG	protein kinase G
PLC-γ1	phospholipase C-γ1
PLL	poly-L-lysine
PM	plasma membrane
PMA	phorbol 12-myristate 13-acetate
PMCA	plasma membrane Ca ²⁺ ATPase
ROS	reactive oxygen species
RP-HPLC	reversed-phase high-performance/pressure liquid chromatography

Abbreviations

RyR1	type 1 ryanodine receptor
RyR3	type 3 ryanodine receptor
SARM1	sterile alpha and TIR motif-containing 1
SEM	standard error of mean
SERCA	sarcoplasmic/endoplasmic reticulum Ca ²⁺ ATPase
SHP-2	Src-homology 2 domain (SH2)-containing protein tyrosine phosphatase (PTP) 2
SOCE	store-operated Ca ²⁺ entry
SR	sarcoplasmic reticulum
STIM	stromal interaction molecule
TBAP	tetrabutylammonium phosphate
Tc cells	T cytotoxic cells
TCR	T cell receptor
Th cells	T helper cells
TNF	tumor necrosis factor
WT	wildtype
ZAP-70	ζ chain-associated protein kinase of 70 kD

Abstract

T cells are a fundamental component of adaptive immune responses and their dysfunctions may lead to autoimmune and inflammatory disorders. Activation of the T cell receptor (TCR) on the surface of T cells is required for immune responses. Once the TCR binds antigenic peptides presented by the antigen-presenting cells (APCs), second messengers are generated and are responsible for propagating signals into the intracellular region. An important transduction mechanism is the rise in free cytosolic Ca^{2+} concentration. Both Ca^{2+} influx from the extracellular space and Ca^{2+} release from intracellular organelles contribute to the increase in free cytosolic Ca^{2+} concentration.

In CD4^+ T cells, nicotinic acid adenine dinucleotide phosphate (NAADP) is rapidly generated within seconds after TCR stimulation. When bound to an NAADP binding protein, hematological and neurologically expressed 1-like protein/Jupiter microtubule-associated homolog 2 (HN1L/JPT2), NAADP is targeting the type 1 ryanodine receptors (RyR1s) in the membrane of the endoplasmic reticulum (ER) and triggering initial Ca^{2+} signals, known as Ca^{2+} microdomains. These initial Ca^{2+} signals are subsequently enhanced by D-*myo*-inositol 1,4,5-trisphosphate (InsP_3)- and cyclic adenosine diphosphate ribose (cADPR)-induced Ca^{2+} release, calcium-induced Ca^{2+} release (CICR) and store-operated Ca^{2+} entry (SOCE). NAADP-evoked initial Ca^{2+} microdomains are critical for T cell activation and downstream function. However, the NAADP forming enzyme in CD4^+ T cells remains elusive.

Using a Ca^{2+} imaging system with high spatial and temporal resolution (25 ms and 368 nm), it is possible to examine Ca^{2+} microdomains emerging within seconds following TCR activation. In this study, the Ca^{2+} microdomains formed within 15 s were used as primary read-out to investigate NAADP synthesis upon T cell activation. In addition, NAADP-evoked initial Ca^{2+} signals are essential for subsequent global Ca^{2+} signaling. Thus, global Ca^{2+} signals within 13 min after TCR stimulation were also analyzed.

It has been revealed that CD38 and the NADPH oxidases are able to generate NAADP in a cell-free system. In this study, CD4^+ T cells derived from different mouse models and CRISPR/Cas designed rat effector T cells were used to evaluate the involvement of these

Abstract

enzymes in NAADP synthesis in intact T cells, i.e., in Ca^{2+} signaling in the early phase of T cell activation. The absence of CD38 did not alter the formation of Ca^{2+} microdomains nor subsequent global Ca^{2+} signaling, indicating that CD38 is not the NAADP forming enzyme in CD4^+ T cells. An isozyme of the NADPH oxidase family, namely dual NADPH oxidase 2 (DUOX2) was identified as responsible for NAADP generation upon T cell activation, given that the absence of DUOX2 significantly reduced Ca^{2+} microdomain formation and global Ca^{2+} signals after TCR stimulation, consistent with previously published phenotypes when the NAADP/ Ca^{2+} pathway was disrupted. Additionally, the role of H_2O_2 , a byproduct of DUOX isozymes, in initial Ca^{2+} signaling was also excluded: the H_2O_2 -degrading enzyme catalase, the ROS scavenger butylated hydroxy anisole (BHA), blocking H_2O_2 uptake, and addition of 80 nM exogenous H_2O_2 did not alter the formation of Ca^{2+} microdomains. Moreover, TCR/CD3 ligation-induced H_2O_2 production is less than 300 nM within seconds post-stimulation, as demonstrated by the ultra-sensitive H_2O_2 indicator HyPer7.

Taken together, DUOX2 was found to play a critical role in NAADP production within seconds after T cell activation and the byproduct H_2O_2 had no effect on initial Ca^{2+} signaling during this period.

Zusammenfassung

T-Zellen gehören zu den Hauptkomponenten der adaptiven Immunantworten und eine Dysfunktion führt zu Autoimmun- und Entzündungserkrankungen.

Die Aktivierung des T-Zell-Rezeptors (TCR) auf der Oberfläche der T-Zellen ist für die Immunreaktion erforderlich. Sobald der TCR antigene Informationen von den Antigen-präsentierenden Zellen (APCs) erkennt, werden sekundäre Botenstoffe (second messengers) gebildet, die für die Weiterleitung der Signale in den intrazellulären Bereich verantwortlich sind. Ein wichtiger Transduktionsmechanismus ist der Anstieg der freien Ca^{2+} -Konzentration im Zytosol. Sowohl der Ca^{2+} -Einstrom aus dem Extrazellulärraum als auch die Ca^{2+} -Freisetzung aus intrazellulären Organellen tragen hierbei zum Anstieg der freien zytosolischen Ca^{2+} -Konzentration bei. In CD4^+ -T-Zellen wird Nikotinsäure-Adenin-Dinukleotid-Phosphat (NAADP) innerhalb von Sekunden nach der TCR-Stimulation gebildet. Wenn NAADP an das hämatologisch und neurologisch exprimierte 1-ähnliche Protein/Jupiter microtubule-associated homolog 2 (HN1L/JPT2) gebunden ist, werden initiale Ca^{2+} -Signale, durch die Öffnung des Typ-1-Ryanodinrezeptors (RyR1s) in der Membran des endoplasmatischen Retikulums (ER) ausgelöst, die als Ca^{2+} -Mikrodomänen beschrieben sind. Diese initialen Ca^{2+} -Signale werden anschließend durch *D-myo*-Inositol-1,4,5-Trisphosphat (InsP_3)- und zyklische Adenindiphosphat-Ribose (cADPR)-induzierte Ca^{2+} -Freisetzung sowie Calcium-induzierte Ca^{2+} -Freisetzung (CICR) und den speichergesteuerten Ca^{2+} -Einstrom (SOCE) verstärkt. Die durch NAADP ausgelösten initialen Ca^{2+} -Signale sind für die T-Zell-Aktivierung und deren nachgeschaltete Funktion entscheidend. Das NAADP-bildende Enzym in T-Zellen ist jedoch nach wie vor nicht bekannt.

Durch den Einsatz eines Mikroskops mit hoher räumlicher und zeitlicher Auflösung (25 ms und 368 nm) ist es möglich, die innerhalb von Sekunden nach der TCR-Aktivierung entstehenden Ca^{2+} -Signale zu untersuchen. In dieser Arbeit wurden die innerhalb von 15 Sekunden gebildeten Ca^{2+} -Mikrodomänen als primäre Messgröße zur Untersuchung der NAADP-Synthese nach der T-Zell-Aktivierung verwendet. Da die durch NAADP ausgelösten initialen Ca^{2+} -Signale maßgeblich für die Entwicklung eines globalen Ca^{2+} -Signals sind wurden darüber hinaus auch die globalen Ca^{2+} -Signale innerhalb von 13 Minuten nach der T-Zell-Aktivierung

analysiert.

Es hat sich gezeigt, dass CD38 und die NADPH-Oxidasen in der Lage sind, NAADP in einem zellfreien System zu bilden. In dieser Studie wurden CD4⁺ T-Zellen aus verschiedenen Mausmodellen und mit CRISPR/Cas entwickelte Ratten-Effektor-T-Zellen verwendet, um die Beteiligung dieser Enzyme an der NAADP-Synthese in intakten T-Zellen zu untersuchen, d. h. die Ca²⁺ Signale während der frühen Phase der T-Zell-Aktivierung,.

Zusammenfassend lässt sich sagen, dass die Abwesenheit von CD38 weder die Bildung von initialen Ca²⁺-Mikrodomänen noch die anschließenden globalen Ca²⁺-Signale verändert, was darauf hindeutet, dass CD38 nicht das NAADP-bildende Enzym in CD4⁺-T-Zellen ist. Ein Isozym der NADPH-Oxidasen, nämlich die duale NADPH-Oxidase 2 (DUOX2), konnte als verantwortlich für die NAADP-Bildung bei der T-Zell-Aktivierung identifiziert werden. Die Abwesenheit von DUOX2 reduzierte signifikant die Bildung von initialen Ca²⁺-Mikrodomänen und die globalen Ca²⁺-Signale nach TCR-Stimulation, was mit den zuvor veröffentlichten Phänotypen übereinstimmt, wenn der NAADP/Ca²⁺-Weg gestört ist. Außerdem konnte die Rolle von H₂O₂, einem Nebenprodukt der DUOX-Enzyme, auf die Entstehung von initialen Ca²⁺-Signalen ausgeschlossen werden: das H₂O₂ abbauende Enzym Kalatase, der ROS-Fänger Butylhydroxyanisol (BHA), die Blockierung der H₂O₂-Aufnahme und die Zugabe von 80 nM exogenem H₂O₂ veränderten die Bildung von initialen Ca²⁺-Mikrodomänen nicht. Darüber hinaus liegt die H₂O₂-Produktion innerhalb 50 s nach der TCR-Stimulation unter 300 nM, wie mit dem H₂O₂-indikator HyPer7 nachgewiesen wurde.

Insgesamt wurde festgestellt, dass DUOX2 innerhalb von Sekunden nach der T-Zell-Aktivierung eine entscheidende Rolle bei der NAADP-Produktion spielt und dass das Nebenprodukt H₂O₂ in diesem Zeitraum keine Auswirkung auf die initialen Ca²⁺ Signale hat.

1. Introduction

1.1. T cells in immunity

The adaptive immune system provides specific and long-lasting protection against pathogens and eliminates dead and faulty cells. T cells are one major component of the adaptive immune responses and fight infections and cancer. On the other hand, abnormal functions of T cells lead to autoimmune and inflammatory diseases. T cells can be further subdivided depending on the co-receptor molecules on their cell surface, i.e., cluster of differentiation (CD)4 and CD8 expression. CD8⁺ T cells are T cytotoxic (T_c) cells that directly kill infected cells. CD4⁺ T cells, also known as T helper (T_h) cells, have limited cytotoxic activity and support the immune responses by secreting cytokines to activate and regulate other immune cells (reviewed in Kesarwani et al., 2013). This study focuses on CD4⁺ T cells.

Mature T cells that have not encountered antigens are referred to as naïve T cells. Peptide antigens, for instance, from ingested external bacteria, are presented to CD4⁺ T cells by major histocompatibility complex (MHC) class II molecules on the surface of the antigen-presenting cells (APCs). Upon recognition, naïve CD4⁺ T cells proliferate and differentiate into effector T cells (Charles A Janeway et al., 2001). The different T_h cells can be distinguished by the cytokines they secrete. For example, T_h 1 cells are characterized by the secretion of interferon- γ (IFN- γ) and tumor necrosis factor- α (TNF- α), which then stimulate macrophages and B cells (Alberts et al., 2002). T_h 17 cells, which were identified later than the traditional T_h 1 and T_h 2 subsets, secrete interleukin-17 (IL-17), IL-21 and IL-22 as their characteristic cytokines. T_h 17 cells mediate host defense and are involved in the pathogenesis of many autoimmune diseases (reviewed in Ouyang et al., 2008), such as multiple sclerosis: the development of experimental autoimmune encephalomyelitis (EAE), the animal model of human demyelinating diseases in the central nervous system (CNS), is significantly ameliorated in *Il-17^{-/-}* mice (Komiyama et al., 2006). Nowadays, more and more T_h subsets are being identified, which participate in the immune responses with diverse functions. A brief overview is given in Table 1.

Table 1: CD4⁺ effector T cell subsets

This table is summarized from (Chen et al., 2019; Eagar and Miller, 2019; Fazilleau et al., 2009;

McKinstry et al., 2010; Veldhoen et al., 2008; Zhu and Paul, 2008).

Th Subset	Signature Cytokines	Functions
Th 1	IFN- γ , TNF- α , IL-2	Intracellular pathogens; autoimmunity
Th 2	IL-4, IL-5, IL-10, IL-13	Extracellular parasites; allergy; asthma
Th 9	IL-9, IL-10	Allergy; tumor immunity
Th 17	IL-17, IL-21, IL-22	Extracellular bacteria; fungi; autoimmunity
Th 22	IL-22 (IL-13, TNF- α)	Epidermal repair
T-follicular helper	IL-4, IL-21	Regulation of B cell-dependent immunity
Regulatory T cell	IL-10	Immune tolerance; lymphocytes homeostasis; regulation of immune responses

1.2. Ca²⁺ signaling upon T cell activation

T cell receptor (TCR) stimulation is fundamental to initiate the T cell response. The majority of T cells are $\alpha\beta$ T cells, based on the nature of TCR expression, which consists of TCR $\alpha\beta$ chains and four CD3 subunits (γ , δ , ϵ , ζ) through non-covalent association. Furthermore, costimulatory receptors, e.g., CD28, are required to completely activate naïve T cells. The strength and duration of TCR stimulation regulate subsequent T cell function, differentiation, and survival. As a consequence of TCR engagement, second messengers are formed and transmit the antigenic signals into the intracellular space (reviewed in Feske, 2007; Hwang et al., 2020).

Calcium ions (Ca²⁺) are a universal messenger molecule for signal transduction. Elevation of free cytosolic Ca²⁺ concentration is essential during T cell activation and reactivation. The free cytosolic Ca²⁺ concentration is from 20 to 100 nM in the absence of TCR stimulation (Diercks et al., 2018; reviewed in Trebak and Kinet, 2019) and rises after T cell activation, originating from both Ca²⁺ entry from the extracellular space and Ca²⁺ release from intracellular organelles. On the other hand, for instance, plasma membrane Ca²⁺ ATPases (PMCA) and sarcoplasmic/endoplasmic reticulum Ca²⁺ ATPases (SERCA) consume energy to pump Ca²⁺ out of the cytosol. There are a number of Ca²⁺ channels and Ca²⁺ pumps expressed in the plasma membrane and the membrane of organelles that fine-tune the Ca²⁺ signaling in T cells spatially and temporally to enable complex immune responses (reviewed in Feske, 2013, 2007; Trebak and Kinet, 2019).

Following TCR stimulation, Ca²⁺ mobilizing second messengers are formed. Nicotinic acid

adenine dinucleotide phosphate (NAADP) is produced within seconds (Gasser et al., 2006), and mediates the initial Ca^{2+} release from the endoplasmic reticulum (ER) via an NAADP binding protein, the hematological and neurological expressed 1-like protein/Jupiter microtubule-associated homolog 2 (HN1L/JPT2), through the type 1 ryanodine receptors (RyR1s) (Dammermann et al., 2009; Diercks et al., 2018; Langhorst et al., 2004; Roggenkamp et al., 2021; Wolf et al., 2015). NAADP-induced initial Ca^{2+} release functions as a co-agonist to D-*myo*-inositol 1,4,5-trisphosphate (InsP_3), which is formed with a peak at 3 min (Guse et al., 1993) and further induces Ca^{2+} release through InsP_3 receptors (reviewed in Berridge, 2016). Another Ca^{2+} mobilizing second messenger, cyclic adenosine diphosphate ribose (cADPR), is produced with highest amplitude from 10 min on (Guse et al., 1999) and induces Ca^{2+} release through the type 3 ryanodine receptors (RyR3s) (Kunerth et al., 2004). All these three second messengers evoke Ca^{2+} release and lead to depletion of Ca^{2+} in the ER, resulting in activation of store-operated Ca^{2+} entry (SOCE): the stromal interaction molecules (STIMs) in the ER membrane sense depletion of Ca^{2+} stores and then activate calcium release-activated calcium channel protein 1 (ORAI1) at ER-PM (plasma membrane) junctions and open the Ca^{2+} release-activated Ca^{2+} (CRAC) channel pore, leading to sustained Ca^{2+} influx (reviewed in Feske, 2013, 2007).

Apart from playing a role in SOCE after TCR stimulation, pre-clusters of STIMs and ORAI1 also contribute to the formation of smaller and lower Ca^{2+} microdomains in the absence of TCR stimulation (Diercks et al., 2018). Furthermore, P2X purinoreceptor cation channels (P2X receptors) gated by adenosine triphosphate (ATP) are also involved in the formation of Ca^{2+} microdomains before and after TCR stimulation (Brock et al., 2022).

A brief introduction of Ca^{2+} signaling within minutes after TCR stimulation is shown in Fig. 1.

Introduction

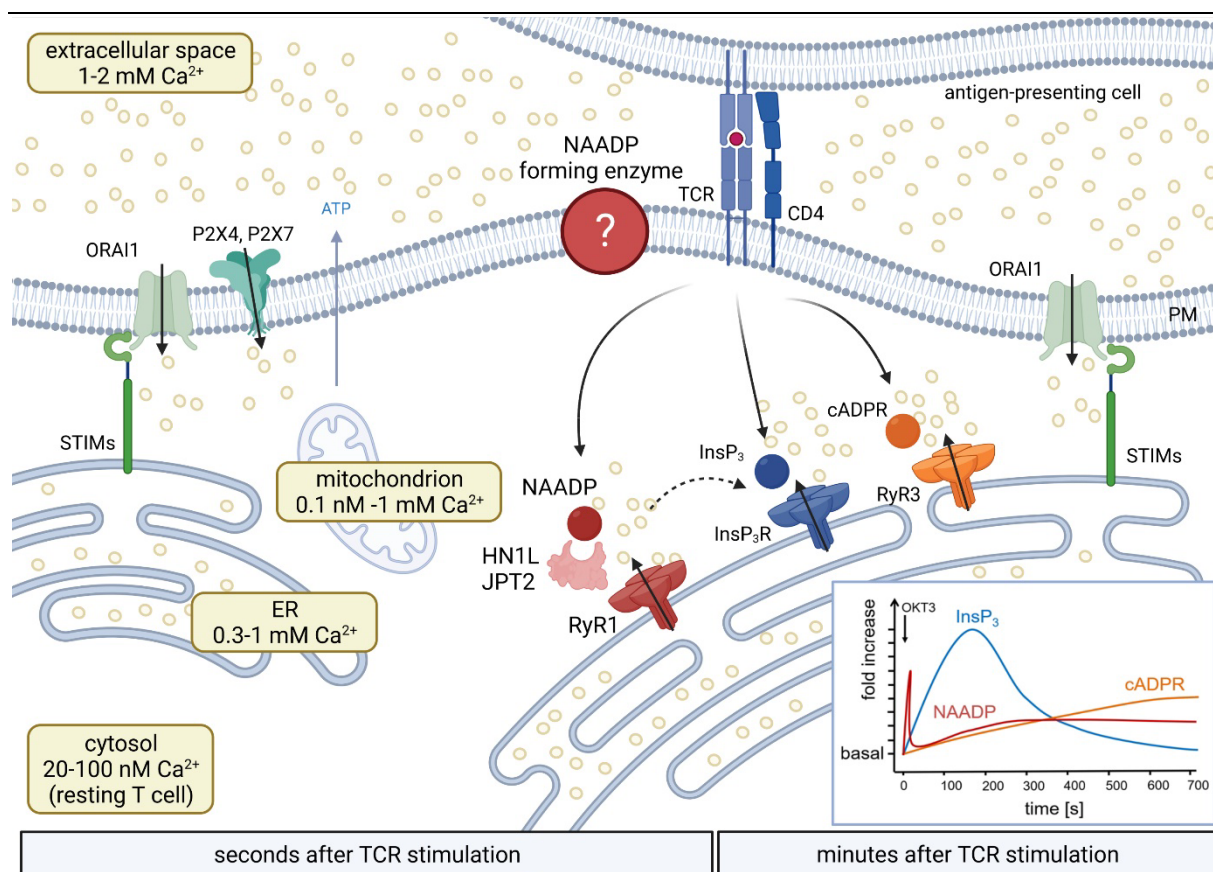


Fig. 1: Ca^{2+} signaling in the early phase of T cell activation.

Upon TCR/CD3 stimulation, the NAADP forming enzyme produces NAADP, which then triggers the initial Ca^{2+} release from the ER through RyR1 together with its binding protein HN1L/JPT2. ATP-gated P2X receptors as well as clusters of STIMs and ORAI1 also contribute to the formation of Ca^{2+} microdomains. These initial Ca^{2+} signals are then amplified by InsP_3 -induced Ca^{2+} signals through CICR (Ca²⁺-induced Ca²⁺ release, indicated by the dashed arrow) and cADPR-mediated Ca^{2+} release. Depletion of Ca^{2+} stores in the ER further stimulates SOCE (store-operated Ca²⁺ entry), which leads to a sustained global Ca^{2+} response. Ca^{2+} concentrations are reviewed in (Trebak and Kinet, 2019) and from (Diercks et al., 2018). The insert is a summary from (Gasser et al., 2006; Guse et al., 1999, 1993). In the insert, the arrow indicates the addition of anti-CD3 antibody (OKT3). The y-axis indicates the fold increase compared with their baseline. Abbreviations: ORAI1: calcium release-activated calcium channel protein 1; STIM: stromal interaction molecule; P2X: ATP-gated P2X purinoreceptor cation channel; HN1L/JPT2: hematological and neurological expressed 1-like protein/Jupiter microtubule-associated homolog 2; RyR: ryanodine receptor; InsP_3 : D-myoinositol 1,4,5-trisphosphate; cADPR: cyclic ADP-ribose; PM: plasma membrane; ER: endoplasmic reticulum. This figure was created with BioRender.com.

This thesis aims to better understand the NAADP/ Ca^{2+} signaling pathway in the early phase of T cell activation, as NAADP functions as the starting point of the Ca^{2+} signaling chain after TCR engagement.

1.3. NAADP-induced Ca²⁺ signaling in CD4⁺ T cells

In 1995, NAADP was first found to trigger Ca²⁺ release from intracellular Ca²⁺ stores using sea urchin egg homogenates, and its signaling pathway is distinct from InsP₃ and cADPR (Lee and Aarhus, 1995). Further reports indicated that NAADP is rapidly formed upon various stimulations and triggers initial Ca²⁺ signals in many mammalian cells (Guse et al., 2013; Guse and Lee, 2008), such as the human Jurkat T cell line (Gasser et al., 2006).

NAADP has unique properties in comparison to other Ca²⁺ mobilizing second messengers, such as self-desensitization: subthreshold concentrations of NAADP inactivate subsequent NAADP-induced Ca²⁺ responses in sea urchin eggs and homogenates (Aarhus et al., 1996; Genazzani et al., 1996). In mammalian cells, high concentration (in the micromolar range) of NAADP leads to self-inactivation (reviewed in Yamasaki et al., 2005), such as in pancreatic β cells (Masgrau et al., 2003) and in T cells (Berg et al., 2000). Especially, in T cells, 10 μ M NAADP not only desensitizes NAADP (50 nM)-induced Ca²⁺ increases, but also inactivates Ca²⁺ responses mediated by InsP₃ (4 μ M), cADPR (10 μ M) and TCR/CD3 ligation (Berg et al., 2000). Such cross-desensitization was not observed in liver microsomes (Mándi et al., 2006) nor in murine pancreatic acinar cells (Cancela et al., 1999). Moreover, the formation of NAADP upon TCR/CD3 ligation shows a bell-shaped concentration-response curve. 5 μ g/mL anti-CD3 antibody (OKT3) induces rapid NAADP generation, as shown in the insert in Fig. 1, whereas 0.1 μ g/mL OKT3 induces the highest NAADP production and 10 μ g/mL OKT3 only slightly increases NAADP concentration compared with its basal level (Gasser et al., 2006).

NAADP plays an essential role in T cell activation and downstream function, as the specific NAADP antagonists BZ194 (Dammermann et al., 2009) and Ned19 (Naylor et al., 2009) diminish global Ca²⁺ signaling upon TCR stimulation and downstream events, such as translocation of nuclear factor of activated T cells (NFAT), expression of proinflammatory cytokines (e.g., IL-2, IL-17, and IFN- γ), T cell proliferation as well as progression of autoimmune and inflammatory diseases (Ali et al., 2016; Cordiglieri et al., 2010; Nawrocki et al., 2021).

However, some questions about NAADP are still under debate, for instance, the ion channel(s)

targeted by NAADP, which has been partially revealed after the identification of NAADP binding proteins (Gunaratne et al., 2021; Roggenkamp et al., 2021; Zhang et al., 2021), and NAADP forming enzyme(s), which was investigated in this thesis.

1.4. NAADP synthases and hydrolases *in vitro*

NAADP is a universal Ca^{2+} trigger and is effective in the low nanomolar range in many cells (reviewed in Guse et al., 2013; Guse and Diercks, 2018). In Jurkat T cells, TCR stimulation gives rise to a rapid NAADP increase from around 4 nM to approximately 34 nM in 10 s, followed by a decrease back to about 10 nM in the following 10 s. Furthermore, there is a second and long-lasting production phase with a moderate peak at 5 min around 15 nM, and by 50 min it is almost back to the baseline level (Gasser et al., 2006). However, synthesis and metabolism of NAADP *in vivo* are still controversially discussed.

It is known that the generation of NAADP by phosphorylation of nicotinic acid adenine dinucleotide (NAAD) and deamidation of nicotinamide adenine dinucleotide phosphate (NADP) has not been successfully identified (Lerner et al., 2001; Schmid et al., 2012). Moreover, NAADP has been reported to be resistant to NADase and apyrase (Graeff and Lee, 2002).

The enzymes identified to date that are capable of forming and degrading NAADP in the cell-free system are indicated in Fig. 2. The details are described below.

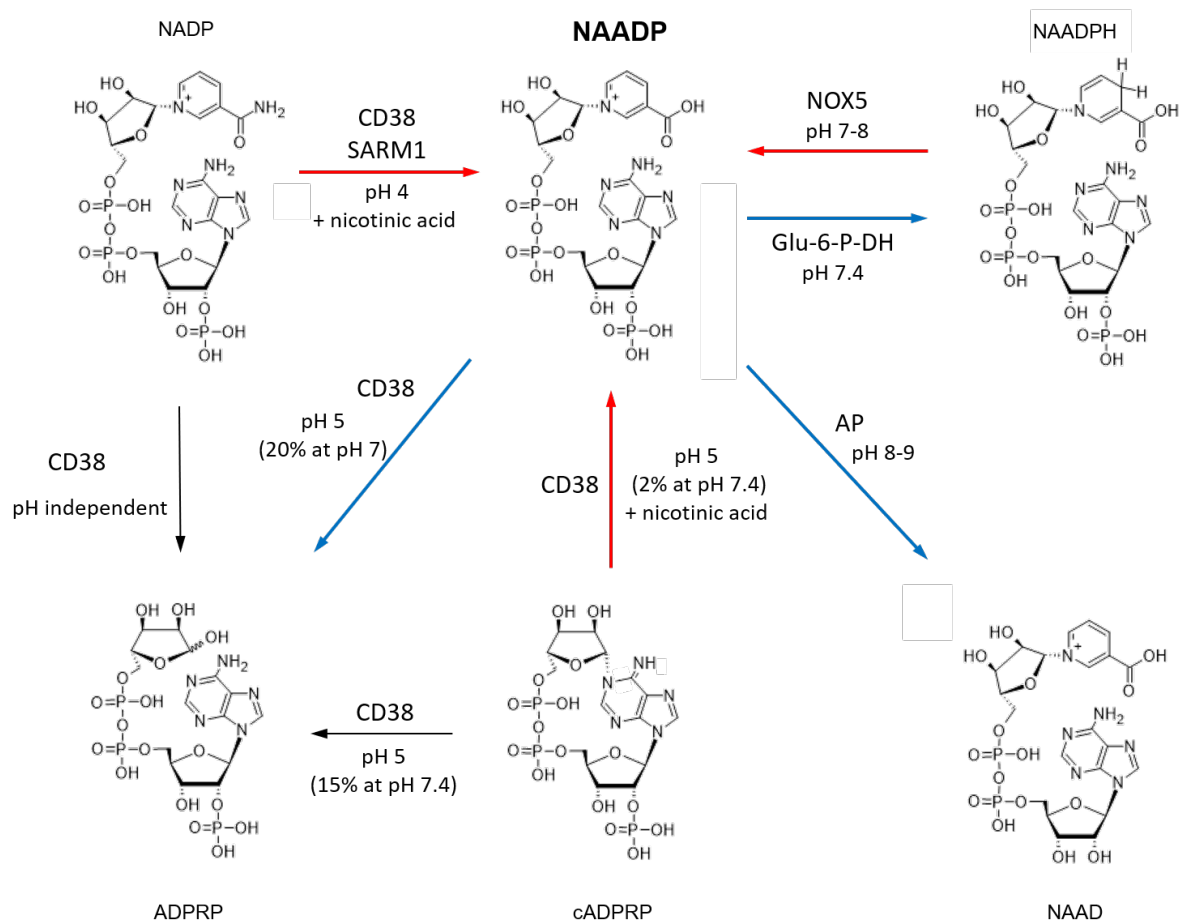


Fig. 2: NAADP generation (arrows in red) and metabolism (arrows in blue) *in vitro*.

The pH values indicated are the optimal pH values for the reactions (Aarhus et al., 1995; Graeff et al., 2006; Gu et al., 2021; Schmid et al., 2012) [except for Glu-6-P-DH, the experiment was carried out only at pH 7.4 (Gu et al., 2021); production of NAADP from cADPRP was compared at pH 7.4 and pH 5 (Moreschi et al., 2006); NAADP production catalyzed by SARM1 was investigated only at pH 4 (Zhao et al., 2019)]. When the reaction can be detected at neutral pH, the percentage of products compared to that at the optimal pH is shown in the bracket. Nicotinic acid is present in the millimolar range. Abbreviations: SARM1, sterile alpha and TIR motif-containing 1; NOX5, NADPH oxidase 5; Glu-6-P-DH, glucose-6-phosphate dehydrogenase; AP, alkaline phosphatase; NADP, nicotinamide adenine dinucleotide phosphate; NAADP, nicotinic acid adenine dinucleotide phosphate; NAADPH, the reduced form of NAADP; ADPRP, 2'-phospho-ADP-ribose; cADPRP, 2'-phospho-cyclic ADP-ribose; NAAD, nicotinic acid adenine dinucleotide.

1.4.1. NAADP synthesis and degradation by CD38

The cluster of differentiation 38 (CD38) is a 42-kilodalton glycoprotein and was first discovered as a surface marker of lymphocytes (Reinherz et al., 1980). A number of reports have demonstrated that CD38 exhibits a structural homology to adenosine diphosphate (ADP)-

ribosyl cyclase of *Aplysia californica*, a species of sea slug, and therefore also functions as an enzyme, catalyzing nicotinamide adenine dinucleotide (NAD) into adenosine diphosphate ribose (ADPR) and cyclic ADP-ribose (cADPR) as well as hydrolyzing cADPR into ADPR (Howard et al., 1993; Summerhill et al., 1993; Takasawa et al., 1993; Zocchi et al., 1993). As a multifunctional enzyme, it also catalyzes a so-called “base-exchange” reaction to produce NAADP (Aarhus et al., 1995), and additionally degrades NAADP (Graeff et al., 2006).

Most CD38 proteins are expressed in type II orientation, with their catalytic domain located in the extracellular leaflet (Jackson and Bell, 1990). Moreover, CD38 is also described as a type III protein in the opposite orientation, and type III CD38 is endogenously expressed in many cells and is enzymatically active, for example, in Jurkat T cells (Fliegert et al., 2017; reviewed in Lee and Zhao, 2019). Given the two opposing orientations of CD38 expressed in the cells, the pH value of the reactions catalyzed by CD38 to produce and degrade NAADP is therefore of interest.

The “base-exchange” reaction was the only identified reaction *in vitro* to produce NAADP for a long time, consuming both NADP and nicotinic acid. Although NADP is only slightly different from NAADP, as indicated in Fig. 2, it is not capable of inducing Ca^{2+} release events. The optimal pH for the “base-exchange” reaction is pH 4. At neutral pH, NAADP production is barely detectable (Aarhus et al., 1995). Furthermore, NAADP synthesis through the “base-exchange” reaction is crucially dependent on nicotinic acid. At pH 5, the half-maximal production of NAADP was observed in the presence of 5 mM nicotinic acid. In the absence of nicotinic acid, NADP is degraded into 2'-phospho-ADP-ribose (ADPRP) by CD38 (Aarhus et al., 1995). Therefore, both an acidic pH and an excess of nicotinic acid are essential for the “base-exchange” reaction to take place.

Another substrate of CD38 for the production of NAADP is 2'-phospho-cyclic ADP-ribose (cADPRP). At pH 5 and in the presence of 5 mM nicotinic acid, CD38 converts cADPRP to NAADP. The value is 43-fold higher than that at neutral pH. In the absence of nicotinic acid, only hydrolysis of cADPRP to ADPRP by CD38 was reported (Moreschi et al., 2006). cADPRP was identified as an endogenous nucleotide with a basal level at tens of fmol/mg protein in bovine tissues (Vu et al., 1997). However, cADPRP has been described as a Ca^{2+} -mobilizing

agent (Guse et al., 1997; Vu et al., 1996). It is therefore questionable whether cADPRP could be a precursor of NAADP.

Because the production of NAADP catalyzed by CD38 prefers an acidic pH, as described above, this may occur in the lumen of acidic organelles, e.g., lysosomes and/or endosomes. The expression of CD38 in early endosomes has been demonstrated in murine pancreatic acinar cells, where CD38 is required for cholecystokinin (CCK)-stimulated NAADP production (Cosker et al., 2010). In IL-8-treated lymphokine-activated killer (LAK) cells, CD38 was also demonstrated to be involved in NAADP synthesis (Nam et al., 2020; Rah et al., 2010). The same group also reported that CD38 is responsible for the formation of cADPR in LAK cells (Park et al., 2019; Rah et al., 2010). In LP-1 cells (a human myeloma cell line) and CD38-overexpressing HeLa cells and HEK293 cells, CD38 is transferred to the lysosomal membranes by nanobody-induced endocytosis and then leads to an increase in NAADP in the presence of 10 mM nicotinic acid (Fang et al., 2018). These pieces of evidence suggest that endo/lysosomal (type II) CD38 is responsible for NAADP production. Along this line, a transporter system is required to import the substrates NADP and nicotinic acid into the endo/lysosomal lumen and transfer the product NAADP in the opposite direction. Connexin-43 hemichannels have been shown to be involved in this transporter system (Ali et al., 2016; Nam et al., 2020). Additionally, a nucleoside transport inhibitor, dipyrindamole, inhibits NAADP-induced Ca^{2+} increase in LAK cells (Rah et al., 2010).

Meanwhile, there are some results that exclude CD38 as an NAADP forming enzyme. First of all is the fact that CD38 is absent in some cell types where NAADP is detectable, e.g., HeLa cells (Schmid et al., 2012). Further, Soares and coworkers demonstrated that CD38 does not catalyze NAADP formation in human myometrial cells and CD38-overexpressing HL60 cells (a human leukemia cell line) (Soares et al., 2007). A similar result was observed in Jurkat T cells: knockdown of CD38 did not affect endogenous NAADP concentration at 10 s (the peak of the first NAADP production phase) and 5 min (the peak of second production phase) after TCR stimulation. Furthermore, in lymphoid tissues from *Cd38*^{-/-} mice, the basal level of NAADP is even higher than that in the WT control, indicating that CD38 instead works as an NAADP degrading enzyme (Schmid et al., 2011). At neutral pH, CD38 hydrolyzes NAADP into ADPRP. However, this reaction prefers a pH of 5, which is approximately 4-fold higher than that at

neutral pH (Graeff et al., 2006). This pH value in the cell-free system indicates that CD38-catalyzed degradation of NAADP may occur in the acidic compartments by type II CD38 preferably or maybe also by type III CD38 in the cytosol.

All these contrary observations lead us to question, whether CD38 is the enzyme responsible for the rapid NAADP synthesis (or degradation) upon T cell activation. Therefore, the role of CD38 in Ca^{2+} signaling in the early phase of T cell activation was investigated in this thesis.

1.4.2. NAADP synthesis by SARM1

Sterile alpha and TIR motif-containing 1 (SARM1), also known as an NAD consuming enzyme, has been linked to axonal degradation in a number of degenerative neuronal diseases. Although SARM1 and CD38 have no sequence and structure similarity at all, it was found that catalysis of SARM1 is very similar to that of CD38, i.e., producing ADPR and cADPR, hydrolyzing cADPR, and catalyzing NAADP synthesis via the “base-exchange” reaction (Zhao et al., 2019). In addition, the same group has recently demonstrated that acidic pH solely (less than pH 5) can activate SARM1, implying that the catalytic compartment of SARM1 in the endo/lysosomal lumen has physiological relevance (Zhao et al., 2021). SARM1 has a low tissue specificity and can be found almost in all tissues. The involvement of SARM1 in NAADP synthesis has to be further investigated.

1.4.3. NAADP degradation by AP

As mentioned above, NAADP can be degraded by CD38 ideally at pH 5. In cells lacking CD38, e.g., HeLa cells (a cell line derived from human cervical cancer cells), endogenous NAADP is present. Alkaline phosphatase (AP) dephosphorylates NAADP into its inactive derivate NAAD at an optimal pH between 8 and 9. The placental AP isozyme is the best candidate that works as an NAADP metabolizing enzyme in HeLa cells (Schmid et al., 2012). AP is not detectable in Jurkat T cells, and in agreement with this, no NAAD production was detected in the presence of NAADP in the cell-free system with isolated Jurkat T cell membranes (Schmid et al., 2012). Furthermore, a 2'-specific Ca^{2+} -dependent phosphatase was found in brain membranes, which

is probably responsible for inactivating of NAADP-induced Ca^{2+} signaling in the brain (Berridge et al., 2002).

1.4.4. NAADP reduction by Glu-6-P-DH

Billington and coworkers have demonstrated that NAADP can be reduced by glucose-6-phosphate dehydrogenase (Glu-6-P-DH) (Billington et al., 2004). Glu-6-P-DH is known to oxidize glucose-6-phosphate, one of the major players in glycolysis, while reducing NADP to NADPH. The enzymatic activity of Glu-6-P-DH that reduces NADP has been identified to be approximately 7.5 nmol/min/mg protein in human lymphocytes (Al-Essa et al., 2013). Since Glu-6-P-DH can reduce NAADP to NAADPH and since NAADPH does not activate Ca^{2+} release in sea urchin egg homogenates (Billington et al., 2004), Glu-6-P-DH may be involved in termination of NAADP-induced Ca^{2+} signaling.

1.4.5. NAADP synthesis by NOX5

A former colleague in the Department of Biochemistry and Molecular Cell Biology, Hannes Roggenkamp, demonstrated that NADPH oxidase 5 (NOX5) is able to oxidize NAADPH to NAADP in a cell-free system (Gu et al., 2021). This finding is the basis of the present study and gives us a new perspective on how NAADP is formed. As mentioned earlier, NAADPH cannot induce Ca^{2+} release (Billington et al., 2004). Therefore, NAADPH was considered to be a possible precursor of NAADP.

NOX5 is one of the isozymes of the NADPH oxidase (NOX/DUOX) family, which has been investigated as an enzyme system with reactive oxygen species (ROS) production as its main function. NOX5 was discovered to be a homolog of the subunit gp91^{phox} of NOX2, which differs from other NOX isozymes as it contains four Ca^{2+} -binding EF-hand domains (Bánfi et al., 2001; Cheng et al., 2001). NOX5 does not require cytosolic organizer or activator subunits, as shown below in Fig. 3, and it has been demonstrated to be active in the absence of cytosolic proteins in a cell-free system (Bánfi et al., 2004, 2001). Therefore, NOX5 was used as a standard model to investigate the ability to oxidize NAADPH. The optimal pH of NOX5 for the oxidation of

NAADPH is between 7 and 8, while that for NADPH is around 8 (Gu et al., 2021).

As mentioned above, NOX5 contains four EF-hand motifs and produces superoxide triggered by Ca^{2+} elevations in a cell-free system. EC_{50} of Ca^{2+} for NOX5 was determined to be 1.06 μM in the presence of 200 μM NADPH (Bánfi et al., 2004). Phorbol 12-myristate 13-acetate (PMA), a protein kinase C (PKC) activator, induces phosphorylation of NOX5 in a time-dependent manner, elevating its Ca^{2+} sensitivity, and therefore enhancing superoxide production (Chen et al., 2014; Jagnandan et al., 2007; Serrander et al., 2007). At the same time, a calmodulin-binding domain at the C-terminus was found to be relevant in its Ca^{2+} sensitivity (Tirone and Cox, 2007). Subsequently, calcium/calmodulin-dependent kinase II (CAMKII) was identified to phosphorylate NOX5 at residues Thr⁴⁹⁴ and Ser⁴⁹⁸ in the *in vitro* phosphorylation assay (Pandey et al., 2011).

NOX5 is the only isozyme of the NOX/DUOX family reported to be absent in rodents (Kawahara et al., 2007), which may suggest that *Nox5* is not an essential gene for mammals.

1.5. Overview of NOX/DUOX family

Considering the ability of NOX5 to generate NAADP from its reduced form, a brief overview may help us understand the NADPH oxidase family better.

Nowadays, seven isozymes of the NOX/DUOX family have been identified, namely NADPH oxidase (NOX) 1-5 and dual NADPH oxidase (DUOX) 1 and 2. All isozymes contain a conserved catalytic core comprising six (seven for DUOX isozymes) transmembrane domains, including NADPH-binding domains and flavin adenine dinucleotide (FAD)-binding sites at C-terminus in the cytosol. They are distinguished from each other by their structure at the N-terminus, subunits, and regulatory proteins, as shown in Fig. 3. They use NADPH as electron donor and molecular oxygen (O_2) as electron acceptor to generate NADP and superoxide radical anion or hydrogen peroxide (H_2O_2). ROS production has been considered as their primary function, and ROS further affect signaling cascades (reviewed in Bedard and Krause, 2007).

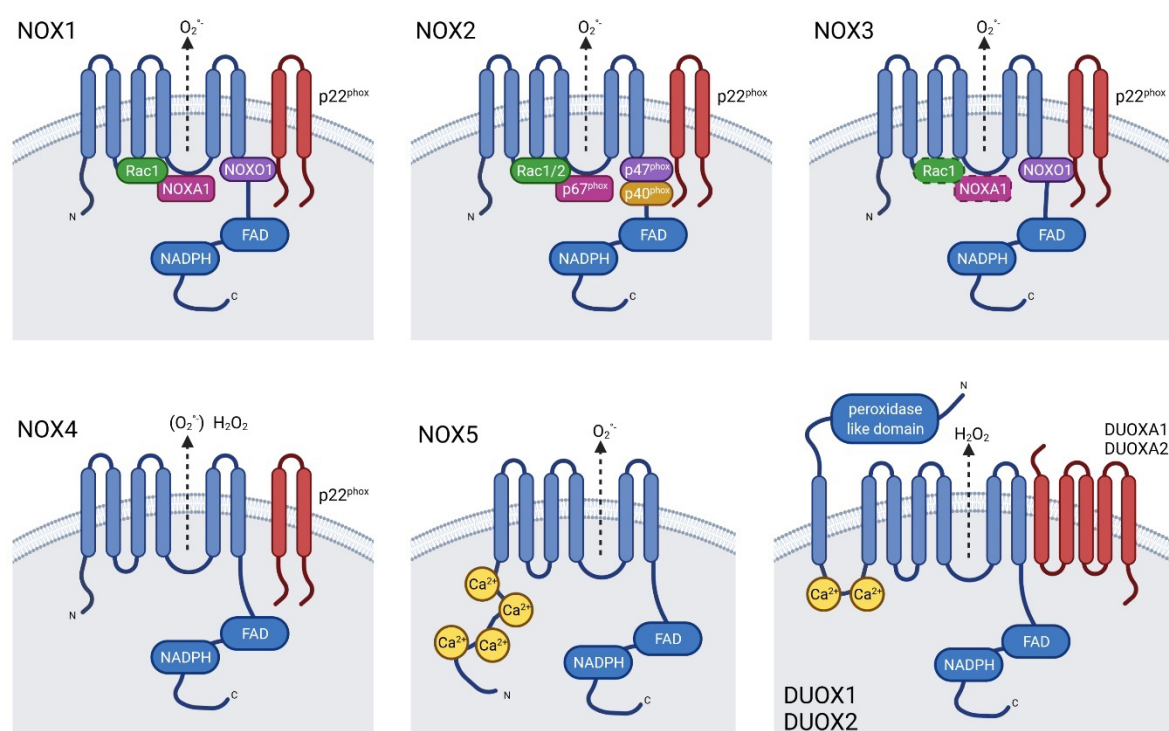


Fig. 3: Structure of isozyms in NADPH oxidase family.

The conserved catalytic core is indicated in blue and consists of six (or seven for DUOX1 and DUOX2) transmembrane domains and a cytosolic C-terminus with NADPH- and FAD-binding domains. The transmembrane subunit p22^{phox} and DUOX maturation factors (DUOXA1 and DUOXA2) are indicated in red. The Ca²⁺-binding EF-hand motifs are shown in yellow. The cytosolic subunits are in other colors. They transfer electrons across the membrane (indicated by the dashed arrow) to oxygen as the final electron acceptor and release reactive oxygen species. This figure was modified from reviews (Altenhöfer et al., 2015; Bedard and Krause, 2007; Belarbi et al., 2017) and created with BioRender.com.

1.5.1. NOX1

NADPH oxidase 1 (NOX1) is the second isozyme identified in this family and exhibits around 60% similarity at the protein level to the prototype NOX2. The gene of NOX1 is located on the X chromosome (reviewed in Bedard and Krause, 2007). It is found in several tissues (Buvelot et al., 2019). In brain cells, the cellular location of NOX1 has been found at the membranes of lysosomes and the nucleus (reviewed in Belarbi et al., 2017). In this study, the role of NOX1 in Ca²⁺ signaling during T cell activation was investigated.

The NOX1 complex is composed of five subunits (Fig. 3): NOX1 is the central catalytic core;

p22^{phox} functions as a stabilizer and binding subunit; NOXO1 is shortened from NOX1 Organizer 1 (p47^{phox} homolog); NOXA1 is NOX1 Activator 1 (p67^{phox} homolog); and the small GTPase Rac serves as guanosine-5'-triphosphate (GTP)-binding protein (Bánfi et al., 2003). In transfected cells, NOX1 can utilize the subunits p47^{phox} and p67^{phox} of NOX2 (reviewed in Bedard and Krause, 2007). NOX1 is inactive in the absence of NOXA1 or NOXO1 and Rac is directly involved in its activation (reviewed in Sumimoto, 2008).

Constitutive activity of the murine NOX1/NOXO1/NOXA1 complex was observed, whereas the human NOX1 complex exhibited only weak constitutive activity. Whether this is a difference between the two species remains unclear (reviewed in Bedard and Krause, 2007). In some transfected cell lines, the PKC activator PMA elevates its superoxide production (Takeya et al., 2003). NOX1 has a significantly higher affinity to NADPH in comparison to NADH as a substrate (Yoshida et al., 2004).

1.5.2. NOX2

NADPH oxidase 2 (NOX2) was the first member of this family to be identified and is the best studied isozyme due to its direct involvement in a hereditary disorder, chronic granulomatous disease (CGD) (Bylund et al., 2005). It is expressed at a high level in neutrophils and macrophages. Therefore, it is also referred to as “phagocyte NADPH oxidase”. However, it is also found in many other cell types, e.g., B cells (reviewed in Bedard and Krause, 2007) and T cells (Jackson et al., 2004). NOX2 is localized to intracellular and plasma membranes (reviewed in Bedard and Krause, 2007; Belarbi et al., 2017). The role of NOX2 in Ca²⁺ signaling upon T cell activation was investigated in this thesis.

Functional NOX2 is composed of six subunits (Fig. 3): the main transmembrane subunit gp91^{phox} (also known as NOX2, is encoded by *Nox2*, also called *Cybb* gene, located on the X chromosome), a transmembrane subunit p22^{phox} that acts as a stabilizer, and the cytosolic organizer p47^{phox}, the activator p67^{phox}, the regulator p40^{phox}, and the GTP-binding protein Rac. The assembly of the NOX2 complex leads to the production of superoxide anion, and the function of the enzyme is affected by mutations in any of the subunits. The role of NOX2 in host defense is well described, most likely due to the “killing” effect and the modification of

intracellular signaling by NOX2-derived ROS (reviewed in Bedard and Krause, 2007).

Its activity has been demonstrated to be regulated by PKC-induced phosphorylation (Raad et al., 2009; Regier et al., 1999). NOX2 has also been identified to use NADH as a substrate, but the K_m value is about 60-fold higher (47 μ M for NADPH versus 2.7 mM for NADH) (Clark et al., 1987).

1.5.3. NOX3

NADPH oxidase 3 (NOX3) is 56% identical to NOX2 and is highly expressed in the inner ear. The enzymatic activity of NOX3 is dependent on p22^{phox} and is enhanced by NOXO1, p67^{phox} and p47^{phox} (reviewed in Bedard and Krause, 2007; Sumimoto, 2008). In a reconstituted system, NOX3 is constitutively activated by NOXO1 (Fig. 3), and human NOX3 can be regulated by the NOX2 subunits p47^{phox} and p67^{phox} (reviewed in Lambeth et al., 2007).

1.5.4. NOX4

NADPH oxidase 4 (NOX4) has only 39% similarity to NOX2. NOX4 is highly expressed in renal epithelial cells and vascular endothelial cells (reviewed in Sumimoto, 2008). The functional NOX4 complex requires only NOX4 and p22^{phox}, and its activity is independent of cytosolic subunits (Fig. 3). Once NOX4 is transfected into cell models, it appears to be constitutively active without the requirement for any activators. A few studies indicate that NOX4 activity in some cells is regulated by unidentified mechanisms (reviewed in Lambeth et al., 2007). The majority of ROS generated by NOX4 are H₂O₂, and the minority are superoxide (Nisimoto et al., 2014). A longer third extracellular loop was found in NOX4 as a switch from superoxide to H₂O₂ production. This loop could serve as a proton source to elevate the dismutation of superoxide to form H₂O₂ (Takac et al., 2011). Protein kinase G (PKG)-mediated phosphorylation of the p22^{phox} subunit has been reported to be involved in NOX4 activation (Park et al., 2019).

1.5.5. NOX5

NADPH oxidase 5 (NOX5) does not require any subunits for activation, and contains a long N-terminus with four Ca²⁺-binding EF-hand domains (Fig. 3), as mentioned previously (Bánfi et al., 2004). NOX5 shows a restricted tissue distribution. By northern blot, NOX5 was detected in the spleen and testis among various human tissues (Bánfi et al., 2001). In a cell-free system, EC₅₀ of Ca²⁺ for NOX5 was determined to be 1.06 μM. Under the same conditions, NADH as an electron donor leads to superoxide production of only around 25% compared to NADPH (Bánfi et al., 2004).

1.5.6. DUOX1 and DUOX2

Dual NADPH oxidase 1 and 2 (DUOX1 and DUOX2) share 83% similarity, and they are approximately 50% identical to NOX2. In addition to the conserved catalytic core (six transmembrane domains with NADPH- and FAD- binding domains), DUOX isozymes contain a seventh transmembrane domain with a peroxidase-homologous domain facing the extracellular space and, like NOX5, with two Ca²⁺-binding EF-hand motifs in the cytosol (reviewed in Bedard and Krause, 2007; Buvelot et al., 2019).

So far, H₂O₂ is the only product detected upon the activation of DUOX isozymes. Whether H₂O₂ is their primary product due to the peroxidase-like domain or is formed after dismutation of superoxide as in NOX4 is still controversial (reviewed in Buvelot et al., 2019). Some studies have shown that they have no peroxidase activity (reviewed in Altenhöfer et al., 2015). DUOX1 and DUOX2 do not require subunits of NOX1 or NOX2, but the so-called DUOX maturation factors, i.e., DUOXA1 and DUOXA2, respectively, have been demonstrated to be essential for their enzyme activity (Fig. 3). In the absence of DUOXA1 and DUOXA2, DUOX isozymes cannot be correctly glycosylated and are retained in the ER instead of being expressed at the plasma membrane (Grasberger and Refetoff, 2006). Further reports suggest that the maturation factors not only promote their maturation but also contribute to H₂O₂ production, given that the unpaired complex produces much less H₂O₂ and leaks superoxide (Morand et al., 2009) and transient expression of immature DUOX2 produces superoxide in a Ca²⁺-dependent manner (Ameziane-EI-Hassani et al., 2005). Functional EF-hand motifs are

essential for the basal activity of both DUOX isozymes. Furthermore, treatment with ionomycin (a Ca^{2+} ionophore that increases intracellular Ca^{2+} concentration) elevates their enzymatic activity. Moreover, the activity of the DUOX1/A1 complex can be further enhanced by phosphorylation at Ser⁹⁵⁵ catalyzed by cyclic adenosine monophosphate (cAMP)-dependent protein kinase A (PKA), whereas the DUOX2/A2 complex requires PKC activation (Rigutto et al., 2009).

Wu and coworkers reported the cryo-EM structure of the human DUOX1/A1 complex, which is in a heterotetrameric form. They demonstrated that the EF-hand motifs and a regulatory pleckstrin homology-like domain (PHLD) contribute to a conformational change at different Ca^{2+} concentrations. The EC_{50} of Ca^{2+} was determined to be 0.38 μM in a cell-free system (Wu et al., 2021). Meanwhile, the cryo-EM structure of the murine DUOX1/A1 complex was also resolved, which is 91% identical to the human complex. However, the conformation of the murine complex changes from a “dimer of dimer” to a heterodimer in the presence or absence of the substrate NADPH (Sun, 2020). Whether this is a difference between the two species or a difference in sample preparation is unclear (Wu et al., 2021).

Both DUOX isozymes are highly expressed in the thyroid gland. However, only deficiency of DUOX2 enzyme leads to congenital hypothyroidism, and DUOX1 may compensate for the function of DUOX2, since the digenic mutations of DUOX1 and DUOX2 are associated with the severe phenotype of congenital hypothyroidism (Aycaan et al., 2017), and the functional double knockout of DUOX1 and DUOX2 (*DuoxA1^{-/-}/A2^{-/-}*) leads to severe congenital hypothyroidism in mice (Grasberger et al., 2012). In addition, DUOX isozymes are expressed in a variety of epithelial cells as well as many other tissues (reviewed in Bedard and Krause, 2007) and are detectable in T cells (Kwon et al., 2010) and B cells (Singh et al., 2005). In this thesis, the role of DUOX1 and DUOX2 in Ca^{2+} signaling upon TCR stimulation was investigated.

1.5.7. Pharmacological inhibitors of NOX/DUOX family

Exploring pharmacological inhibitors of the NOX/DUOX family is a hot topic, because oxidative stress is likely an underlying mechanism for many diseases, such as neurodegenerative disorders (ND). Increased oxidant formation is known to be a central feature in ND (reviewed

in Sorce et al., 2017). In one of the ND mouse models, upregulation of NOX2 and DUOXA was observed in the spinal cord (Seredenina et al., 2016). Apocynin, commonly advertised as a NOX inhibitor, has been shown to have beneficial effects on ND in some animal models. However, it was later shown that apocynin is not a NOX inhibitor and instead functions as an oxidant scavenger (reviewed in Sorce et al., 2017). ROS production is most commonly used as an indicator to quantify the activity of these enzymes. Therefore, some inhibitors partially function as ROS scavengers and/or have redox activity that interferes with the reagents used in the enzyme assay. Furthermore, the highly conserved backbone of the NOX/DUOX family makes it difficult to develop a selective inhibitor (reviewed in Altenhöfer et al., 2015). Reis and coworkers investigated twenty-four NOX inhibitors, and only three of them appear to provide “real or clean” inhibition: DPI (diphenylene iodonium), VAS2870, and VAS3947 (Reis et al., 2020).

DPI is the most commonly used inhibitor in NOX/DUOX studies. It potently inhibits all the isozyms, most likely by irreversible binding to the FAD-binding domains (O'Donnell et al., 1993). Therefore, it also inhibits other flavoproteins involved in a wide range of biological processes. DPI has also been demonstrated to be a potent inhibitor of cholinesterases with an IC_{50} in the micromolar range. In addition, DPI inhibits SERCA pumps in isolated microsomes from pig coronary artery (30 μ M DPI inhibits Ca^{2+} uptake by 18%, whereas 1 μ M thapsigargin inhibits 71% as a positive control) (Tazzeo et al., 2009), which in turn induces SOCE.

VAS2870 and VAS3947 inhibit NOX isozyms by covalent ligation at the NADPH-binding domains. VAS3947 significantly inhibits NOX4 after 10 min of incubation. Nevertheless, they are pan-NOX inhibitors (Reis et al., 2020). Additionally, they have been reported to reduce platelet activation through a NOX-independent pathway (Lu et al., 2019). An off-target effect of VAS2870 is the direct modification of cysteine thiols of RyR1 (Sun et al., 2012).

Therefore, when using pharmacological NOX/DUOX inhibitors in cell-based experiments, both the off-target effect as well as ROS scavenging and redox activity have to be considered. In this study, CD4⁺ T cells derived from different mouse models were used to discriminate between different NOX/DUOX isozyms.

2. Study aims

T cell activation is a hallmark of the adaptive immune response. NAADP is produced within seconds after the stimulation of T cell receptor. NAADP-induced Ca^{2+} signals function as a trigger of T cell activation and play a central role in subsequent global Ca^{2+} signaling as well as downstream events, and therefore in the progression of many inflammatory diseases. The importance of NAADP in T cell activation led to the question: how is NAADP formed in CD4^+ T cells? It has been known that CD38 generates NAADP in the cell-free system at acidic pH. Further, in the course of the experimental part of this thesis, NADPH oxidases (NOX/DUOX) were established as enzymes oxidizing NAADPH to NAADP. Hence, their potential roles in intact CD4^+ T cells stimulated via the TCR/CD3 complex were investigated in this thesis.

The rapid formation of NAADP upon TCR/CD3 ligation evokes initial local Ca^{2+} signals, termed Ca^{2+} microdomains. Hence, Ca^{2+} microdomains were used as the main read-out to identify the NAADP forming enzyme in CD4^+ T cells. Subsequent global Ca^{2+} signals upon T cell activation were also analyzed.

- 1) CD38 has long been the only identified enzyme capable of producing NAADP in cell-free system. However, due to its ability to also degrade NAADP, the situation appears complex. Therefore, Ca^{2+} responses in T cells from *Cd38*^{-/-} mice were first investigated.
- 2) The NADPH oxidase family, which produces NAADP from its reduced form in the cell-free system, was then investigated. Since no selective pharmacological inhibitors were available, primary CD4^+ T cells isolated from different mouse models were used to distinguish the isozymes expressed in T cells, namely NOX1, NOX2, DUOX1, and DUOX2. Because the single knockout of DUOX1 and DUOX2 mouse models were not available, the difference between DUOX isozymes was determined using CRISPR/Cas designed rat CD4^+ effector T cells.
- 3) NADPH oxidases generate reactive oxygen species (ROS) as a second product. ROS are known to act as signaling molecules. Therefore, several experimental approaches were conducted to analyze effects of ROS on Ca^{2+} signaling in the first seconds after T cell activation.

3. Methods and materials

3.1. Materials

The following fluorescent dyes, kits, antibodies, chemicals, and adenine nucleotides standards were used for this project. All compounds were prepared, stored, and used according to the manufacturer's instructions.

Table 2: List of compounds and devices used for Ca²⁺ imaging

Product	Manufacturer
Ca²⁺ indicators	
Fura2-AM	EMD Millipore, Merck, USA
Fluo4-AM	Invitrogen, Life Technologies, USA
FuraRed-AM	Invitrogen, Life Technologies, USA
T cell isolation	
EasySep™ CD4+ T Cell Isolation Kit	STEMCELL Technologies, Canada
Cell Strainer (40 µmNylon, 352340)	BD Falcon, USA
antibodies and magnetic beads	
anti-mouse CD3 monoclonal antibody	BD Biosciences, USA
anti-mouse CD28 monoclonal antibody	BD Biosciences, USA
anti-rat CD3 monoclonal antibody	BD Biosciences, USA
anti-rat CD28 monoclonal antibody	BD Biosciences, USA
PureProteome™ Protein G Magnetic Beads	EMD Millipore, Merck, USA
additional compounds	
thapsigargin	EMD Millipore, Merck, USA
ionomycin	Merck, Germany
EGTA	Sigma-Aldrich Co, USA or Sigma-Aldrich Chemie GmbH, Germany
BZ194	provided from Prof. Chris Meier from Organic Chemistry, University of Hamburg
catalase	Sigma-Aldrich Co, USA or Sigma-Aldrich Chemie GmbH, Germany
BHA	Sigma-Aldrich Co, USA or Sigma-Aldrich Chemie GmbH, Germany
DFP00173	Axon Medchem, Nederland
H ₂ O ₂	Sigma-Aldrich Co, USA or Sigma-Aldrich Chemie GmbH, Germany
pCMV-HyPer7-MEM	Addgene #136465
Neon Transfection system 100 µL kit	Invitrogen, USA
Pure water (Aqua)	B. Braun Melsungen, Germany
slides coating	
PLL	Sigma-Aldrich Co, USA or Sigma-Aldrich Chemie

Methods and materials

Product	Manufacturer
	GmbH, Germany
BSA	SIGMA Life Science, USA
ACK buffer	
NH ₄ Cl	Merck, Germany
KHCO ₃	Merck, Germany
EDTA	Sigma-Aldrich Co, USA or Sigma-Aldrich Chemie GmbH, Germany
Ca²⁺ buffer	
(D)-glucose • 6 H ₂ O	Merck, Germany
KCl	Merck, Germany
MgSO ₄ • 7 H ₂ O	Merck, Germany
NaCl	Sigma-Aldrich Co, USA or Sigma-Aldrich Chemie GmbH, Germany
CaCl ₂ • 2 H ₂ O	Merck, Germany
NaH ₂ PO ₄ • H ₂ O	Merck, Germany
HEPES	Carl Roth, Germany

Table 3: List of adenine nucleotides standards used for HPLC assay

Product	Manufacturer
adenine	Sigma-Aldrich Co, USA or Sigma-Aldrich Chemie GmbH, Germany
adenosine	Sigma-Aldrich Co, USA or Sigma-Aldrich Chemie GmbH, Germany
ADP	Sigma-Aldrich Co, USA or Sigma-Aldrich Chemie GmbH, Germany
ADPR	Sigma-Aldrich Co, USA or Sigma-Aldrich Chemie GmbH, Germany
ADPRP	Biolog, Germany
AMP	Sigma-Aldrich Co, USA or Sigma-Aldrich Chemie GmbH, Germany
ATP	Sigma-Aldrich Co, USA or Sigma-Aldrich Chemie GmbH, Germany
NAAD	Sigma-Aldrich Co, USA or Sigma-Aldrich Chemie GmbH, Germany
NAADP	Biolog, Germany
NAD	Roche, Switzerland
NADP	Sigma-Aldrich Co, USA or Sigma-Aldrich Chemie GmbH, Germany
NADPH	Roche, Switzerland
nicotinic acid	Sigma-Aldrich Co, USA or Sigma-Aldrich Chemie GmbH, Germany
nicotinamide	Sigma-Aldrich Co, USA or Sigma-Aldrich Chemie GmbH, Germany

Table 4: List of compounds and devices used for enzyme assay

Product	Manufacturer
Enzyme assay buffer	
FAD	Sigma-Aldrich Co, USA or Sigma-Aldrich Chemie GmbH, Germany
phosphatidic acid	Sigma-Aldrich Co, USA or Sigma-Aldrich Chemie GmbH, Germany
NTA	Sigma-Aldrich Co, USA or Sigma-Aldrich Chemie GmbH, Germany

Methods and materials

Product	Manufacturer
MgCl ₂ • 6 H ₂ O	Merck, Germany
CaCl ₂ • 2 H ₂ O	Merck, Germany
HEPES	Carl Roth, Germany
EDTA	Sigma-Aldrich Co, USA or Sigma-Aldrich Chemie GmbH, Germany
HPLC buffer	
KH ₂ PO ₄	Sigma-Aldrich Co, USA or Sigma-Aldrich Chemie GmbH, Germany
methanol	Merck, Germany
TBAP	Sigma-Aldrich Co, USA or Sigma-Aldrich Chemie GmbH, Germany
NAADPH production	
NAADP	Biolog, Germany
NaHCO ₃	Merck, Germany
sodium dithionite	Sigma-Aldrich Co, USA or Sigma-Aldrich Chemie GmbH, Germany
NaCl	Sigma-Aldrich Co, USA or Sigma-Aldrich Chemie GmbH, Germany
additional devices	
VIVASPIN 500	Sartorius Stedim Lab, UK
HiTrap DEAE FF 1 mL column	GE Healthcare, Sweden

Table 5: List of other compounds used for buffer solution and medium

Product	Manufacturer
RPMI 1640 + GlutaMAX™-I + 25mM HEPES	Gibco, Life Technologies, USA
DEME (1X) + GlutaMAX™-I	Gibco, Life Technologies, USA
PenStrep	Gibco, Life Technologies, USA
PBS (Ca ²⁺ - and Mg ²⁺ -free)	Gibco, Life Technologies, USA
NCS	Biochrom, Germany
FCS	Biochrom, Germany
sodium pyruvate	Gibco, Life Technologies, USA
L-asparagine	Sigma-Aldrich Co, USA or Sigma-Aldrich Chemie GmbH, Germany
2-mercaptoethanol (50 mM)	Gibco, Life Technologies, USA
MEM non-essential amino acids	Gibco, Life Technologies, USA
NaOH	J.T. Baker, Netherland
KOH	Merck, Germany
DMSO	Sigma-Aldrich Co, USA or Sigma-Aldrich Chemie GmbH, Germany

3.2. Solutions

Ca²⁺ buffer for imaging: 20 mM HEPES, 140 mM NaCl, 5 mM KCl, 1 mM MgSO₄, 1 mM CaCl₂, 1 mM NaH₂PO₄, 5.5 mM glucose; pH 7.4 adjusted with 7 M NaOH

ACK buffer: 4.3 g NH₄Cl, 0.5 g KHCO₃, 0.00186 g Na₂-EDTA in 400 mL H₂O; pH 7.2 – 7.4

PBS-T: 10 x PBS with 0.1% (v/v) Tween 20

Buffer for enzyme assay: 50 mM HEPES, 5.5 μM phosphatidic acid, 10 μM FAD, 450 μM NTA, 450 μM EDTA, 1 mM MgCl₂, 1.4 mM CaCl₂; pH 7.1 adjusted with 7 M NaOH

HPLC buffer A1 (with ion pair reagent): 20 mM KH₂PO₄, 1% (v/v) TBAP, pH 6.0 adjusted with 7 M KOH

HPLC buffer B1: 50% buffer A1 (v/v), 50% methanol

HPLC buffer A2 (without ion pair reagent): 20 mM KH₂PO₄, pH 6.0 adjusted with 7 M KOH

HPLC buffer B2: 50% buffer A2 (v/v), 50% methanol

Buffer for chemical NAADPH production: 744 μM NAADP, 400 mM NaHCO₃, 115 mM sodium dithionite

Buffer A for NAADPH elution: 20 mM HEPES; pH 8.0 adjusted with 7 M NaOH

Buffer B for NAADPH elution: 20 mM HEPES, 300 mM NaCl; pH 8.0 adjusted with 7 M NaOH

3.3. Mediums

Medium for rat T cells: 96% (v/v) DMEM + GlutaMAXTM -I supplemented with 4.5 g/L D-glucose, 1% (v/v) MEM non-essential amino acids, 1% (v/v) sodium pyruvate (final concentration 1 mM), 1% (v/v) PenStrep (final concentration 100 U/mL), 1% (v/v) L-asparagine (final concentration 1 mM), 0.1% (v/v) 2-mercaptoethanol (final concentration 50 μM)

Medium for murine T cells and Jurkat T cells clone JMP: RPMI medium 1640 + GlutaMAXTM -I supplemented with 25 mM HEPES and phenol red, additionally supplemented with 1% (v/v) PenStrep (final concentration 100 U/mL) and 7.5% NCS

Medium for transfection: RPMI medium 1640 + GlutaMAXTM -I + 25 mM HEPES, supplemented with 10% (v/v) FCS

3.4. Mouse models

Cd38^{-/-} (B6.129P2-Cd38^{tm1Lnd}/J) (Cockayne et al., 1998) and WT (C25BL/6) mice were bred in the animal facility of the University Medical Center Hamburg-Eppendorf. In collaboration with Prof. Hans-Willi Mittrücker, the isolated murine spleens and lymph nodes in DEME medium were kept on wet ice before T cell isolation.

Nox1^{y/-} mouse model was reported in (Gavazzi et al., 2006). **Nox2**^{-/-} (B6.129S-Cybb^{tm1Din}/J) were purchased from the Jackson Laboratory. Breeding was performed by crossing homozygote **Nox1**^{-/-} or **Nox2**^{-/-} females with WT males, giving rise to WT^(+/+) or KO^(y/-) male littermates. In collaboration with Prof. Katrin Schröder from Goethe-University Frankfurt, the isolated murine spleens and lymph nodes were shipped to Hamburg in DEME medium on wet ice.

3.5. Isolation of primary murine T cells

Before T cell isolation, the spleens and lymph nodes were kept in cold RPMI medium on wet ice. Then they were crushed by pressing them into a sieve with a syringe plunger. Cells were washed with additional medium through the filter and were centrifuged (1200 rpm, 5 min, 4°C). Cells were then resuspended in ACK buffer and incubated on wet ice for 5 min to lyse the red blood cells. After centrifuging the suspension (1200 rpm, 5 min, 4°C), the supernatant was discarded. CD4⁺ T cells were isolated by EasySepTM Mouse CD4⁺ T Cell Isolation Kit by negative selection. Briefly, unwanted cells are eliminated precisely using biotinylated antibodies directed against non-CD4⁺ T cells that are coupled to streptavidin-coated magnetic particles (RapidSpheresTM). A magnet was used to remove the magnetic particles and bound cells from the solvent. CD4⁺ T cells were present in the solution.

3.6. DUOX1 and DUOX2 single knockouts in rat effector T cells

In collaboration with Prof. Alexander Flügel from University Medical Center Göttingen, CRISPR/Cas designed DUOX1 and DUOX2 single knockout rat CD4⁺ effector T cells were shipped to Hamburg in DMEM medium on wet ice.

Briefly, retroviral short guide RNA expression constructs were cloned into a modified pMSCV vector pMPuChe-U6zero from Clontech. A long terminal repeat (LTR) promoter drives expression of a puromycin resistance gene linked to the red fluorescent protein mCherry. U6 promoter controls the expression of crRNA. Oligonucleotides targeted to protospacer in the exon 2 of rat *Duox1* gene (CCTGGATCCTCCTTTTTGGGATG) or exon 3 of rat *Duox2* gene (CCTGGGCGCTCTGTTGACTGGAC) were annealed and ligated into Bbs I digested vector. Control short guide RNA was made to target intronic sequence in the rat *Rosa26* locus. After 7 days of puromycin (1 µg/mL) selection, flow cytometry was used to sort survivor packaging cells. These cells were then subcloned by limited dilution. Effector T cell lines specific for ovalbumin or myelin basic protein on a transgenic background expressing Cas9 nuclease were described previously (Flügel et al., 1999). In culture, more than 95% of cells were positive for Cherry after two rounds of restimulation, as demonstrated by flow cytometry.

3.7. Imaging of initial Ca²⁺ microdomains and analysis

Identification of local Ca²⁺ microdomains, image processing, calibration, and comparison for subcellular compartments has been reported in detail in (Diercks et al., 2019). Briefly, freshly isolated murine CD4⁺ T cells or rat CD4⁺ effector T cells were loaded with a combination of 10 µM Fluo4-AM and 20 µM FuraRed-AM for 50 min at room temperature in RPMI medium (murine T cells) or DMEM medium (rat T cells). In between, 2 mL medium was added at 20 min intervals. After washing, cells were resuspended in Ca²⁺ buffer. The stimulating beads were PureProteome™ Protein G Magnetic Beads coated with anti-CD3 and anti-CD28 antibodies. Coverslips were coated with bovine serum albumin (BSA; 5 mg/mL) and poly-L-lysine (PLL; 0.1 mg/mL) to facilitate T cell adhesion.

Cells were preincubated at room temperature with 1000 to 2500 units/mL catalase for 5 min (control with equal volume Ca²⁺ buffer) or with 50 µM BHA for 5 min or with 25 µM DFP00173 for 10 min [control with 0.5% (v/v) DMSO] before measurements. Commercial H₂O₂ (10 M) was diluted with commercial pure water to a 50 µM stock solution and then diluted into 0.8 µM with Ca²⁺ buffer. The H₂O₂ stock solution was prepared shortly before the measurements and kept on ice.

Imaging was performed on a Leica IRBE2 microscope (100-fold magnification) using a Sutter DG-4 light source and electron-multiplying charge-coupled device camera (C9100, Hamamatsu). Exposure time was 25 ms (40 frames/s) in 14-bit mode with 2-fold binning. A Dual-View module (Optical Insights, PerkinElmer Inc.) was used to split the emission wavelengths, with filters: 480/40 for excitation; 495 for beam splitter; 542/50 for emission 1 and 650/57 for emission 2. Volocity software (version 6.6.2; PerkinElmer) was used for image acquisition, and Ca^{2+} microdomain analysis was done with MATLAB (MathWorks). All pixel Ca^{2+} concentration value in the microdomain was required to be at least within an increase more than 90 nM, greater than the frame-specific mean Ca^{2+} concentration of the considered cell to identify Ca^{2+} microdomain in cell images. A method called "dartboard projection" was developed to compare subcellular compartments. Every individual cell was matched to a circular, dartboard-like template. The recognized local Ca^{2+} signals were allocated to the relevant dartboard based on their geographical positions. Rotation was used to equalize each dartboard to the bead contact site to 1 o'clock. The dartboard information for all individual cells was then combined and analyzed. Data are shown as the mean of the number of Ca^{2+} microdomains per cell and frame.

3.8. Imaging of global Ca^{2+} signals and analysis

Freshly isolated murine T cells or rat effector T cells were loaded with 4 μM Fura2-AM for 30 min at 37°C in RPMI medium (murine T cells) or DMEM medium (rat T cells). In between, 2 mL medium was added at 15 min intervals. Cells were washed twice, resuspended in Ca^{2+} buffer, and kept at room temperature for 20 min.

Cells were preincubated with 500 μM NAADP antagonist BZ194 [control with 1% (v/v) DMSO] overnight at 37°C and 5% CO_2 in a humidified cell incubator; or with 1000-2500 units/mL catalase for 5 min (control with equal volume Ca^{2+} buffer) on coverslips coated with BSA (5 mg/mL) and PLL (0.1 mg/mL). Anti-CD3 antibody (final concentration: 1 $\mu\text{g}/\text{mL}$ for rat T cells or 10 $\mu\text{g}/\text{mL}$ for murine T cells) was added at 2 min to stimulate T cells, and thapsigargin (final concentration 1.67 μM) was added at 15 min as a positive control.

Imaging was carried out using a Leica IRBE microscope with 40-fold magnification. A Sutter

DG-4 was used as a light source, and frames were acquired with an electron-multiplying charge-coupled device camera (Hamamatsu). The time-lapse rate was 2 s/frame with a Fura2 filter set (excitation, HC 340/26 nm and HC 387/11 nm; beam splitter, 400 DCLP; emission, 510/84 nm; AHF Analysentechnik).

Before calculating the ratio of 340ex/380ex, the background was corrected. The free cytosolic Ca^{2+} concentration $[Ca^{2+}]_i$ was calibrated using the equation provided in (Grynkiewicz et al., 1985):

$$[Ca^{2+}]_i = Kd * \frac{R - Rmin}{Rmax - R} * \frac{F(380)max}{F(380)min}$$

Kd refers to the dissociation constant 224 nM. Rmax (ratio of 340ex/380ex) and F(380)max (fluorescence upon excitation at 380 nm) were measured in Ca^{2+} buffer with 5 μ M ionomycin; Rmin and F(380)min were measured in Ca^{2+} buffer containing 4 mM EGTA and 5 μ M ionomycin using WT murine or rat T cells, respectively.

3.9. Cell culture of Jurkat T cells

Jurkat T cells are an immortalized CD4+ human T cell line. In present study, a subclone JMP was used. Jurkat T cells were cultured at 37°C and 5 % CO₂ in a CO₂ incubator. Every 2 to 3 days the cell density was determined and adjusted to a concentration of 0.3x10⁶ cells/mL with RPMI medium.

3.10. Determination of H₂O₂ using HyPer7 sensor

To examine H₂O₂ generation, 2x10⁶ WT Jurkat T cells (clone JMP) were electroporated with 5 μ g of pCMV-HyPer7-MEM according to the manufacturer's recommendation using the Neon Transfection System (Invitrogen). V. Belousov kindly provided the vector (Addgene, plasmid no. 136465) as a gift. Before transfection, cells were washed in phosphate-buffered saline (PBS; without Ca^{2+} and Mg^{2+}) and resuspended in 100 μ l of resuspension buffer R (an Invitrogen proprietary buffer). Two 1400-V pulses, each lasting 20 ms, were used for electroporation. After electroporation, cells were incubated overnight at 37°C and 5% CO₂ in

humanized incubator.

For image acquisition, cells were seeded on coverslips coated with BSA (5 mg/mL) and PLL (0.1 mg/mL) and images were acquired at 100-fold magnification using a spinning-disk confocal imaging system (Visitron). HyPer7 fluorescence was acquired for 400 ms with 40% laser power using 405 nm and 488 nm lasers. Emission from both lasers was measured using a 525/50 emission filter in front of a sCMOS camera (Orca-Flash 4.0, C13440-20CU, Hamamatsu). After 30 s, OKT3 (final concentration 1 μ g/mL), Ca^{2+} buffer, or the appropriate H_2O_2 concentrations were added (final concentrations: 80 nM, 100 nM, 200 nM, 300 nM, 400 nM, and 10 μ M). H_2O_2 was freshly prepared as described in methods and materials section 3.7. Before calculating the ratio of 488ex/405ex, the background was corrected, and finally, the ratio was normalized to the time point of stimulation (R/R_{stim}).

3.11. NAADPH production

The procedure for production of the reduced form of NAADP was described in a previous report (Billington et al., 2004). 744 μ M NAADP was dissolved in buffer containing 400 mM NaHCO_3 and 115 mM sodium dithionite. Under a steady argon flow, the solution was incubated in the dark for 2 h. Then, the solution was loaded onto a HiTrap DEAE FF 1 mL column using a peristaltic pump at a 1 mL/min flow rate and equilibrated with 20 mM HEPES (pH 8.0). A linear gradient of 0 to 300 mM NaCl was then used to elute NAADPH. 1 mL fractions were collected, 12 μ l of each fraction was then analyzed on HPLC, the fractions with the greatest absorption at 340 nm were then used as substrate for the enzyme assay. The rest of the fractions was immediately aliquoted, argon-treated, and stored at -80°C until used.

HPLC (Agilent Technologies, 1260 Infinity and 1200 Infinity) was used to control the quality and quantity of each batch, using a BDS Multohyp 5 μ column (250 x 4.60 mm, particle size 5 μ m). Buffer A1 [20 mM KH_2PO_4 , 1% (v/v) tetrabutylammonium phosphate (TBAP) at pH 6.0] and buffer B1 [50% (v/v) buffer A1, 50% (v/v) methanol] were used to analyze the product at a flow rate 0.8 mL/min. The gradient was 30% buffer B1 (0 to 3.5 min), linearly increased B1 to 62.5% (3.5 to 11 min), 62.5% buffer B1 (11 to 15 min), linearly increased B1 to 100% (15 to 25 min), decreased B1 to 30% (25 to 27min), and 30% B1 (29 to 38 min). Because NADPH (6220

1/cm/M) and NAADPH (6228 1/cm/M) have similar absorption coefficients at 340 nm (Billington et al., 2004), NADPH was used as the standard for quantification of NAADPH. The wavelengths of the diode array detector (Agilent Technologies) were 260 nm (for nucleotides) and 340 nm (for the reduced form of nucleotides). ChemStation Software (Rev. C.01.05, Agilent Technologies) was used for peak integration.

3.12. Enzyme assay in a cell-free system and HPLC conditions

In collaboration with Prof. Karl-Heinz Krause from the University of Geneva, membranes were isolated from human DUOX1/A1 or human DUOX2/A2 overexpressing HEK293 cells, then aliquoted and shipped on dry ice to Hamburg. Purification of these membranes was described in detail in (Augsburger et al., 2019), and protein concentration was determined using the Bradford reagent. Membranes were then immediately stored at -80°C and thawed shortly before the measurements and incubated at 37°C in the enzyme assay buffer at pH 7.1 containing 50 mM HEPES, 5.5 µM phosphatidic acid, 10 µM FAD, 450 µM NTA, 450 µM EDTA, 1.4 mM CaCl₂, 1 mM MgCl₂ and 50 µM NAADPH or NADPH as positive control.

Samples were analyzed by HPLC (Agilent Technologies, 1260 Infinity and 1200 Infinity) equipped with a C8 column [Phenomenex Luna 5µ C8(2) 100A (250 x 4.60 mm, particle size 5 µm)] and a guard cartridge (4 x 3.0 mm) containing a C8 filter element (Phenomenex). Analysis was carried out at a flow rate of 0.8 mL/min in a running buffer A2 (20 mM KH₂PO₄ at pH 6.0) with a linear methanol gradient [buffer B2: 50% (v/v) buffer A2 and 50% (v/v) methanol]. The gradient was 0% B2 (0 to 5 min), linearly increased B2 to 25% (5 to 27.5 min), 25% B2 (27.5 to 30 min), decreased B2 to 0% (30 to 32 min), and 0% B2 (32 to 43 min). The wavelengths of the diode array detector (Agilent Technologies) were 260 nm (for nucleotides) and 340 nm (for the reduced form of nucleotides). ChemStation Software (Rev. C.01.05, Agilent Technologies) was used for peak integration. Enzyme activity was calculated using the difference in NAADP or NADP after incubation with and without enzyme-containing membranes.

4. Results

The physiological mechanism of generation of NAADP in CD4⁺ T cells is still unknown. In this study, Ca²⁺ microdomains generated within 15 s and global Ca²⁺ signals up to 13 min after TCR stimulation were monitored as read-out for the synthesis of NAADP in intact T cells. The results section mainly consists of two parts:

In the first part, CD4⁺ primary T cells derived from different mouse models and CRISPR/Cas designed rat CD4⁺ effector T cells were used. These T cells lack the enzymes reported to synthesize NAADP in the cell-free system. One enzyme was identified that is responsible for the rapid NAADP formation upon T cell activation.

In the second part, the role of H₂O₂ in initial Ca²⁺ signaling upon T cell activation was excluded. To obtain these data, master students Aileen Krüger and Franziska Möckl helped with a part of the measurements and analyses.

4.1. Role of CD38 in Ca²⁺ signaling upon TCR/CD3 ligation

CD38 has long been the only identified mammalian enzyme capable of synthesizing NAADP *in vitro*, either by the “base-exchange” reaction (Aarhus et al., 1995) or from cADPRP (Moreschi et al., 2006). Both reactions prefer an acidic pH and require the presence of nicotinic acid in the millimolar range. Without nicotinic acid or at neutral pH, CD38 can hydrolyze NADP and cADPRP into ADPRP (Aarhus et al., 1995; Moreschi et al., 2006). On the other side, CD38 can also function as an NAADP degrading enzyme (Graeff et al., 2006; Schmid et al., 2011).

Therefore, the role of CD38 in NAADP production (or NAADP metabolism) was first investigated. In collaboration with Prof. Hans-Willi Mittrücker from the University Medical Center Hamburg-Eppendorf, CD4⁺ T cells isolated from spleens and lymph nodes of WT and *Cd38*^{-/-} mice were used. The results are summarized in Fig. 4.

Results

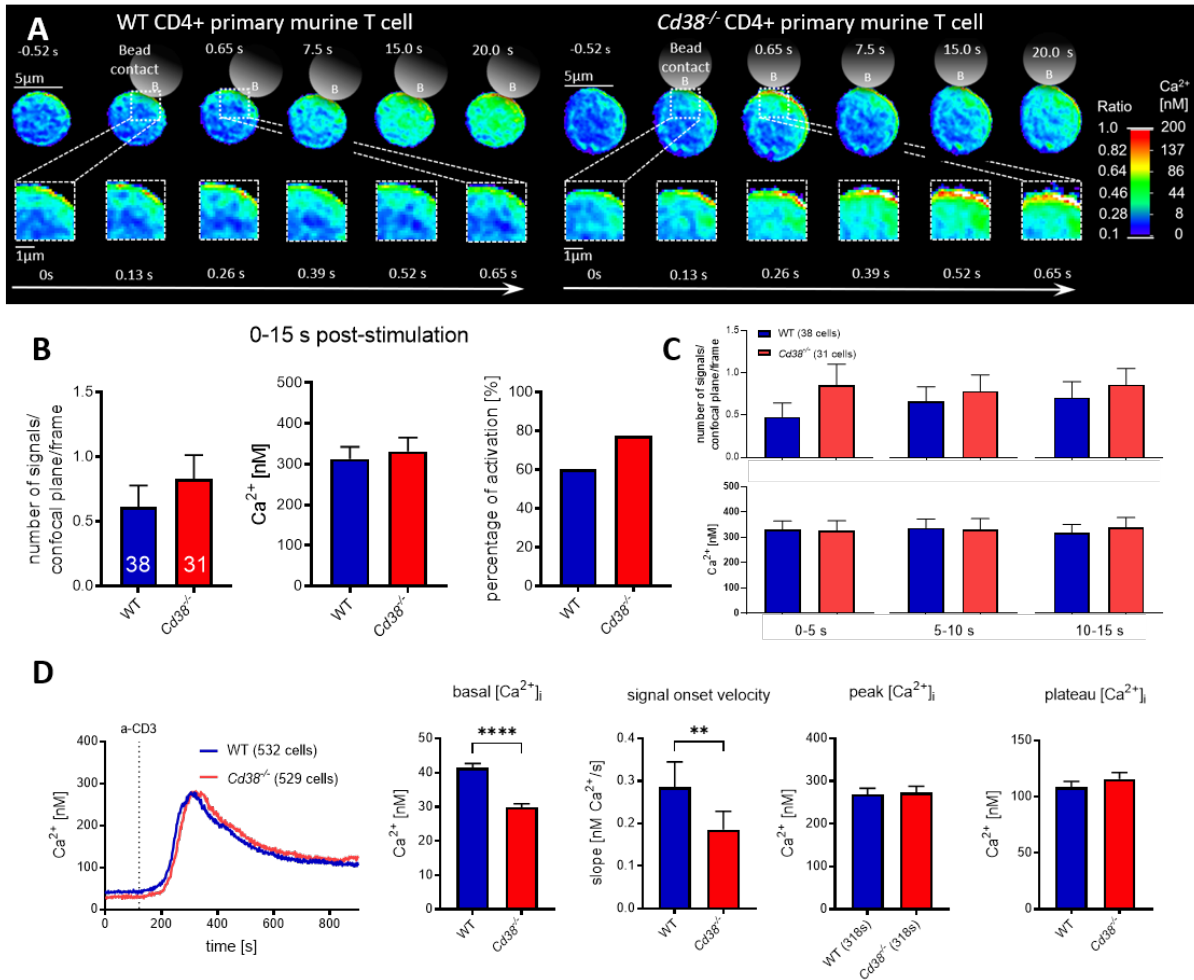


Fig. 4: Lack of CD38 has no effect on Ca²⁺ microdomain formation or global Ca²⁺ signals in response to TCR stimulation.

CD4⁺ primary T cells were extracted from lymphoid tissues of WT or Cd38^{-/-} mice and loaded with 10 μM Fluo4-AM and 20 μM FuraRed-AM for Ca²⁺ microdomain imaging (A-C) or 4 μM Fura2-AM for global Ca²⁺ imaging (D). (A) High resolution Ca²⁺ images of a WT T cell (left) and a Cd38^{-/-} T cell (right) after stimulation with anti-CD3 and anti-CD28 coated beads (indicated schematically). The heatmap suggests emission ratios between Fluo4 and FuraRed ranging from 0.1 to 1.0; ratio data was then transformed to 0 to 200 nM intracellular Ca²⁺ concentration using external calibration. Scale bars are 5 μm for complete cells and 1 μm for the magnified region at the bead contact site. (B) Analysis of Ca²⁺ microdomains in whole cells within the first 15 s following bead stimulation, revealing the number of signals per confocal plane per frame, average Ca²⁺ concentration in responding cells, and percentage of activated cells. Data are shown as mean ± SEM and were collected from at least three independent experiments; cell numbers are indicated in the column (WT n=38 cells; Cd38^{-/-} n=31 cells); a non-parametric Mann-Whitney U test revealed no significant differences. (C) Analysis of the number of signals per confocal plane per frame and average Ca²⁺ concentration in responding cells from (B) after bead stimulation in a shorter period (5 s as indicated). No significant difference was observed in statistical analysis as in (B). (D) Analysis of global Ca²⁺ signals showing mean Ca²⁺ traces after 10 μg/mL anti-CD3 addition, basal Ca²⁺ concentration, the slope of Ca²⁺ concentration increase within 100 s after stimulation, and peak (as indicated) and plateau (at 816s) amplitudes. The data are mean ± SEM from at least three different

Results

experiments; cell numbers are shown in legends (WT n=532 cells and *Cd38*^{-/-} n=529 cells). Non-parametric Mann-Whiney U test was used for statistical analysis: ** p<0.005, **** p<0.0001. This dataset is modified from Fig. 1 in (Gu et al., 2021).

In the characteristic Ca²⁺ images in Fig. 4A, the local Ca²⁺ increase below the plasma membrane near the stimulating site can be seen in both T cells from 0.13 s after stimulation. Quantitative analysis of the formation of Ca²⁺ microdomains in the whole cells indicated that the absence of CD38 did not show any significant effect on the Ca²⁺ microdomain formation within 15 s after stimulation: the average number of Ca²⁺ microdomains was 0.62 signals per frame in WT T cells and 0.83 signals per frame in *Cd38*^{-/-} T cells, as shown in Table 6. The Ca²⁺ microdomains occurred in 60% of WT T cells with an average concentration of 313 ± 30 nM (mean ± SEM), and more CD38-deficient cells (77%) showed the Ca²⁺ microdomains with an amplitude of 331 ± 34 nM (mean ± SEM) (Fig. 4B). Furthermore, there was no significant difference in shorter periods, as shown in Fig. 4C and Table 6.

Table 6: Number of Ca²⁺ microdomains per frame (mean ± SEM) in WT versus CD38-deficient T cells shown in Fig. 4 B and C.

	0 – 15 s		
WT (n=38)	0.62 ± 0.16		
<i>Cd38</i> ^{-/-} (n=31)	0.83 ± 0.18		
	0 – 5 s	5 – 10 s	10 – 15 s
WT (n=38)	0.48 ± 0.16	0.66 ± 0.18	0.71 ± 0.19
<i>Cd38</i> ^{-/-} (n=31)	0.85 ± 0.25	0.79 ± 0.19	0.84 ± 0.19

Moreover, imaging data of global Ca²⁺ signals (Fig. 4D) confirmed that the absence of CD38 did not affect NAADP-induced Ca²⁺ signaling upon T cell activation. Although a decreased slope was observed in the absence of CD38 [0.19 ± 0.04 nM/s (mean ± SEM)] compared with WT T cells [0.28 ± 0.06 nM/s (mean ± SEM)], the profile of global Ca²⁺ signaling, e.g., peak amplitude [269 ± 14 nM (mean ± SEM) in WT cells versus 273 ± 15 nM (mean ± SEM) in *Cd38*^{-/-} cells] and plateau amplitude [108 ± 5 nM (mean ± SEM) in WT cells versus 116 ± 6 nM (mean ± SEM) in *Cd38*^{-/-} cells], was almost identical.

Therefore, CD38 does not appear to function as either an NAADP synthesizing enzyme or its major degrading enzyme in intact T cells upon TCR stimulation.

4.2. Role of NADPH oxidases in Ca²⁺ signaling upon T cell activation

A former colleague in the Department of Biochemistry and Molecular Cell Biology, Hannes Roggenkamp, demonstrated that NOX5, as a standard model of the NOX/DUOX family, can also oxidize NAADPH, and the optimal pH for oxidation of NAADPH is between 7 and 8 (Gu et al., 2021). NOX5 is known to be absent in rodents (Kawahara et al., 2007). Among other isozymes, NOX1, NOX2, DUOX1, and DUOX2 are detectable in murine and rat T cells by qPCR (Gu et al., 2021). In this study, T cells extracted from different mouse models and CRISPR/Cas designed rat T cells were used.

4.2.1. Role of NOX1 in Ca²⁺ signaling upon TCR/CD3 ligation

NOX1 produces superoxide and requires two cytosolic subunits (Geiszt et al., 2003). The *Nox1* gene is located on the X chromosome. A NOX1 deficient mouse model (*Nox1*^{Y/-}) was established and described in (Gavazzi et al., 2006).

In collaboration with Prof. Katrin Schröder from Goethe University Frankfurt, CD4⁺ primary murine T cells were isolated from lymphoid tissues of *Nox1*^{Y/-} mice in comparison to male WT littermates and the Ca²⁺ response was analyzed (Fig. 5).

Results

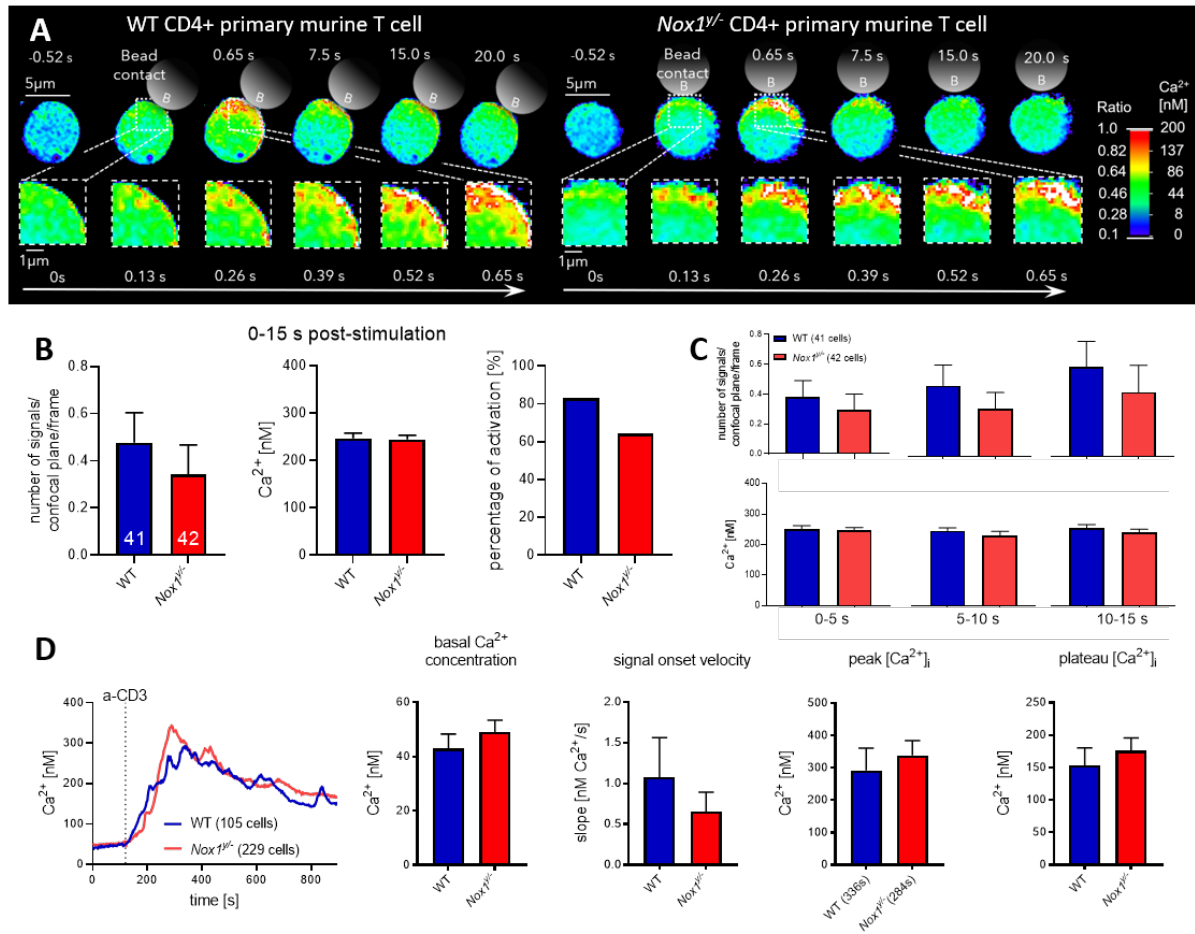


Fig. 5: Absence of NOX1 affects neither Ca²⁺ microdomain formation nor the global Ca²⁺ signals upon TCR stimulation.

CD4⁺ primary T cells were freshly isolated from lymphoid tissues of WT or NOX1-deficient mice and were loaded with Fluo4-AM (10 μM) and FuraRed-AM (20 μM) for Ca²⁺ microdomain imaging (A-C) or Fura2-AM (4 μM) for global Ca²⁺ imaging (D). (A) High resolution Ca²⁺ images of a WT T cell (left) and a *Nox1*^{-/-} T cell (right) after stimulation with anti-CD3 and anti-CD28 coated beads (indicated schematically). The heatmap suggests emission ratios between Fluo4 and FuraRed ranging from 0.1 to 1.0; ratio data were then converted using external calibration corresponding to 0 to 200 nM intracellular Ca²⁺ concentration. 5 μm scale bar is shown for whole cells and 1 μm for the magnified region at the bead contact site. (B) Analysis of Ca²⁺ microdomains in the whole cells across the first 15 s after bead stimulation shown as the number of signals per confocal plane per frame, average Ca²⁺ concentration in the responding cells, and the percentage of activation. Data are presented as mean ± SEM and were collected from at least three independent experiments; cell number indicated in the column (WT n=41 cells; *Nox1*^{-/-} n=42 cells); no significant difference was indicated using a non-parametric Mann-Whitney U test. (C) Analysis of the number of signals per confocal plane per frame and average Ca²⁺ concentration from (B) in a shorter period (5 s as indicated) after bead stimulation. Statistical analysis as in (B), no significant difference was indicated. (D) Analysis of global Ca²⁺ measurements showing mean Ca²⁺ traces upon 10 μg/mL anti-CD3 addition, basal Ca²⁺ concentration, the slope of Ca²⁺ concentration increase within 100 s after stimulation and peak (as indicated) and plateau (at 816s) amplitudes. Data are mean ± SEM and were collected from at least three independent experiments; cell

Results

number is shown in legends (WT n=105 cells; *Nox1*^{−/−} n=229 cells). No significant difference was shown using a non-parametric Mann-Whiney U test. The global imaging data were published in (Gu et al., 2021) in Fig. 3.

In the characteristic Ca²⁺ images of the *Nox1*^{−/−} T cell, strong Ca²⁺ microdomain formation was observed near the plasma membrane from 0.13 s after bead stimulation, like the WT T cell (Fig. 5A). In the analysis of whole cells in the first 15 s post-stimulation (Fig. 5B), the NOX1-deficient T cells showed no significant difference in the number of signals per frame compared to the WT control (0.48 signals per frame in WT T cells versus 0.34 signals per frame in *Nox1*^{−/−} T cells, as shown in Table 7). The Ca²⁺ microdomains occurred in 83% WT T cells with an average Ca²⁺ concentration of 247 ± 11 nM (mean ± SEM) and in 64% *Nox1*^{−/−} T cells with an amplitude of 245 ± 9 nM (mean ± SEM). Similar results in the number of signals per frame could be observed in every 5 s period, as shown in Fig. 5C and Table 7.

Table 7: Number of Ca²⁺ microdomains per frame (mean ± SEM) in WT versus NOX1-deficient T cells shown in Fig. 5 B and C.

	0 – 15 s		
WT (n=41)	0.48 ± 0.13		
<i>Nox1</i> ^{−/−} (n=42)	0.34 ± 0.12		
	0 – 5 s	5 – 10 s	10 – 15 s
WT (n=41)	0.38 ± 0.11	0.47 ± 0.14	0.59 ± 0.17
<i>Nox1</i> ^{−/−} (n=42)	0.30 ± 0.11	0.32 ± 0.11	0.42 ± 0.17

Moreover, the deficiency of NOX1 did not affect the subsequent global Ca²⁺ signals (Fig. 5D): the average peak Ca²⁺ concentration was 292 ± 69 nM (mean ± SEM) in WT cells and 339 ± 45 nM (mean ± SEM) in *Nox1*^{−/−} T cells. The amplitudes in the plateau phase were similar as well, 153 ± 27 nM (mean ± SEM) in WT cells and 176 ± 20 nM (mean ± SEM) in knockout T cells.

Therefore, NOX1 does not seem to be involved in NAADP synthesis upon TCR stimulation.

4.2.2. Role of NOX2 in Ca²⁺ signaling upon TCR/CD3 ligation

Next, the role of NOX2 was analyzed. NOX1 and NOX2 have 60% sequence similarity at the

Results

protein level and both require cytosolic subunits and produce superoxide. Moreover, the location of the *Nox2* gene (also known as the *Cybb* gene) is also on the X chromosome (reviewed in Bedard and Krause, 2007).

From our collaborator Prof. Katrin Schröder from Goethe University in Frankfurt, lymphoid tissues of NOX2-deficient mice were shipped to Hamburg on wet ice. Ca^{2+} signaling after TCR stimulation was analyzed in isolated CD4⁺ T cells (Fig. 6).

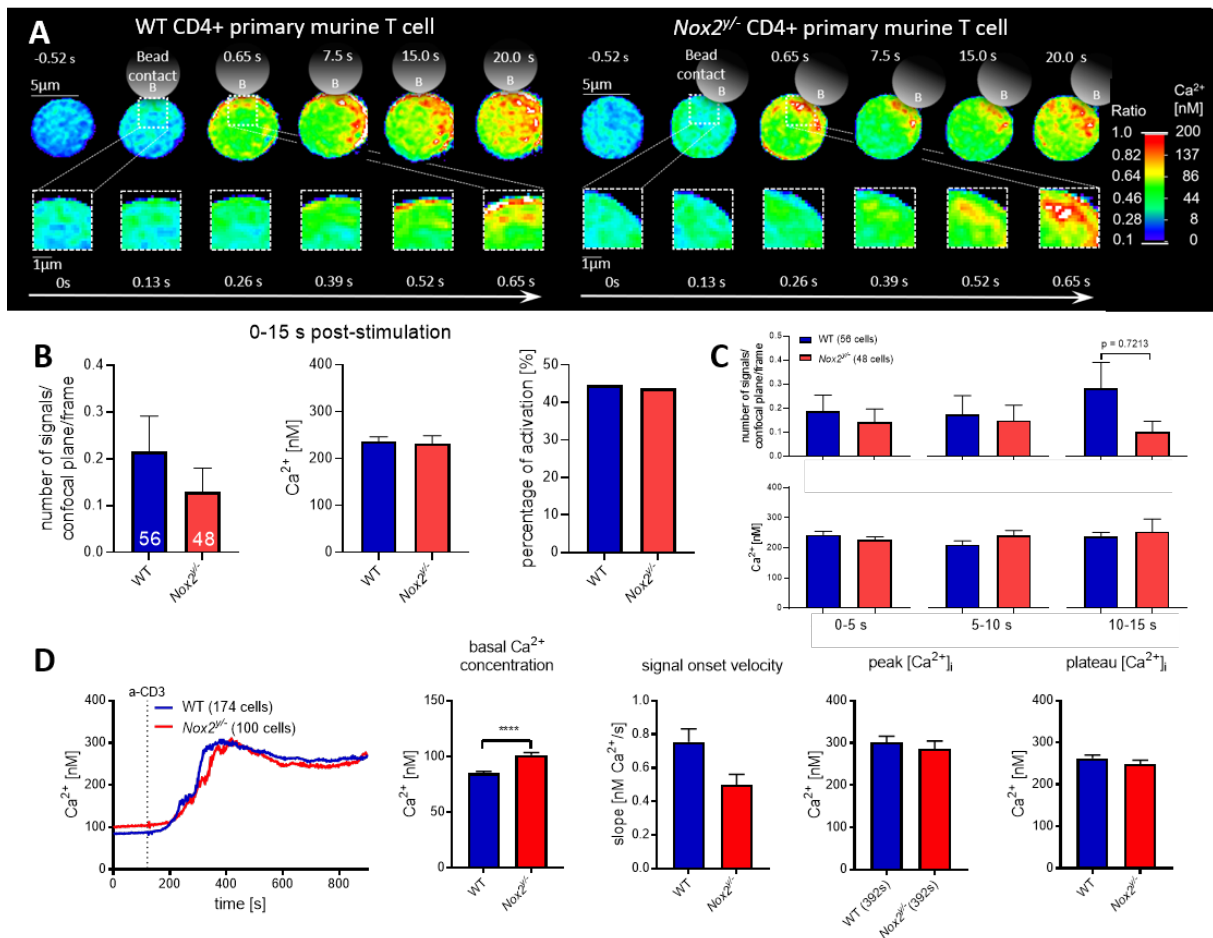


Fig. 6: Lack of NOX2 affects neither the Ca^{2+} microdomains nor the overall Ca^{2+} signals after TCR stimulation.

Freshly isolated CD4⁺ primary T cells from WT or NOX2-deficient mice's lymphoid tissues were loaded with 10 μM Fluo4-AM and 20 μM FuraRed-AM for Ca^{2+} microdomain imaging (A-C) or 4 μM Fura2-AM for global Ca^{2+} imaging (D). (A) High resolution Ca^{2+} images of a WT T cell (left) and a NOX2-deficient T cell (right) stimulated with anti-CD3 and anti-CD28 coated beads (indicated schematically). The heatmap shows emission ratios between Fluo4 and FuraRed ranging from 0.1 to 1.0; ratio data was then translated to 0 to 200 nM intracellular Ca^{2+} concentration using external calibration. 5 μm scale bar is shown for complete cells and 1 μm scale bar for the magnified region near the stimulating bead. (B) Ca^{2+} microdomains in whole cells within the first 15 seconds after bead stimulation, indicating the

Results

number of signals per confocal plane per frame, average Ca^{2+} concentration in the responding cells, and percentage of activated cells. Data are reported as mean \pm SEM and were obtained from at least three different experiments; cell number is indicated in the column (WT n=56 cells; *Nox2*^{-/-} n=48 cells); a non-parametric Mann-Whitney U test revealed no significant differences. (C) Analysis of the number of signals per confocal plane per frame and average Ca^{2+} concentration from (B) after bead stimulation over a shorter period (as indicated). There is no significant change after statistical analysis, as shown in (B). (D) Mean Ca^{2+} traces following 10 $\mu\text{g}/\text{mL}$ anti-CD3 addition, basal Ca^{2+} concentration, the slope of Ca^{2+} concentration increase within 100 s of stimulation, and peak (as indicated) and plateau (at 816s) amplitudes. The data are mean \pm SEM from at least three different experiments; cell numbers are as stated in legend (WT n=174 cells; *Nox2*^{-/-} n=100 cells). A non-parametric Mann-Whitney U test was used for the statistical analysis: **** $p < 0.0001$. The global imaging dataset was published in (Gu et al., 2021) in Fig. 3.

As shown in Fig. 6A, similar to the results of NOX1, a strong and fast Ca^{2+} increase was observed within 0.65 s in the *Nox2*^{-/-} T cell at the bead contact site. In whole cell analysis of Ca^{2+} microdomains within the first 15 s (Fig. 6B), 0.22 signals per frame were observed in WT cells and 0.13 signals per frame were observed in *Nox2*^{-/-} T cells, as shown in Table 8. Further, a similar number of Ca^{2+} microdomains was observed in the first 10 s. Except from 10 to 15 s, there were 0.28 signals per frame in WT T cells and 0.10 signals per frame in *Nox2*^{-/-} T cells (Table 8) with a high p value (0.7213), as shown in Fig. 6C.

Table 8: Number of Ca^{2+} microdomains per frame (mean \pm SEM) in WT versus NOX2-deficient T cells shown in Fig. 6 B and C.

	0 – 15 s		
WT (n=56)	0.22 \pm 0.076		
<i>Nox2</i> ^{-/-} (n=48)	0.13 \pm 0.050		
	0 – 5 s	5 – 10 s	10 – 15 s
WT (n=56)	0.19 \pm 0.066	0.18 \pm 0.078	0.28 \pm 0.11
<i>Nox2</i> ^{-/-} (n=48)	0.14 \pm 0.057	0.15 \pm 0.064	0.10 \pm 0.045

Furthermore, absence of NOX2 did not influence the subsequent global Ca^{2+} signals upon TCR stimulation (Fig. 6D). Peak amplitudes were 302 \pm 14 nM (mean \pm SEM) in WT cells and 286 \pm 19 nM (mean \pm SEM) in *Nox2*^{-/-} T cells and plateau amplitudes were 263 \pm 7 nM (mean \pm SEM) in WT cells and 249 \pm 9 nM (mean \pm SEM) in *Nox2*^{-/-} cells.

Hence, NOX2 is unlikely to be the enzyme involved in NAADP synthesis in T cells.

4.2.3. The role of DUOX isozymes

DUOX1 and DUOX2 are unique members in this family: i) they require maturation factors (DUOXA1 and DUOXA2, respectively) instead of cytosolic subunits; ii) their activation is dependent on the binding of intracellular Ca^{2+} on EF-hand motifs (like NOX5); iii) they contain an extracellular peroxidase-homologs domain and produce H_2O_2 upon activation (H_2O_2 production like NOX4) (reviewed in Bedard and Krause, 2007). They both share 50% identity at the protein level with NOX2, and DUOX1 and DUOX2 share 83% sequence similarity (De Deken et al., 2000). In the next step, the role of these two DUOX isozymes was further investigated.

4.2.3.1. DUOX1 and DUOX2 oxidize NAADPH to NAADP in cell-free system

In collaboration with Prof. Karl-Heinz Krause from the University of Geneva, membranes isolated from human DUOX1-DUOXA1 (hDUOX1/A1) and DUOX2-DUOXA2 (hDUOX2/A2) over-expressing HEK293 cells were shipped in dry ice. Their enzyme activity was analyzed on RP-HPLC (Fig. 7).

Results

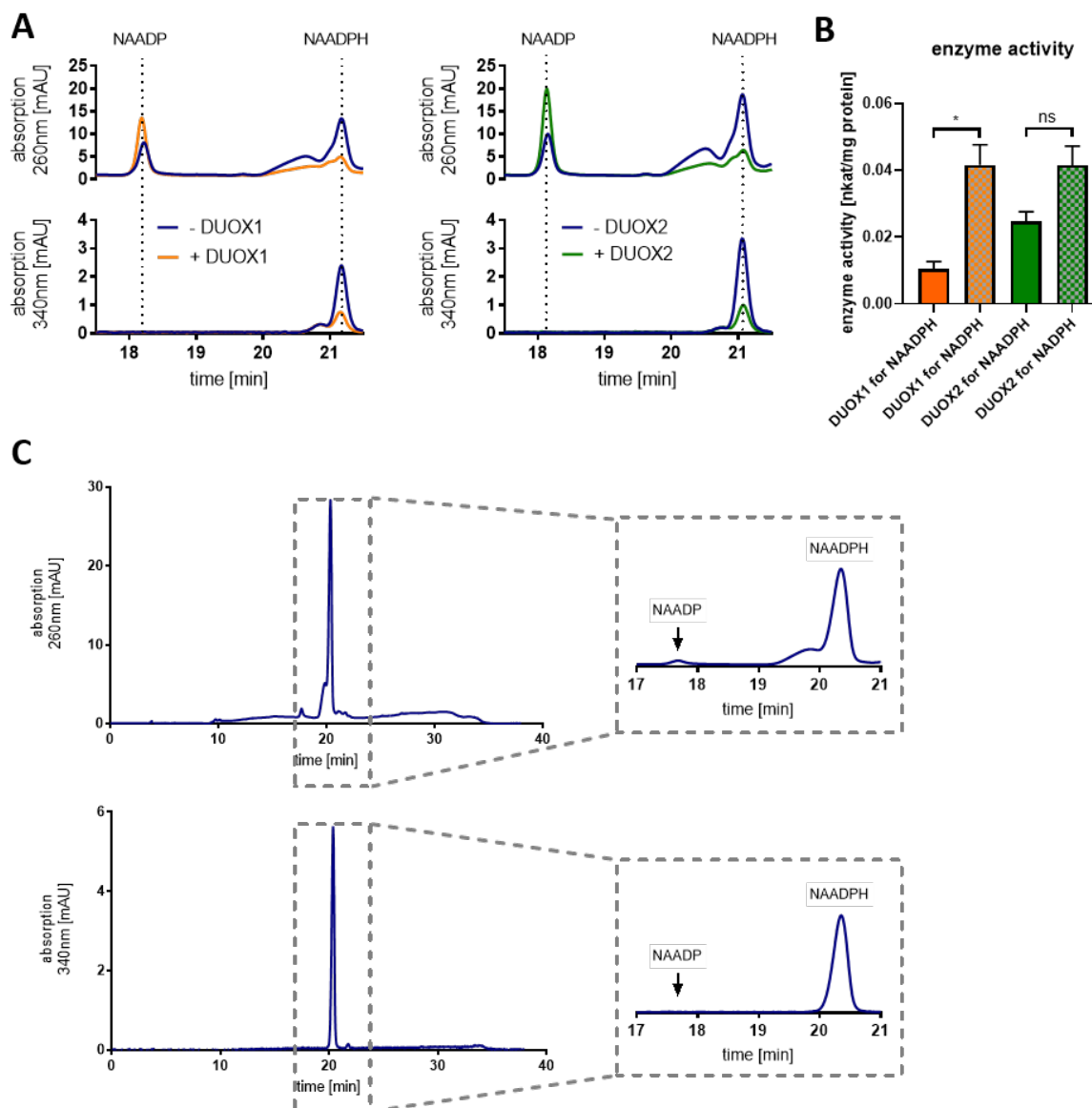


Fig. 7: Synthesis of NAADP from its reduced form NAADPH *in vitro* by DUOX1 and DUOX2.

(A) Synthesis of NAADP from NAADPH (produced by chemical reduction see section 3.11.) in the presence or absence of DUOX1- or DUOX2 containing HEK cell membranes (0.3 mg protein/mL) in the buffer with 50 μ M NAADPH or NADPH, 5.5 μ M phosphatidic acid, 1.4 mM CaCl₂, 1 mM MgCl₂, 450 μ M NTA, 450 μ M EDTA, 10 μ M FAD and 50 mM HEPES at pH 7.1. As described in section 3.12., samples were analyzed by reversed-phase (RP)-HPLC. A characteristic HPLC chromatogram from five tests is displayed. (B) Comparison of the enzyme activity of DUOX1 and DUOX2 using NADPH and NAADP as substrates. Enzyme activity was calculated by the increase in NAADP or NADP after incubation with and without enzyme-containing membranes. Data are mean \pm SEM, n=5; Non-parametric Mann-Whitney U test was used: * p<0.05. (C) Purity of NAADPH. The chemical reduction was used to create NAADPH, then purified using semi-preparative HPLC. The image shows a typical HPLC chromatogram from at least three different tests. The purity of the product was determined using RP-HPLC. NAADPH was identified at wavelengths of 260 nm (top) and 340 nm (bottom). The latter wavelength was used to detect the reduced form of nucleotides. This dataset was published in (Gu et al., 2021) in Fig. 2 and Fig. S1.

As shown in Fig. 7A, both DUOX1/A1 and DUOX2/A2 complexes oxidize NAADPH in the cell-free system at neutral pH and 37°C. The purity of chemically reduced NAADPH is shown in Fig. 7C, a small amount of NAADP is present (chemical production of NAADPH as described in section 3.11.). Therefore, the enzyme activity shown in Fig. 7B was calculated from the difference of NAADP (and NADP as positive control) after the incubation with and without enzyme-containing membranes. DUOX2 complex did not show significant specificity consuming NAADPH and NADPH [0.025 ± 0.0029 nkat/mg protein (mean \pm SEM) for NAADPH versus 0.041 ± 0.0058 nkat/mg protein (mean \pm SEM) for NADPH], whereas DUOX1 complex significantly preferred NADPH as substrate [0.010 ± 0.0022 nkat/mg protein (mean \pm SEM) for NAADPH versus 0.042 ± 0.0060 nkat/mg protein (mean \pm SEM) for NADPH].

It is known that EC_{50} of Ca^{2+} for DUOX1/A1 complex is $0.38 \mu\text{M}$ (Wu et al., 2021). From other publications we know that smaller and lower Ca^{2+} microdomains are present close to the plasma membrane in the absence of TCR stimulation, where the local Ca^{2+} concentration is supposed to be approximately 230 nM (Brock et al., 2022; Diercks et al., 2018). As for NOX1 and NOX2, any role of the DUOX isozymes in Ca^{2+} signaling was further investigated in intact T cells.

4.2.3.2. DUOX1 and DUOX2 affect Ca^{2+} microdomain formation differently

Since DUOX1 and DUOX2 single knockout mouse models were not available, CRISPR/Cas designed CD4⁺ rat effector T cells from Prof. Alexander Flügel's group in the University Medical Center Göttingen were used for further analysis of Ca^{2+} response to distinguish the DUOX isozymes (Fig. 8). The expression and localization of DUOX1 and DUOX2 were validated by STED super-resolution microscope (Gu et al., 2021).

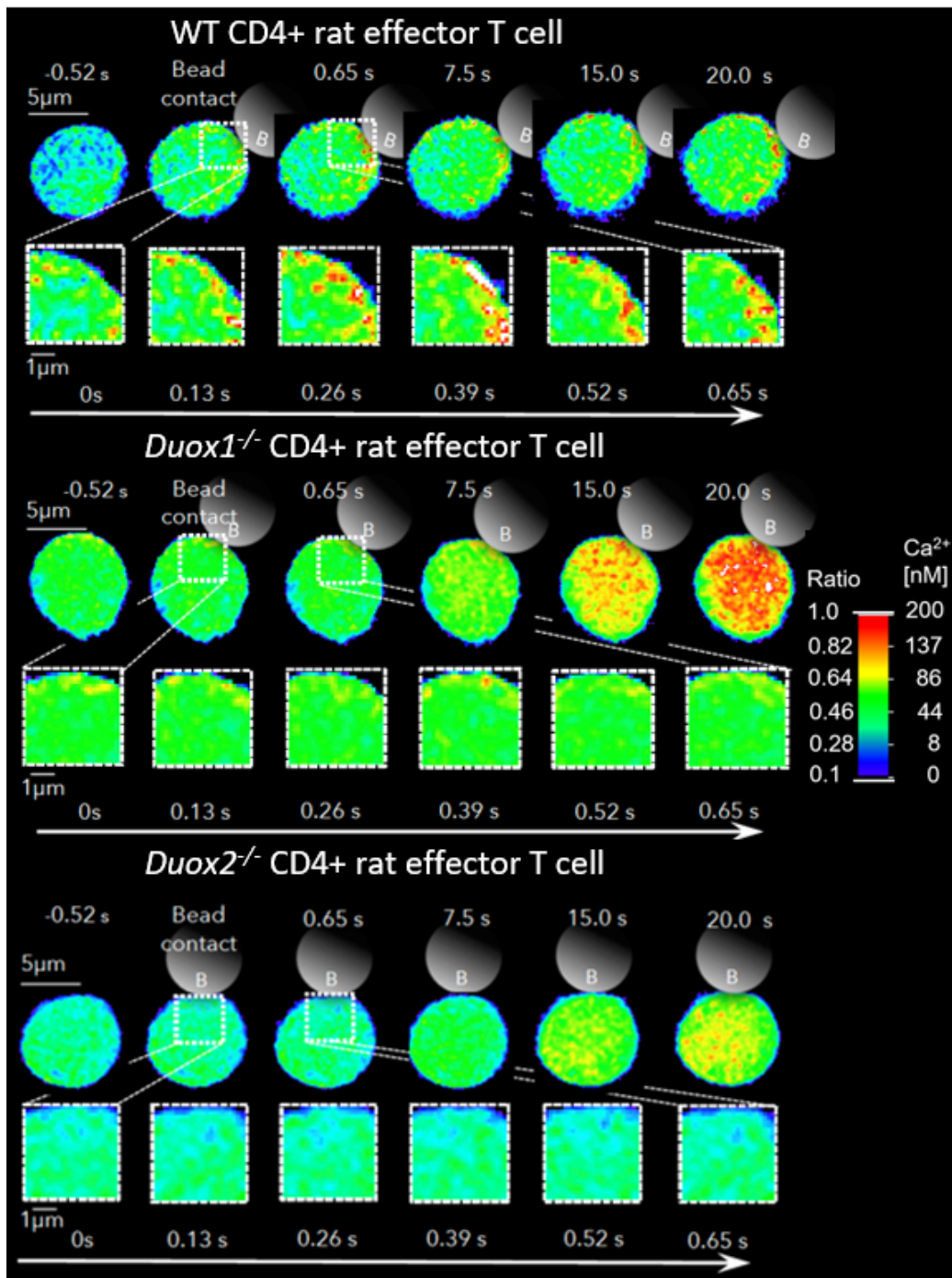


Fig. 8: Single knockouts of DUOX1 and DUOX2 in CD4⁺ effector rat T cells reduce Ca²⁺ microdomain formation in the first 15 s.

CD4⁺ rat effector T cells created using CRISPR/Cas were loaded with 10 μ M Fluo4-AM and 20 μ M FuraRed-AM for Ca²⁺ microdomain imaging. Ca²⁺ images of a WT T cell (upper), a *Duox1*^{-/-} T cell (middle), and a *Duox2*^{-/-} T cell (lower) following stimulation with anti-CD3 and anti-CD28 coated beads (indicated schematically). The heatmap shows emission ratios between Fluo4 and FuraRed ranging from 0.1 to 1.0; ratio data was then translated to 0 to 200 nM intracellular Ca²⁺ concentration using external calibration. 5 μ m scale bar is shown for whole cells and 1 μ m scale bar for the enlarged region at the bead contact site.

Results

In Fig. 8, increased local Ca^{2+} concentration close to the plasma membrane was observed in the WT T cell already within 0.65 s; in this period, less Ca^{2+} microdomains occurred in *Duox1*^{-/-} T cell and almost no Ca^{2+} microdomains were seen in *Duox2*^{-/-} T cell. In whole cell analysis within first 15 s, there were 0.89 signals per frame in the WT T cells, 0.79 signals per frame in *Duox1*^{-/-} T cells and 0.70 signals per frame in *Duox2*^{-/-} T cells. Then this dataset was further analyzed in 5 s periods (Table 9).

Table 9: Number of Ca^{2+} microdomains per frame (mean \pm SEM) in WT versus DUOX1- or DUOX2-single knockout T cells in the first 15 s and in 5 s periods.

	0 – 15 s		
WT (n=23)	0.89 \pm 0.29		
<i>Duox1</i> ^{-/-} (n=23)	0.79 \pm 0.26		
<i>Duox2</i> ^{-/-} (n=25)	0.70 \pm 0.26		
	0 – 5 s	5 – 10 s	10 – 15 s
WT (n=23)	0.95 \pm 0.36	1.04 \pm 0.39	1.33 \pm 0.45
<i>Duox1</i> ^{-/-} (n=23)	0.42 \pm 0.13	0.60 \pm 0.20	1.37 \pm 0.52
<i>Duox2</i> ^{-/-} (n=25)	0.27 \pm 0.11	0.60 \pm 0.25	1.17 \pm 0.45

As shown in Table 9, the differences between WT and DUOX1-and DUOX2-deficient T cells are not significant using a non-parametric Kruskal-Wallis test and Dunn's correction for multiple testing. However, in the first 5 s, there were only 0.27 signals per frame in the absence of DUOX2. Therefore, a finer analysis was performed and compared with other datasets as shown below in Fig. 9.

A coworker in the Department of Biochemistry and Molecular Cell Biology, Aileen Krüger, analyzed the initial Ca^{2+} signaling in the CD4⁺ T cells derived from *DuoxA1*^{-/-}/*A2*^{-/-} mice, the functional double knockout mouse model of DUOX1 and DUOX2 as reported in (Grasberger et al., 2013), and observed a strong phenotype in Ca^{2+} microdomain formation upon TCR stimulation (Gu et al., 2021). This dataset is shown in Fig. 9 A and B as a comparison.

It is also known that NAADP requires its binding protein HN1L/JPT2 to evoke initial Ca^{2+} release events (Roggenkamp et al., 2021). Ca^{2+} microdomain formation at the bead contact site in *Hn1l*^{-/-} CD4⁺ rat effector T cells is shown in Fig. 9C as a comparison.

Results

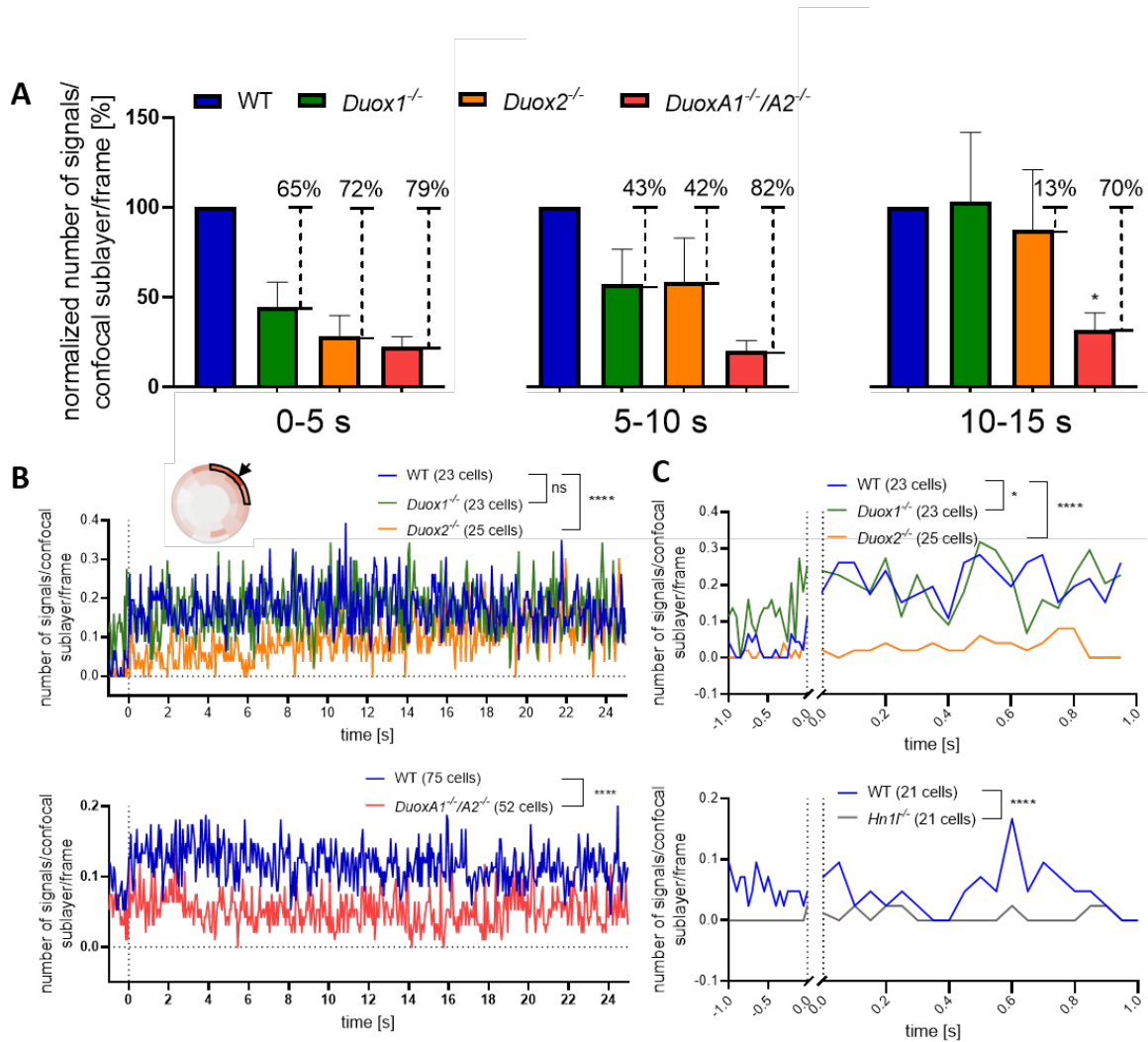


Fig. 9: DUOX2 is essential for initial NAADP formation

(A) The normalized number of signals per confocal plane per frame in DUOX1 and DUOX2 single knockout T cells from Table 9 (no significant difference as revealed by non-parametric Kruskal-Wallis test and Dunn's correction for multiple testing) as well as in functional double knockout of DUOX1 and DUOX2 T cells (Gu et al., 2021) in 5 s periods (as indicated) after bead stimulation. The data in the functional double knockout T cells were performed by Aileen Krüger (WT: n=75 cells; *DuoxA1*^{-/-}/*A2*^{-/-}: n=52 cells). Statistical analysis was carried out using a non-parametric Mann-Whitney U test, * p<0.05). The percentage above column represents the reduction of Ca²⁺ microdomains compared to WT control, respectively. (B) Kinetics of the number of Ca²⁺ microdomains in the subcellular layer underneath the plasma membrane (as shown in the inset) near the stimulating bead (as shown by the arrow) 1 s before and during the first 25 s after TCR stimulation. The data are the averages of at least three different experiments. For multiple comparisons testing, the non-parametric and paired Friedman test and Dunn's correction were used for WT against *Duox1*^{-/-} or *Duox2*^{-/-} (**** p<0.0001). For the dataset of WT versus *DuoxA1*^{-/-}/*A2*^{-/-} T cells, statistical analysis was carried out using the non-parametric and paired Wilcoxon test (**** p<0.0001). (C) Magnification of (B, upper) 1 s before and after the bead stimulation (upper) and the kinetics of the number of Ca²⁺ microdomains in the sublayer indicated in (B) in WT versus *Hn1f*^{-/-} rat T cells (lower, cell number as shown in the legends: WT n=21 cells; *Hn1f*^{-/-} n=21 cells). The data

Results

are the averages of at least three different experiments. Statistical analysis for WT against *Duox1*^{-/-} or *Duox2*^{-/-} (* p<0.05; **** p<0.0001) is the same as in (B); Wilcoxon matched-pairs signed rank test was used for WT against *Hn1*^{-/-} (**** p<0.0001). The dataset of DUOX1 and DUOX2 single knockouts was published in (Gu et al., 2021) in Fig. 5; (C) of HN1L-deficient T cells was published in (Roggenkamp et al., 2021) in Fig. 5.

The decrease of Ca²⁺ microdomain formation compared with WT control in 5 s periods is shown in Fig. 9A, including the data in *DuoxA1*^{-/-}/*A2*^{-/-} CD4⁺ primary murine T cells as a comparison. In the first 5 s, the decrease of the signals per frame in *Duox2*^{-/-} T cells was similar to that observed in *DuoxA1*^{-/-}/*A2*^{-/-} CD4⁺ murine T cells, above 70%, which indicates that DUOX2 seems to be the major enzyme responsible for NAADP formation in this period. In the following 5 s, reduced Ca²⁺ microdomain formation were recovered in both *Duox1*^{-/-} and *Duox2*^{-/-} T cells, which accounted approximately to half of the decrease in *DuoxA1*^{-/-}/*A2*^{-/-} T cells. This indicates that in the absence of single isozyme they may start to compensate each other. From 10 to 15 s, there was still 70% decrease in *DuoxA1*^{-/-}/*A2*^{-/-} T cells, whereas no and only 13% reduction was observed in *Duox1*^{-/-} and *Duox2*^{-/-} T cells, respectively.

Furthermore, in Fig. 9B, the kinetics of Ca²⁺ microdomains in the sublayer underneath the plasma membrane at stimulating site, significantly diminished formation of Ca²⁺ microdomains were seen in the *Duox2*^{-/-} T cells from the very beginning after bead stimulation up to around 20 s, whereas in *DuoxA1*^{-/-}/*A2*^{-/-} T cells a strong phenotype was shown throughout the first 25 s (Gu et al., 2021). A significant effect was observed in *Duox2*^{-/-} T cells already in the first second after bead stimulation (Fig. 9C upper), and a similar decrease was shown in *Hn1*^{-/-} CD4⁺ rat effector T cells (Fig. 9C lower), i.e., in the absence of NAADP binding protein (Roggenkamp et al., 2021). This further confirmed that DUOX2 plays a major role in NAADP synthesis in the first seconds of T cell activation, and DUOX1 may partially and slowly compensate DUOX2 to produce NAADP and therefore recover the formation of Ca²⁺ microdomains in the single knockout T cells.

4.2.3.3. DUOX1 and DUOX2 affect global Ca²⁺ signaling differently

To further confirm the role of DUOX1 and DUOX2 in NAADP formation, global Ca²⁺ signals in the rat CD4⁺ effector T cells were measured. A specific NAADP antagonist BZ194 was used

Results

as control (Fig. 10). BZ194 is a specific NAADP antagonist and does not influence InsP_3 - and cADPR-induced Ca^{2+} signals (Dammermann et al., 2009). It has been used in many studies to investigate the role of NAADP (not only but as examples in Cordiglieri et al., 2010; Diercks et al., 2018; Nawrocki et al., 2021; Nebel et al., 2013; Zhang et al., 2018).

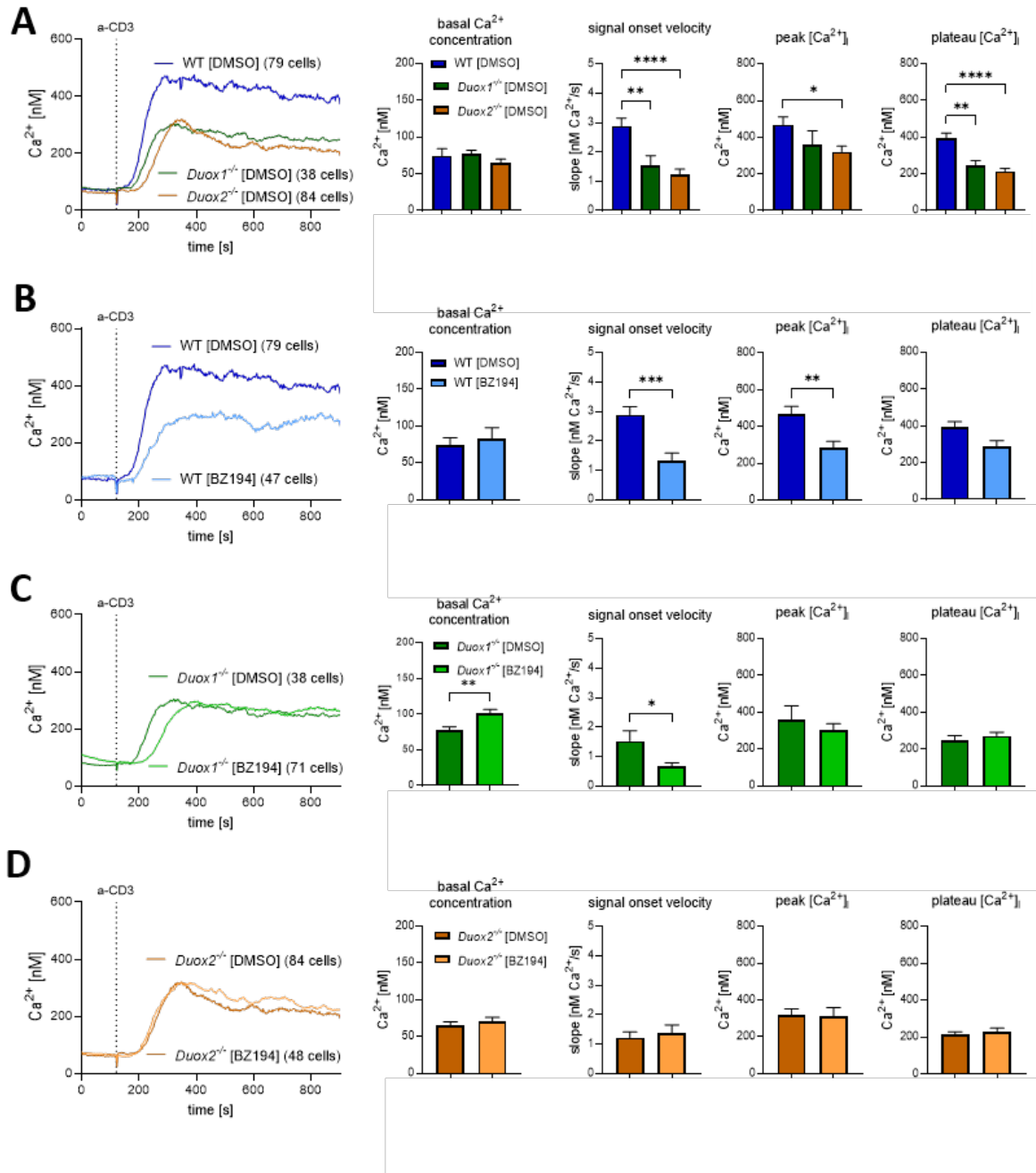


Fig. 10: Single knockouts of DUOX1 and DUOX2 in CD4⁺ effector rat T cells influence global Ca^{2+} signaling differently.

WT versus *Duox1*^{-/-} or *Duox2*^{-/-} T cells loaded with 4 μM Fura2-AM in terms of global Ca^{2+} signaling. (A) From left to right: kinetics of mean Ca^{2+} traces after 1 $\mu\text{g}/\text{mL}$ anti-CD3 stimulation, basal Ca^{2+} concentration, signal onset velocity (slope of Ca^{2+} concentration from 120 s to 300 s), peak Ca^{2+}

Results

concentration (WT in DMSO at 290 s; *Duox1*^{-/-} in DMSO at 332 s; *Duox2*^{-/-} in DMSO at 346 s), and plateau (at 816 s). The data are presented as means ± SEM, with cell numbers specified in the legend (WT in DMSO n=79 cells; *Duox1*^{-/-} in DMSO n=38 cells; *Duox2*^{-/-} in DMSO n=84 cells). A non-parametric Kruskal-Wallis test with Dunn's correction for multiple testing was used for the statistical analysis, *p<0.05, **p<0.005, ****p<0.0001. (B) WT T cells treated with DMSO [1% (v/v)] versus WT T cells treated with NAADP antagonist BZ194 (500 μM in DMSO) overnight. From left to right: kinetics of mean Ca²⁺ traces after anti-CD3 stimulation (1 μg/mL), basal Ca²⁺ concentration, signal onset velocity, peak Ca²⁺ concentration (WT in DMSO at 290 s; WT with BZ194 at 396 s), and plateau Ca²⁺ concentration (at 816 s). The data are shown as means ± SEM, with cell numbers indicated in the legend (WT in DMSO n=79 cells; WT in BZ194 n=47 cells). A non-parametric Mann-Whitney U test was used: **p<0.005, ***p<0.001. (C) DMSO-treated *Duox1*^{-/-} T cells versus BZ194-treated *Duox1*^{-/-} T cells overnight as in (B). The dynamics of mean Ca²⁺ traces after 1 μg/mL anti-CD3 addition, baseline Ca²⁺ concentration, signal onset velocity, peak (*Duox1*^{-/-} in DMSO at 332 s; *Duox1*^{-/-} with BZ194 at 394 s) Ca²⁺ concentrations, and plateau (at 816 s) Ca²⁺ concentrations are shown from left to right. The data are presented as means ± SEM, with cell numbers indicated in the legend (DMSO control n=38 cells; BZ194-treated *Duox1*^{-/-} n=71 cells). Statistical analysis was carried out as in (B); *p < 0.05, **p< 0.005. (D) DMSO-treated *Duox2*^{-/-} T cells versus BZ194-treated *Duox2*^{-/-} T cells, treated as in (B). From left to right: kinetics of mean Ca²⁺ traces after anti-CD3 addition (1 μg/mL), basal Ca²⁺ concentration, signal onset velocity, peak (at 346 s) and plateau (at 816 s) Ca²⁺ concentrations. The data are presented as means ± SEM, with cell numbers as indicated in the legend (*Duox2*^{-/-} in DMSO n=84 cells; BZ194-treated *Duox2*^{-/-} n=48 cells). No significant difference in statistical analysis as in (B). This dataset is modified from Fig. 6 in (Gu et al., 2021).

In Fig. 10A, both *Duox1*^{-/-} and *Duox2*^{-/-} T cells showed delayed Ca²⁺ signals as well as decreased peak and plateau amplitudes (details see Table 10), the effect at the peak phase is similar to that of NAADP antagonism as shown in Fig. 9B and Table 10. The phenotype observed in *Duox1*^{-/-} T cells was further diminished by BZ194 in the signal onset velocity. In Fig. 9C, the slope of the Ca²⁺ increase was 1.53 nM/s in DMSO-treated *Duox1*^{-/-} T cells and was only 0.66 nM/s in BZ194-treated *Duox1*^{-/-} T cells. In contrast, global Ca²⁺ signals in *Duox2*^{-/-} T cells were identical to that of NAADP antagonism. In Fig. 9D, the slope was 1.22 nM/s in *Duox2*^{-/-} T cells with DMSO and was 1.38 nM/s in *Duox2*^{-/-} T cells treated with BZ194. These data further indicate that DUOX2 plays a major role in NAADP formation upon T cell activation.

Results

Table 10: Parameters (mean \pm SEM) of global Ca²⁺ signals in WT versus DUOX1- or DUOX2-single knockout T cells shown in Fig. 10.

	signal onset velocity [nM/s]	peak amplitude [nM]	plateau amplitude [nM]
WT [DMSO] (n=79)	2.89 \pm 0.27	467 \pm 43	393 \pm 29
WT [BZ194] (n=47)	1.33 \pm 0.26	285 \pm 35	286 \pm 33
<i>Duox1</i> ^{-/-} [DMSO] (n=38)	1.53 \pm 0.34	361 \pm 75	249 \pm 25
<i>Duox1</i> ^{-/-} [BZ194] (n=71)	0.66 \pm 0.13	303 \pm 35	272 \pm 19
<i>Duox2</i> ^{-/-} [DMSO] (n=84)	1.22 \pm 0.19	321 \pm 31	214 \pm 16
<i>Duox2</i> ^{-/-} [BZ194] (n=48)	1.38 \pm 0.27	313 \pm 47	230 \pm 19

The reduced signal onset velocity by BZ194 in *Duox1*^{-/-} T cells may suggest that there might be another Ca²⁺ signaling pathway(s) involved. DUOX isozymes produce H₂O₂ as a byproduct and H₂O₂ is known as one of the signaling molecules (reviewed in Di Marzo et al., 2018). Low micromolar exogenous H₂O₂ was reported to be able to increase the cytosolic free Ca²⁺ concentration in endothelial cells (Avdonin et al., 2017). These led us to the second part of the results section to understand the role of the byproduct H₂O₂ in the early phase of T cell activation.

4.2.3.4. Role of H₂O₂, the byproduct of DUOX forming NAADP

The role of the byproduct H₂O₂ in the early phase of T cell activation was investigated in this section using H₂O₂-degrading enzyme catalase, and a ROS scavenger butylated hydroxy anisole (BHA), an inhibitor of H₂O₂ transporter, as well as an ultra-sensitive H₂O₂ indicator.

4.2.3.4.1. Catalase has no effect on Ca²⁺ signaling

The peroxidase-like domain of DUOX1 and DUOX2 faces the extracellular space, and they release H₂O₂ into the extracellular space. It was reported that degradation of extracellular H₂O₂ by catalase inhibits the proliferation of fibroblasts (Preston et al., 2001). Therefore, primary CD4⁺ T cells from WT mice were pre-incubated with catalase in the extracellular buffer to cleave extracellular H₂O₂ and were used to analyze the Ca²⁺ response upon TCR stimulation,

Results

as shown in Fig. 11.

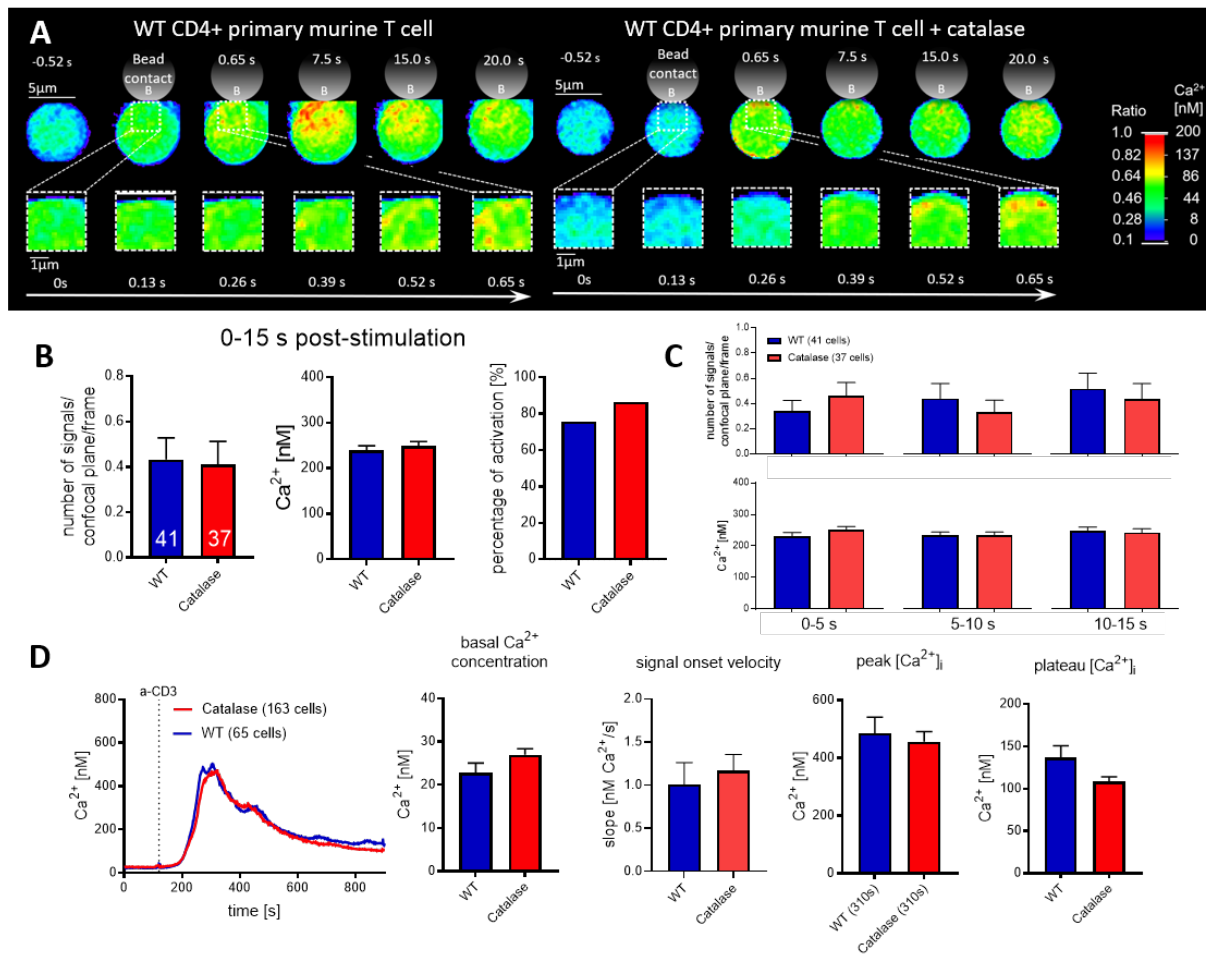


Fig. 11: H₂O₂-consuming catalase in extracellular buffer affects neither Ca²⁺ microdomain formation nor the global Ca²⁺ signals in primary T cells upon TCR stimulation.

CD4⁺ primary T cells were extracted from lymphoid tissues of WT mice and labeled with Fluo4-AM (10 μM) and FuraRed-AM (20 μM) for Ca²⁺ microdomain imaging (A-C) or Fura2-AM (4 μM) for global Ca²⁺ imaging (D). Before measurements, cells were treated in buffer or additional catalase (1000-2500 units/mL) for 5 min. (A) High resolution Ca²⁺ images of a WT T cell (left) and a WT T cell incubated with catalase (right) after stimulation with antibodies-coated beads (anti-CD3/anti-CD28) (indicated schematically). The heatmap reveals emission ratios between Fluo4 and FuraRed ranging from 0.1 to 1.0; ratio values were then transformed to 0 to 200 nM intracellular Ca²⁺ concentration using external calibration. The whole cells have a scale bar of 5 μm, the enlarged region near the bead contact site has a scale bar of 1 μm. (B) The number of signals per confocal plane per frame in whole cells within the first 15 s after bead stimulation, as well as the average Ca²⁺ concentration of the microdomains in the responding cells and the percentage of stimulated cells, are displayed. Data are presented as mean ± SEM and were obtained from at least three different experiments; cell number is indicated in the column (WT n=41 cells; WT+catalase n=37 cells); a non-parametric Mann-Whitney U test revealed no significant difference. (C) Analysis of the number of signals per confocal plane per frame and average Ca²⁺ concentration from (B) following bead stimulation in a shorter period (as indicated). No significant difference was revealed in statistical analysis as in (B). (D) Mean Ca²⁺ traces after 10 μg/mL anti-CD3

Results

addition, baseline Ca^{2+} concentration, the slope of Ca^{2+} concentration rise within 100 s after stimulation, and peak (as indicated) and plateau (at 816 s) amplitudes are shown in the analysis of global Ca^{2+} readings. The data are represented as mean \pm SEM and were gathered from at least three different tests; the cell number is as stated in the legend (WT n=65 cells and WT+catalase n=163 cells). No significant difference was observed using a non-parametric Mann-Whitney U test. This dataset was published in (Gu et al., 2021) in Fig. 7 and S6.

As shown in Fig. 11A, both T cells with and without catalase showed similar formation of Ca^{2+} microdomains below the plasma membrane at the bead contact site. Further, whole cell analysis confirmed that the addition of extracellular catalase did not result in a difference in Ca^{2+} microdomain formation, in neither the first 15 s (Fig. 11B and Table 11) nor the 5 s periods (Fig. 11C and Table 11).

Table 11: Number of Ca^{2+} microdomains per frame (mean \pm SEM) in WT T cells with and without catalase shown in Fig. 11 B and C.

	0 – 15 s		
WT (n=41)	0.43 \pm 0.096		
WT + catalase (n=37)	0.41 \pm 0.10		
	0 – 5 s	5 – 10 s	10 – 15 s
WT (n=41)	0.34 \pm 0.083	0.44 \pm 0.11	0.52 \pm 0.12
WT + catalase (n=37)	0.46 \pm 0.10	0.33 \pm 0.094	0.44 \pm 0.12

Moreover, in global Ca^{2+} signals after TCR stimulation, the average Ca^{2+} concentration at the peak was 486 \pm 56 nM (mean \pm SEM) in WT control cells and was 457 \pm 34 nM (mean \pm SEM) in catalase-treated T cells. Additionally, the amplitude at the plateau phase was 137 \pm 14 nM (mean \pm SEM) in the cells without catalase and was 108 \pm 6 nM (mean \pm SEM) in the cells with catalase (Fig. 10D).

Therefore, removal of extracellular H_2O_2 by catalase did not influence the Ca^{2+} signaling upon TCR stimulation.

4.2.3.4.2. Aquaporin3 inhibitor has no effect on Ca^{2+} microdomain formation

Next, the diffusion of H_2O_2 across the plasma membrane was considered. Aquaporins (AQPs), also known as water channels, have been identified to facilitate H_2O_2 distribution across

Results

cellular membranes, specially AQP3 and AQP8 in mammalian cells (reviewed in Bienert and Chaumont, 2014; Di Marzo et al., 2018). AQP8 is not detectable in human lymphocytes (Moon et al., 2004), and AQP3 mediated H_2O_2 uptake was reported in CD4⁺ murine T cells (Hara-Chikuma et al., 2012). Here, a specific AQP3 inhibitor DFP00173 (Sonntag et al., 2019) was used to block the H_2O_2 uptake through AQP3 (Fig. 12).

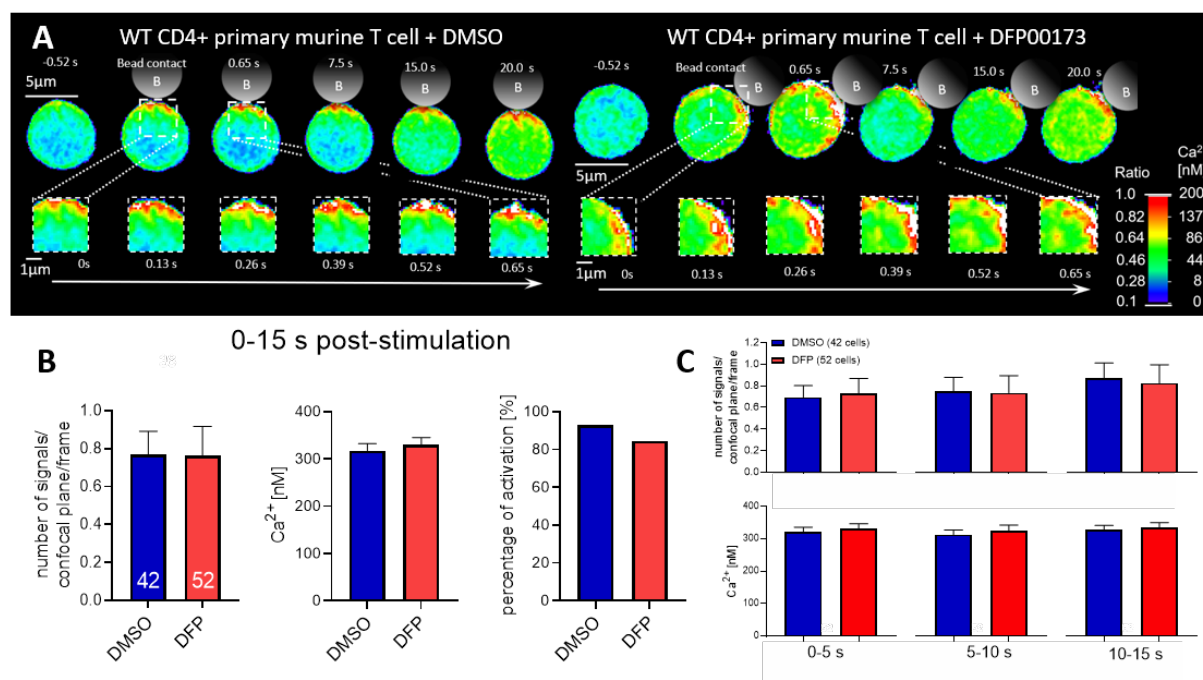


Fig. 12: DFP00173, an AQP3 inhibitor, has no effect on the formation of Ca^{2+} microdomains in primary T cells after TCR activation.

CD4⁺ primary T cells were extracted from lymphoid tissues of WT mice and loaded with 10 μM Fluo4-AM and 20 μM FuraRed-AM for the Ca^{2+} microdomain imaging. Before measurements, cells were treated in DMSO [0.5% (v/v)] or DFP00173 (25 μM) for 10 min. (A) High resolution Ca^{2+} images of a WT T cell in DMSO (left) and a WT T cell treated with DFP00173 (right) after stimulation with anti-CD3 and anti-CD28 coated beads (indicated schematically). The heatmap reveals emission ratios between Fluo4 and FuraRed ranging from 0.1 to 1.0; ratio data was then transformed to 0 to 200 nM intracellular Ca^{2+} concentration using external calibration. Scale bar of 5 μm is shown for whole cells and 1 μm for the enlarged region near the bead contact site. (B) Analysis of Ca^{2+} microdomains in the whole cells across the first 15 s after bead stimulation shows the number of signals per confocal plane per frame, average Ca^{2+} concentration in the responding cells, and the activation percentage. Data are presented as mean \pm SEM and were collected from at least three independent experiments; cell number is indicated in the column (WT in DMSO n=42 cells and WT with DFP00173 n=52 cells); no significant difference was shown using a non-parametric Mann-Whitney U test. (C) Analysis of the number of signals per confocal plane per frame and average Ca^{2+} concentration from (B) in a shorter period (as indicated) after bead stimulation. Statistical analysis was carried out as in (B), no significant difference is detected. This dataset was modified from Fig. 7 and S7 in (Gu et al., 2021).

Results

In the characteristic T cell pre-incubated with DFP00173, the formation of Ca^{2+} microdomains was similar to that in the DMSO-treated T cell (Fig. 12A). The average number of Ca^{2+} microdomains within 15 s was 0.77 signals per frame in T cells with DMSO and was 0.76 signals per frame in DFP00173-treated T cells (Fig. 12B and Table 12). Again, in the 5 s periods after bead stimulation, the number of Ca^{2+} microdomains per frame was almost identical in T cells with and without AQP3 blockage (Fig. 12C and Table 12).

Table 12: Number of Ca^{2+} microdomains per frame (mean \pm SEM) in WT T cells with and without AQP3 inhibitor DFP00173 shown in Fig. 12 B and C.

	0 – 15 s		
WT + DMSO (n=42)	0.77 \pm 0.12		
WT + DFP00173 (n=52)	0.76 \pm 0.16		
	0 – 5 s	5 – 10 s	10 – 15 s
WT + DMSO (n=42)	0.69 \pm 0.11	0.75 \pm 0.13	0.87 \pm 0.14
WT + DFP00173 (n=52)	0.73 \pm 0.14	0.74 \pm 0.16	0.83 \pm 0.17

Taken together, blocking the uptake of H_2O_2 by DFP00173, an AQP3 inhibitor, had no effect on initial Ca^{2+} response after TCR stimulation.

4.2.3.4.3. BHA has no effect on Ca^{2+} microdomain formation

It was reported that in a transfected cell model, the transient expression of partially glycosylated DUOX2 generates superoxide in a Ca^{2+} -dependent manner (Ameziiane-El-Hassani et al., 2005). Therefore, a membrane-permeable ROS scavenger butylated hydroxy anisole (BHA) was used to scavenge ROS produced in the cytosol (Fig. 13). BHA is a lipophilic organic compound and is commonly used as standard antioxidant in many studies to scavenge free radicals and H_2O_2 .

Results

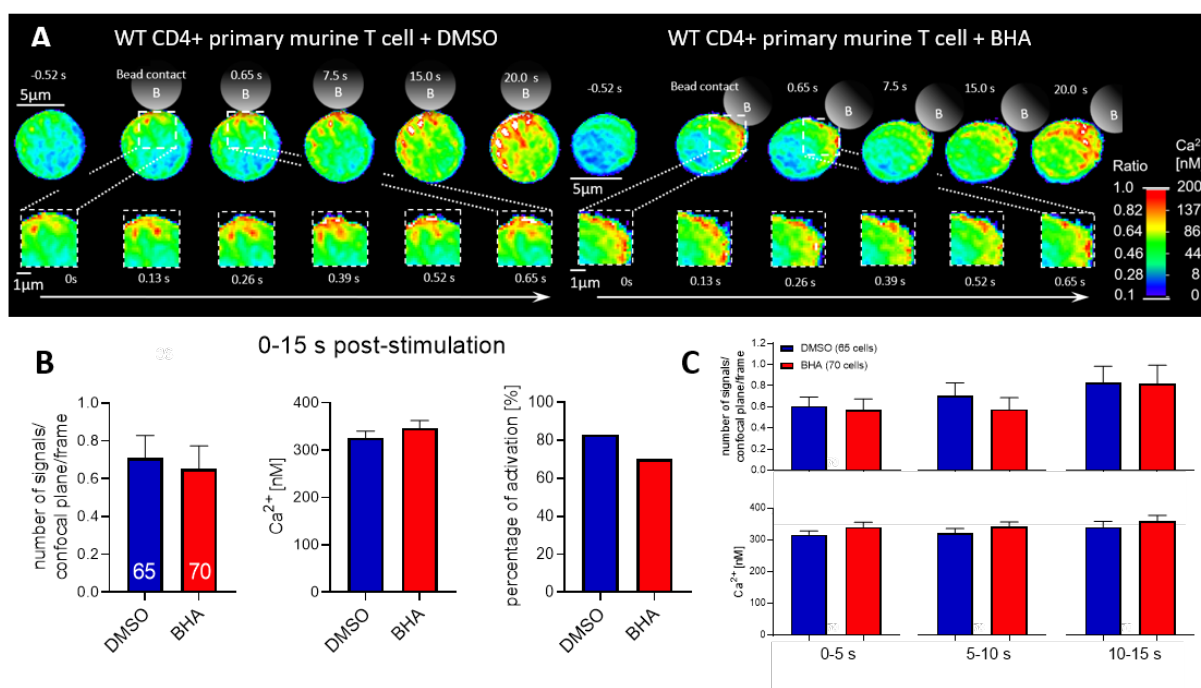


Fig. 13: Membrane-permeable ROS scavenger BHA does not affect Ca^{2+} microdomain formation in primary T cells upon TCR stimulation.

For Ca^{2+} microdomain imaging, CD4^{+} primary T cells were extracted from lymphoid tissues of WT mice and loaded with Fluo4-AM (10 μM) and FuraRed-AM (20 μM). Before measurements, cells were incubated in DMSO [0.5% (v/v)] or BHA (50 μM in DMSO) for 5 min. (A) High resolution Ca^{2+} images of a WT T cell preincubated in DMSO (left) and a WT T cell treated with BHA (right) after stimulation with anti-CD3 and anti-CD28 coated beads (indicated schematically). The heatmap reveals emission ratios between Fluo4 and FuraRed ranging from 0.1 to 1.0; ratio values were then transformed to 0 to 200 nM intracellular Ca^{2+} concentration using external calibration. The whole cells have a scale bar of 5 μm , and the enlarged region near the bead contact site has a scale bar of 1 μm . (B) Analysis of Ca^{2+} microdomains in whole cells throughout the first 15 s following bead stimulation, revealing the number of signals per confocal plane per frame, average Ca^{2+} concentration in responding cells, and percentage of activation. Data are reported as mean \pm SEM and were obtained from at least three different experiments; cell number is indicated in the column (WT in DMSO $n=65$ cells and BHA-treated $n=70$ cells); a non-parametric Mann-Whitney U test revealed no significant difference. (C) Analysis of the number of signals per confocal plane per frame and average Ca^{2+} concentration from (B) following bead stimulation in a shorter period (as indicated). No significant difference was detected in statistical analysis as in (B). These results were published in (Gu et al., 2021) in Fig. 7 and S7.

As shown in Fig. 13A, BHA did not influence the increase of local Ca^{2+} concentration below the plasma membrane. The whole cell analysis confirmed that BHA had no effect on Ca^{2+} microdomain formation upon TCR stimulation. In Fig. 13B and Table 13, the formed Ca^{2+} microdomains in the first 15 s were 0.71 signals per frame in DMSO-treated T cells and were 0.65 signals per frame in BHA-treated T cells. Further analysis in 5 s periods did not show any

effect either (Fig. 13C and Table 13).

Table 13: Number of Ca²⁺ microdomains per frame (mean ± SEM) in WT T cells with and without ROS scavenger BHA shown in Fig. 13 B and C.

	0 – 15 s		
WT + DMSO (n=65)	0.71 ± 0.12		
WT + BHA (n=70)	0.65 ± 0.12		
	0 – 5 s	5 – 10 s	10 – 15 s
WT + DMSO (n=65)	0.61 ± 0.087	0.70 ± 0.12	0.83 ± 0.16
WT + BHA (n=70)	0.57 ± 0.10	0.58 ± 0.11	0.82 ± 0.18

In summary, scavenging intracellular ROS by BHA did not affect initial Ca²⁺ signals after TCR stimulation.

4.2.3.4.4. Exogenous H₂O₂ has no effect on Ca²⁺ microdomain formation

As the byproduct of NAADP generation by DUOX isozymes, H₂O₂ is expected to be equal to NAADP, approximately 34 nM at 10 s post TCR stimulation (Gasser et al., 2006). Considering a higher local concentration near the plasma membrane, 80 nM exogenous H₂O₂ was added to WT murine CD4⁺ T cells instead of bead stimulation. Here, Ca²⁺ buffer was added as a negative control and thapsigargin, an inhibitor of sarco/endoplasmic reticulum Ca²⁺ ATPase (SERCA) that induces store-operated Ca²⁺ entry (SOCE), was added as a positive control (see Fig. 14).

Results

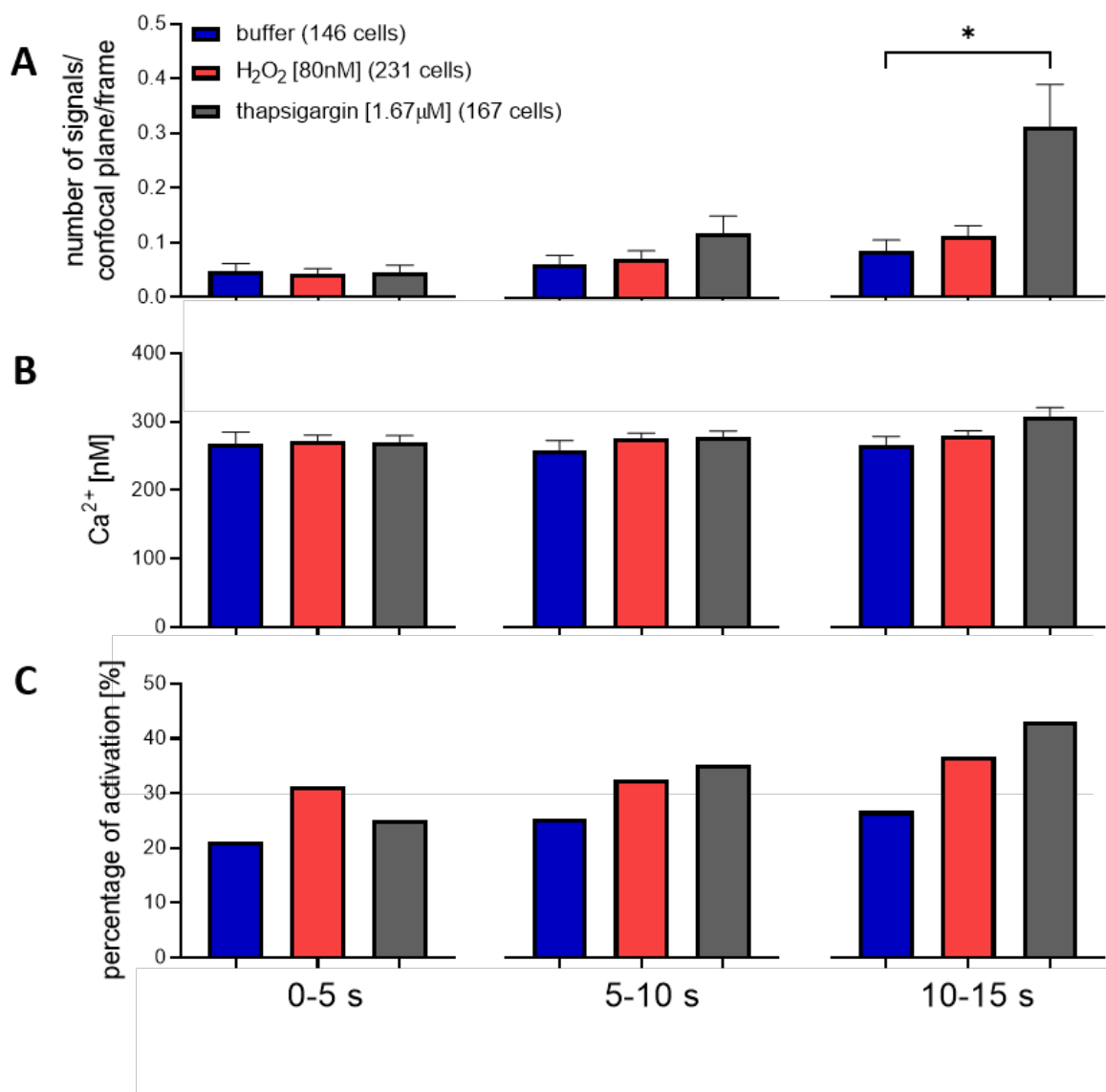


Fig. 14: Exogenous H₂O₂ at 80 nM does not increase Ca²⁺ microdomains in primary T cells without bead stimulation.

For Ca²⁺ microdomain imaging, CD4⁺ primary T cells were extracted from lymphoid tissues of WT mice and loaded with 10 μM Fluo4-AM and 20 μM FuraRed-AM. Analysis of Ca²⁺ microdomains in whole cells after addition of Ca²⁺ buffer (negative control), 80 nM exogenous H₂O₂, and 1.67 μM thapsigargin (positive control) in 5 s periods, shown as the number of signals per confocal plane per frame (top), average Ca²⁺ concentration in the responding cells (middle), and percentage of activated cells (bottom). Data were obtained from at least three different experiments and are given as mean ± SEM; cell number is indicated in the legend (buffer control n=146 cells; 80 nM H₂O₂ n=231 cells and thapsigargin n=167 cells); statistical analysis was carried out using a non-parametric Kruskal-Wallis test and Dunn's correction for multiple testing: *p<0.05. These data were modified from Fig. 7 in (Gu et al., 2021).

In Fig. 14A and Table 14, thapsigargin significantly increased Ca²⁺ microdomain formation from

Results

10 to 15 s after the addition. In this period, the average number of Ca^{2+} microdomains was 0.31 signals per frame after thapsigargin addition, 0.084 signals per frame after buffer addition, and 0.11 signals per frame after 80 nM H_2O_2 addition. Furthermore, thapsigargin also increased the percentage of responding cells, from 25% in the first 5 s, then 35%, and 43% in the last 5 s. In contrast, 80 nM H_2O_2 did not elevate the number of Ca^{2+} microdomains per frame, and only approximately 30% of cells showed Ca^{2+} microdomains (Fig. 14C and Table 14).

Table 14: Number of Ca^{2+} microdomains per frame (mean \pm SEM) and percentage of responding cells in WT T cells with 80 nM exogenous H_2O_2 shown in Fig. 14 A and C.

	0 – 5 s	5 – 10 s	10 – 15 s
	number of signals/confocal plane/frame		
WT + buffer (n=146)	0.048 \pm 0.014	0.060 \pm 0.017	0.084 \pm 0.020
WT + 80 nM H_2O_2 (n=231)	0.044 \pm 0.0089	0.072 \pm 0.014	0.11 \pm 0.018
WT+ thapsigargin (n=167)	0.046 \pm 0.013	0.12 \pm 0.032	0.31 \pm 0.078
	percentage of activation [%]		
WT + buffer (n=146)	21	25	27
WT + 80 nM H_2O_2 (n=231)	31	32	37
WT+ thapsigargin (n=167)	25	35	43

In short, 80 nM exogeneous H_2O_2 did not elevate initial Ca^{2+} signals in the absence of TCR stimulation.

4.2.3.4.5. No detectable H_2O_2 production within 15 s post TCR/CD3 ligation

The classical substrate of the NOX/DUOX family is NADPH. Whether the activation of DUOX isozymes after TCR stimulation results in endogenous H_2O_2 production was analyzed using a genetically encoded H_2O_2 indicator HyPer7 (Pak et al., 2020). The version targeted to the cytosolic side of the plasma membrane (PRID: Addgene_136465) was used to determine endogenous H_2O_2 after TCR stimulation, as shown in Fig. 15.

Results

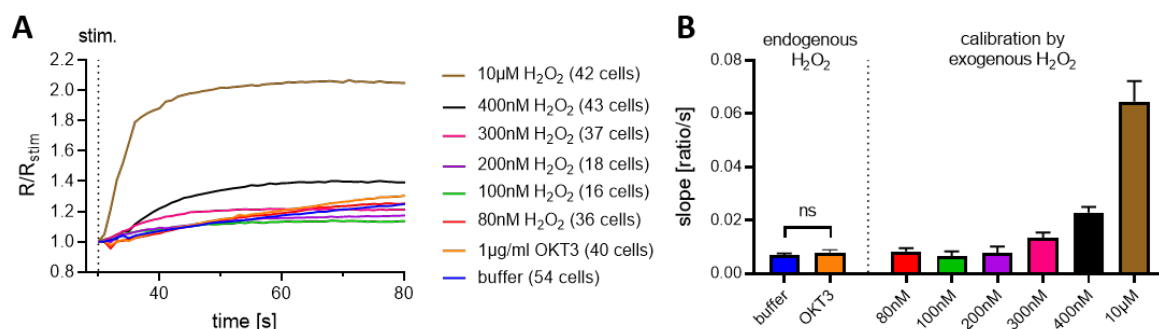


Fig. 15: No measurable H_2O_2 generation after TCR/CD3 stimulation by using ultrasensitive H_2O_2 indicator HyPer7.

WT Jurkat T cells were transfected with 5 μ g/mL pCMV-HyPer7-MEM (PRID: Addgene_136465) and stimulated with buffer, OKT3 (1 μ g/mL), or freshly diluted H_2O_2 (concentration as indicated). (A) Mean tracings of the HyPer7-MEM 488ex/405ex ratio adjusted to the stimulation time point (R/R_{stim}). Cell numbers are provided in the legends (buffer n=54 cells; OKT3 n=40 cells; 80 nM H_2O_2 n=36 cells; 100 nM H_2O_2 n=16 cells; 200 nM H_2O_2 n=18 cells; 300 nM H_2O_2 n=37 cells; 400 nM H_2O_2 n=43 cells; 10 μ M H_2O_2 n=42 cells). (B) Signal onset velocities (slopes within 15 s after addition) of the tracings in (A). The data are provided as means \pm SEM and the cell numbers as shown in (A). The non-parametric Mann-Whitney U test was used for statistical analysis, with no significant difference between buffer control and 1 μ g/mL OKT3. This dataset was published in (Gu et al., 2021) in Fig.7.

As shown in Fig. 15 and Table 15, 10 μ M H_2O_2 resulted in a rapidly increased HyPer7 signal within around 5 s after addition (slope 0.065 ratio/s), and 300 nM exogenous H_2O_2 is sufficient to evoke a detectable increase of the HyPer7 signal (slope 0.013 ratio/s). TCR stimulation by OKT3 (slope 0.0078 ratio/s) did not result in statistically significant difference compared to the buffer control (slope 0.0068 ratio/s).

Table 15: Slope of HyPer7 signals (mean \pm SEM) shown in Fig. 15B.

	1 μ g/mL OKT3			buffer		
slope [ratio/s]	0.0078 \pm 0.0011			0.0068 \pm 0.00075		
H_2O_2	80 nM	100 nM	200 nM	300 nM	400 nM	10 μM
slope [ratio/s]	0.0083 \pm 0.0012	0.0065 \pm 0.0018	0.0078 \pm 0.0023	0.013 \pm 0.0020	0.023 \pm 0.0021	0.065 \pm 0.0076

As indicated by HyPer7, TCR/CD3 ligation induced H_2O_2 production is less than 300 nM in the analyzed period.

5. Discussion

5.1. Key findings in this study

NAADP functions as a trigger for Ca^{2+} signaling in many cells (reviewed in Guse and Lee, 2008). In T cells, it plays an essential role in T cell activation, differentiation, and function, and is therefore critical in the progression of many inflammatory diseases (Ali et al., 2016; Berg et al., 2000; Cordiglieri et al., 2010; Dammermann et al., 2009; Nawrocki et al., 2021). NAADP is rapidly formed within 10 s after T cell activation and decreases over the next 10 s, followed by a second production phase that peaks at 5 min after TCR stimulation in Jurkat T cells (Gasser et al., 2006), as indicated in the insert in Fig. 16. The aim of this thesis was to answer the question: which enzyme(s) produces NAADP in CD4^+ T cells? Here, dual NADPH oxidase 2 (DUOX2) was identified as the major enzyme responsible for rapid NAADP generation upon TCR stimulation (Fig. 16).

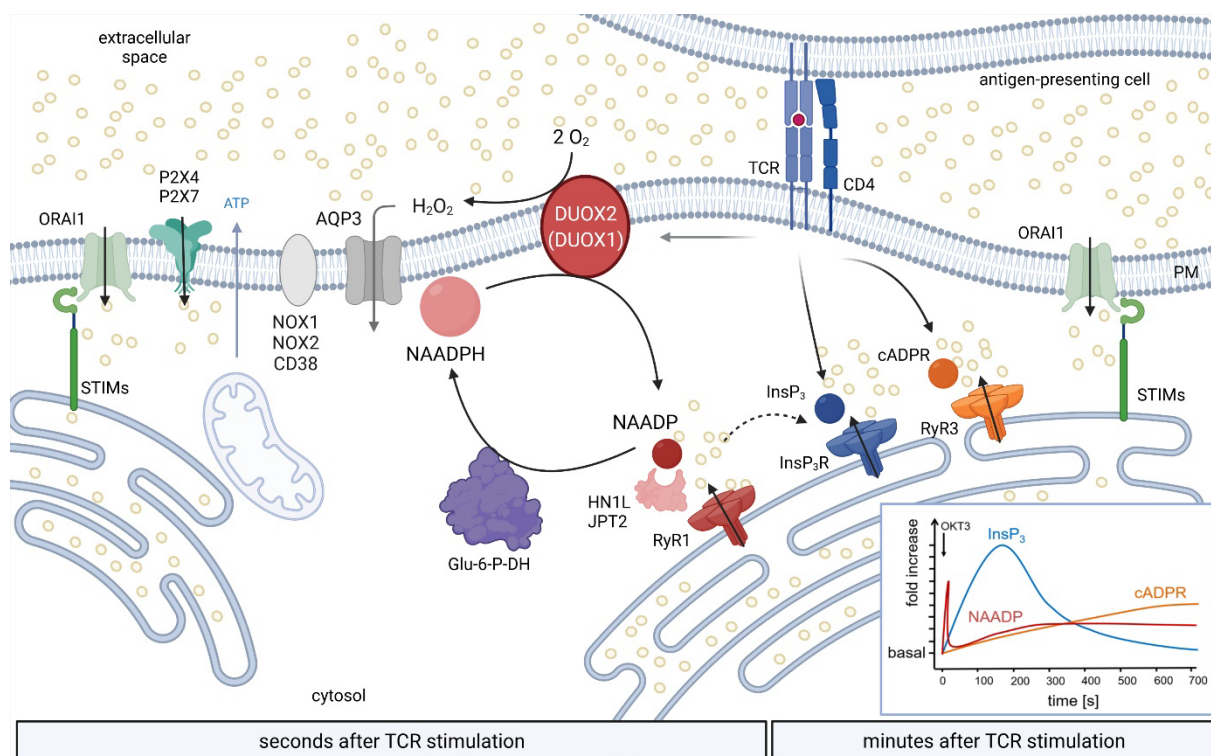


Fig. 16: Ca^{2+} signaling upon TCR stimulation and key findings in this thesis.

Upon TCR stimulation, NAADP is rapidly formed within 10 s [as shown in the insert in red (Gasser et al., 2006)], and induces the initial Ca^{2+} signals, termed Ca^{2+} microdomains. In the first 15 s, the absence of CD38, NOX1, and NOX2 did not influence Ca^{2+} microdomain formation (shown in grey); DUOX2 was established to be the major enzyme responsible for the rapid NAADP generation, whereas DUOX1 could

compensate NAADP production in the absence of DUOX2. The byproduct H_2O_2 , diffusing through the PM via AQP3, had no effect on Ca^{2+} microdomain formation during this period, as indicated in grey. Glu-6-P-DH may be responsible for the rapid NAADP degradation from 10 to 20 s by reducing NAADP (Gu et al., 2021). NAADP-induced Ca^{2+} signals are then amplified by $InsP_3$ -induced Ca^{2+} release [kinetics of $InsP_3$ production is shown in the insert in blue (Guse et al., 1993)], cADPR-induced Ca^{2+} release [kinetics of cADPR generation is shown in the insert in yellow (Guse et al., 1999)], Ca^{2+} -induced Ca^{2+} release as indicated by the dashed arrow and store-operated Ca^{2+} entry, originating from clusters of STIMs and ORAI1 as indicated in green. In the first 13 min after TCR/CD3 ligation, global Ca^{2+} signals in T cells, in which CD38, NOX1 and NOX2 were deleted, were identical to those in WT T cells. The phenotype of global Ca^{2+} signals in *Duox2*^{-/-} T cells was identical to NAADP antagonism, whereas the peak in *Duox1*^{-/-} T cells was further delayed by the specific NAADP antagonist BZ194. In the insert, the arrow indicates the addition of anti-CD3 antibody (OKT3). The y-axis indicates the fold increase compared with their baseline. This figure was created with BioRender.com.

5.1.1. Understanding the role of CD38 upon TCR stimulation

In 1995, the first report indicated that CD38 can produce NAADP through the “base-exchange” reaction in the cell-free system, which requires an acidic pH and nicotinic acid in the millimolar range (Aarhus et al., 1995). Then accumulating reports pointed out that CD38 is responsible for NAADP formation in some cell types (Cosker et al., 2010; Fang et al., 2018; Nam et al., 2020; Rah et al., 2010). In contrast, other observations exclude CD38 as an NAADP forming enzyme or even suggest it is an NAADP degrading enzyme (Schmid et al., 2011; Soares et al., 2007).

In this study, the absence of CD38 did not influence initial Ca^{2+} signals, termed Ca^{2+} microdomains, nor subsequent global Ca^{2+} signals upon TCR stimulation in CD4⁺ primary murine T cells. These results demonstrate that CD38 is not involved in the rapid NAADP generation, which is consistent with the previous report that CD38 does not alter the endogenous NAADP levels at 10 s after TCR stimulation in Jurkat T cells (Schmid et al., 2011). Moreover, this may also suggest that CD38 is not the enzyme, at least not the major one, responsible for the rapid degradation of NAADP from 10 to 20 s after T cell activation.

It should be noted that in this study, T cells were incubated in a neutral buffer and without the presence of nicotinic acid. It is known that the “base-exchange” reaction requires an excess of nicotinic acid, half the maximum of NAADP production was observed in the presence of 5 mM nicotinic acid at pH 5 (Aarhus et al., 1995). In LP-1 cells and HEK293 cells expressing

lysosomal CD38, CD38 elevates cellular NAADP levels in the presence of 10 mM nicotinic acid (Fang et al., 2018). Nicotinic acid, also known as niacin or a form of vitamin B₃, is an essential human nutrient. It can be synthesized from the amino acid tryptophan and is a precursor of NAD and NADP. The recommended daily intake of nicotinic acid for adults is 14–18 mg/day, which corresponds to 0.11–0.14 mmol/day (“Niacin,” 2014). Hence, it is unlikely that nicotinic acid is present in the millimolar range in the cytosol under physiological conditions. Nevertheless, it is worth considering whether T cells can reach higher local concentrations of nicotinic acid, for instance, in lymph nodes or at inflamed site or under pathophysiological conditions. Moreover, researchers also mentioned that lysosomal CD38 regulates cellular NAADP levels via substrate access rather than enzyme activation (Fang et al., 2018). Whether this mechanism represents a physiological role of CD38 in regulating NAADP in resting T cells needs to be further investigated.

5.1.2. DUOX2, the major NAADP forming enzyme in CD4+ T cells

The NADPH oxidase family has been identified to generate NAADP from its reduced form NAADPH in the cell-free system under physiological conditions (in this study and Gu et al., 2021). NAADPH is not able to evoke Ca²⁺ signals (Billington et al., 2004), so it is a possible inactive precursor of NAADP. The isozymes in this family have a highly conserved catalytic core (Fig. 3). NOX5 does not require any subunits for its activation, and consequently, it was used as a standard model. The optimal pH of NOX5 for oxidation of NAADPH is between 7 and 8 (Gu et al., 2021).

NOX5 is known to be absent in rodents (Kawahara et al., 2007), and from the other isozymes expressed in murine primary CD4+ T cells, NOX1 and NOX2 did not influence Ca²⁺ microdomain formation in the first 15 s nor subsequent global Ca²⁺ signaling up to 13 min upon TCR stimulation. These results confirm with the observations from other groups: i) NOX1 and NOX2 produce superoxide, and TCR/CD3 ligation induces the generation of superoxide mainly from 45 to 90 min in Jurkat T cells (Kwon et al., 2010), and ii) oxidation of 2',7'-dichlorodihydrofluorescein diacetate [DCFDA, an H₂O₂ indicator, reported in (McLennan and Esposti, 2000)] indicates that H₂O₂ is produced within minutes after T cell activation (Jackson

et al., 2004; Kwon et al., 2010, 2003). The deficiency of NOX2, i.e., the subunits gp91^{phox} and p47^{phox}, does not influence DCFDA oxidation in the first minutes after T cell activation in primary murine T blasts (Jackson et al., 2004). iii) Furthermore, CD4⁺ T cells in *Nox1*^{-/-} mice produce increased IL-2, IFN- γ , and TNF- α (the characteristic cytokines of Th 1, as shown in Table 1) after the infection of influenza A virus (Hofstetter et al., 2016). Similarly, the absence of NOX2 in CD4⁺ murine T blasts leads to an increase in the production of IL-2, IFN- γ , and TNF, as well as a decrease in the secretion of IL-4 and IL-5 (the signature cytokines of Th 2, as shown in Table 1) (Jackson et al., 2004). In contrast, the expression of IL-2, IFN- γ , and IL-17 (signature cytokines of Th 1 and Th 17, as shown in Table 1) is downregulated in *Duox1*^{-/-} and *Duox2*^{-/-} CD4⁺ rat effector T cells (Gu et al., 2021), which is in line with the effect of NAADP antagonism on T cell function (Ali et al., 2016; Cordiglieri et al., 2010; Dammermann et al., 2009).

Indeed, both DUOX isozymes oxidize NAADPH to NAADP under physiological conditions in the cell-free system. Moreover, DUOX1 significantly preferred NADPH as a substrate, whereas DUOX2 exhibited comparable enzyme activity for both substrates. Wu and coworkers solved the cryo-EM structure of the human DUOX1/A1 complex. They reported that the hDUOX1/A1 complex is present in a heterotetrametric form. Briefly, a cytosolic layer consisting of a regulatory PHL- domain and the Ca²⁺-binding EF-hand motifs contributes to a conformational change at low- and high-Ca²⁺ states (Wu et al., 2021). This explains the fact that the treatment with ionomycin increases DUOX1 (and DUOX2) enzyme activity (Rigutto et al., 2009). Compared with the enzyme activity of hDUOX1/A1 for NADPH reported in (Wu et al., 2021), approximately 2.2 nmol/s/mg protein at 50 μ M NADPH, the enzyme activity of hDUOX1/A1 for NADPH (0.042 nmol/s/mg protein) determined in this study is about 52-fold lower. This could be due to different expression levels of hDUOX1/A1 in the HEK293 cell system or different methods for determining protein concentration. The membranes used in this study were determined using the Bradford reagent with bovine serum albumin (BSA) as a standard, whereas the membranes they used were established by GFP-tagged DUOX1 (Wu et al., 2021), which allows a more accurate determination of enzyme concentration.

The enzyme assay in this study was performed in a buffer with a concentration of 670 μ M free Ca²⁺, which refers to the high Ca²⁺ state (\geq 500 μ M) for hDUOX1/A1, and EC₅₀ of Ca²⁺ for the hDUOX1/A1 complex is 0.38 μ M in the presence of 100 μ M NADPH (Wu et al., 2021). It is

known that in the absence of TCR stimulation, there are smaller and less frequent Ca^{2+} microdomains close to the plasma membrane, where the average Ca^{2+} concentration reaches 200 to 250 nM (Brock et al., 2022; Diercks et al., 2018). This Ca^{2+} concentration is much lower than that in the cell-free enzyme assay. Therefore, it is then questionable whether the DUOX1 (and DUOX2) complex may be activated in intact T cells? The studies of NOX5 may give us a hint. NOX5, as mentioned above, another isozyme with Ca^{2+} -binding EF-hand domains like DUOX1 and DUOX2, was reported to have an EC_{50} around 1 μM of Ca^{2+} in the cell-free system (Bánfi et al., 2004). In intact Cos-7 cells, PMA-dependent phosphorylation increases the sensitivity of NOX5 to Ca^{2+} (Chen et al., 2014; Jagnandan et al., 2007; Serrander et al., 2007). Furthermore, a calmodulin-binding domain is found at the C-terminus of NOX5, which is involved in its Ca^{2+} sensitivity (Tirone and Cox, 2007). In a later study, calcium/calmodulin-dependent kinase II (CAMKII) was reported to phosphorylate NOX5 in the *in vitro* phosphorylation assays directly (Pandey et al., 2011). In this regard, phosphorylation may function similarly to DUOX1 and DUOX2 complexes, which require cAMP-dependent PKA and PKC, respectively, in Cos-7 cells (Rigutto et al., 2009). Therefore, in intact T cells, the DUOX1/A1 and DUOX2/A2 complexes may be able to generate NAADP in the presence of 200 to 250 nM local Ca^{2+} near the plasma membrane.

As shown in this study, the absence of DUOX isozymes impaired Ca^{2+} signaling in intact T cells. However, their effect on Ca^{2+} signaling was different. First, NAADP is produced in the first 10 s after TCR stimulation in Jurkat T cells (Gasser et al., 2006). When both DUOX isozymes are nonfunctional in T cells (*DuoxA1^{-/-}/A2^{-/-}*), the formation of Ca^{2+} microdomains was reduced by more than 70% within 15 s after TCR stimulation (Gu et al., 2021). A comparable reduction was observed only in the first 5 s in *Duox2^{-/-}* T cells; in the following 5 s, the decrease in Ca^{2+} microdomains in single knockout T cells was around half that in functional double knockout T cells; from 10 to 15 s, DUOX1 no longer affected Ca^{2+} microdomain formation, and only a 13% reduction was observed in DUOX2-deficient T cells. Furthermore, a substantial reduction can be observed in the sublayer below the plasma membrane at the stimulating site in the *DuoxA1^{-/-}/A2^{-/-}* T cells throughout the first 25 s after bead stimulation (Gu et al., 2021), whereas the absence of DUOX2 resulted in a significantly decreased formation of Ca^{2+} microdomains from the first second up to around 20 s. It appears that DUOX1 is able to slowly

compensate for the generation of NAADP in the lack of DUOX2, and therefore, to recover Ca²⁺ microdomain formation. Moreover, the apparent phenotype observed in the first second at the bead contact site in *Duox2*^{-/-} T cells is similar to that in *DuoxA1*^{-/-}/*A2*^{-/-} T cells (Gu et al., 2021), in the absence of the NAADP binding protein HN1L/JPT2 (Roggenkamp et al., 2021), as well as in *Ryr1*^{-/-} T cells and NAADP antagonism (Diercks et al., 2018). Additionally, the byproduct H₂O₂ had no effect on Ca²⁺ signaling in the first 15 s after TCR stimulation. Second, NAADP-induced initial Ca²⁺ signals are essential for subsequent global Ca²⁺ signals (reviewed in Wolf and Guse, 2017). Global Ca²⁺ signals in DUOX2-deficient T cells were identical to global Ca²⁺ signals observed upon NAADP antagonism. All of the above results suggest that DUOX2 is the primary enzyme responsible for the rapid NAADP generation upon T cell activation, and that DUOX1 can compensate for NAADP production in the absence of DUOX2.

5.2. Limitations of this study

The role of CD38, NOX1, NOX2, and the synergy of DUOX1 and DUOX2 in Ca²⁺ signaling was examined in freshly isolated primary murine CD4⁺ T cells, which are a mixture of naïve, memory, and effector T cells, whereas the effect of DUOX1 or DUOX2 alone was determined in rat CD4⁺ effector T cells constructed with CRISPR/Cas, because the individual knockout mouse models were not available. Differences between naïve, memory, and effector T cells have been reported, such as responsiveness to antigen and requirement for co-stimulation (reviewed in Berard and Tough, 2002; Croft, 1994). Because the concentration of OKT3 alters NAADP production in Jurkat T cells (Gasser et al., 2006), 1 µg/mL anti-CD3 antibody was used to stimulate rat effector T cells for global Ca²⁺ signaling, whereas 10 µg/mL anti-CD3 antibody was used to stimulate primary murine T cells. Cordiglieri and coworkers reported that naïve and memory T cells are less susceptible to NAADP antagonist BZ194, but this effect correlated with different expression of RyR1 (Cordiglieri et al., 2010). Although i) the Ca²⁺ signaling observed in this study was very similar after TCR stimulation in murine and rat T cells, and ii) Ali and coworkers also reported a similar profile of NAADP-induced Ca²⁺ signaling as well as downstream events in murine naïve and effector T cells (Ali et al., 2016), it is still not clear whether the upstream mechanism of NAADP-induced Ca²⁺ signaling, i.e., regulation of NAADP

production, is altered in different CD4⁺ T cell subsets or even in the two species.

The enzyme assay of DUOX1 and DUOX2 was performed with the human DUOX1- and DUOX2-complexes, and their role in intact T cells was investigated in primary murine T cells (Gu et al., 2021) and rat T cells. The cryo-EM structures of the murine and human DUOX1 complexes were recently published by two independent groups. Although the murine DUOX1 shares about 91% sequence identity with the human ortholog, they reveal two different activation modes: the murine complex shows a conformational change from an inactive state “dimer of dimer” to an active state “heterodimer” in the absence or presence of NADPH, respectively (Sun, 2020), whereas the human complex is present in a heterotetrameric form with the conformational change of the regulatory PHL-domain and EF-hand motifs in the intracellular layer in the low and high Ca²⁺ states (Wu et al., 2021). This difference was mentioned in the latter publication, and the authors concluded that it remains unclear whether it results from different protein preparation procedure or different species (Wu et al., 2021).

More direct evidence that DUOX2 is the NAADP forming enzyme will be provided measuring the endogenous level of NAADP in the absence of DUOX2 after TCR stimulation using the enzymatic cycling assay described in (Gasser et al., 2006). However, this enzymatic cycling assay requires 1.6x10⁸ Jurkat T cells for one data point. Considering the diameter of murine and rat T cells, which is around half that of Jurkat T cells, too many mice would be required to attain one data point. Consequently, the endogenous NAADP will be possibly determined until a stable DUOX2 knockout or knockdown Jurkat T cell line is established.

Furthermore, the results of this study only suggest that DUOX2 (and DUOX1) is responsible for NAADP generation within seconds after T cell activation, i.e., the first NAADP production phase, as indicated in Fig. 17. It is unclear whether they also play a role in the second NAADP production phase. A decreased plateau amplitude of global Ca²⁺ signals was observed in both *Duox1*^{-/-} and *Duox2*^{-/-} T cells, and the decrease was identical to the global Ca²⁺ signal-phenotype during NAADP antagonism. However, cADPR-induced Ca²⁺ release and store-operated Ca²⁺ entry play a significant role in maintaining cytosolic free Ca²⁺ concentration in this phase (reviewed in Feske, 2007). It is unclear how NAADP, produced in its second production phase, contributes to the maintenance of cytosolic free Ca²⁺ concentration. If a

NAADP sensor may be established in the future, it may allow to monitor NAADP generation in living cells. In that case, this would be a better solution to explore further details of the NAADP/Ca²⁺ signaling during T cell activation.

5.3. H₂O₂ in the early phase of T cell activation

Another issue that was clarified in this study is that the byproduct H₂O₂ did not affect the initial Ca²⁺ signaling within seconds of T cell activation. The kinetics of ROS production after T cell activation are shown in Fig. 17. H₂O₂ production indicated by HyPer7 (Pak et al., 2020) within the first 30 s after OKT3 stimulation was measured in this study, and ROS production indicated by DCFDA and dihydroethidium (DHE) has been reported previously (Kwon et al., 2010). DCFDA is commonly used to characterize cellular H₂O₂ production (McLennan and Esposti, 2000), and DHE is commonly used as a probe for superoxide production (Zamzami et al., 1995). Dye oxidation was calculated as the percentage of increased fluorescence of stimulated cells compared with non-stimulated cells, as described in (Kwon et al., 2010). HyPer7 signals after OKT3 stimulation or the addition of 300 nM H₂O₂ shown in Fig. 17 were calculated in the same way, relative to the buffer control.

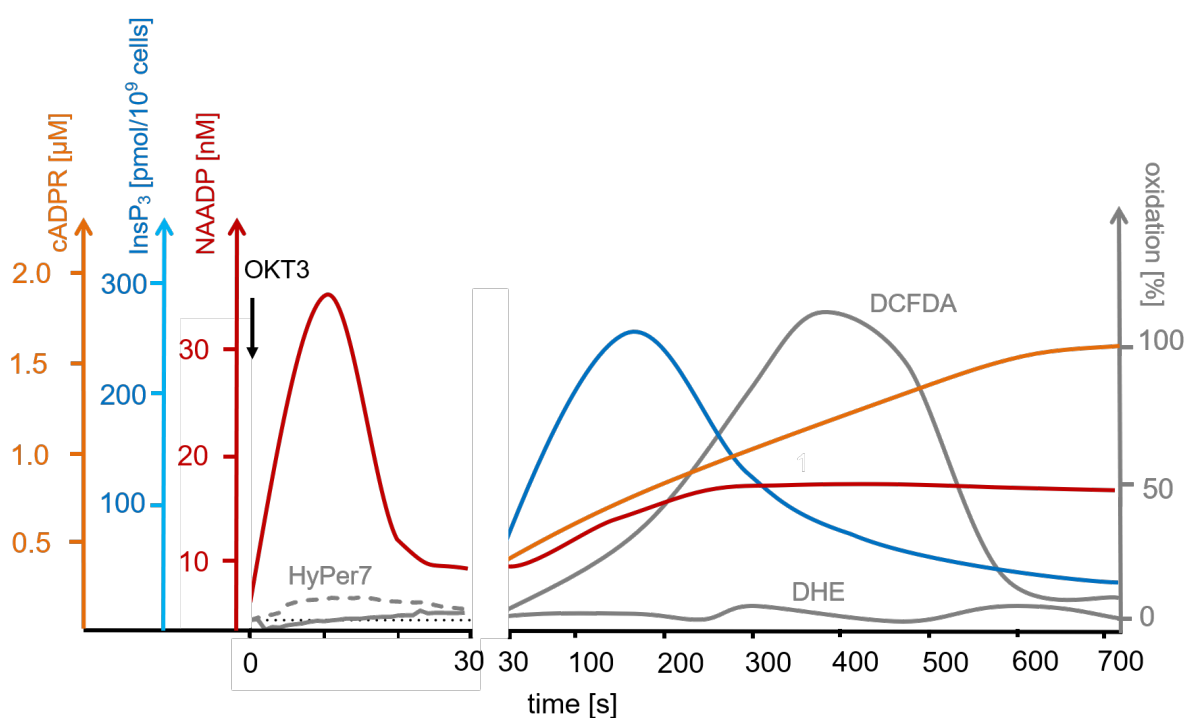


Fig. 17: Kinetics of production of Ca²⁺ releasing second messengers and ROS in the first 12 min

upon TCR/CD3 ligation.

NAADP is rapidly produced within 10 s after TCR/CD3 ligation, followed by a second production phase peaking at around 5 min (Gasser et al., 2006). InsP_3 is subsequently produced with a peak at 3 min (Guse et al., 1993). cADPR shows a sustained production with highest amplitude from 10 min on after T cell activation (Guse et al., 1999). The right y-axis indicates the percentage of increased fluorescence of HyPer7, DCFDA, and DHE compared with their signals without T cell activation. HyPer7 is an ultrasensitive H_2O_2 indicator (Pak et al., 2020) used in this study to measure H_2O_2 production (see results section 4.2.3.4.5). The solid grey line in the first 30 s shows the increased HyPer7 signals after T cell activation, and the dashed grey line shows the heightened HyPer7 signals after 300 nM H_2O_2 addition for comparison. The horizontal dashed line in this period indicates the zero point of the right y-axis. DCFDA and DHE oxidation was reported in (Kwon et al., 2010). The arrow indicates that anti-CD3 antibody (OKT3) stimulates Jurkat T cells.

Many reports indicate the oxidation of DCFDA after T cell activation, e.g., a peak of DCFDA oxidation at around 6 min in Jurkat T cells, as shown in Fig. 17 (Kwon et al., 2010), as well as in human and murine T blasts (Jackson et al., 2004; Kwon et al., 2003). However, this fluorogenic dye, DCFDA, is sensitive not only to H_2O_2 but also to other ROS, such as hydroxyl radical, hydroperoxides, and peroxynitrite, albeit with reduced sensitivity (Yang et al., 2014). The ultrasensitive H_2O_2 indicator HyPer7 used in this study is more suitable for studying physiological H_2O_2 production in real-time imaging with high specificity (Pak et al., 2020). To better understand the role of DUOX isozymes or H_2O_2 in Ca^{2+} signaling, it is meaningful to know the physiological H_2O_2 concentration over a long period of time after T cell activation. In addition, the low oxidation of DHE reported in (Jackson et al., 2004; Kwon et al., 2010, 2003) also indicates that in the early phase of T cell activation, H_2O_2 is produced directly rather than by dismutation of superoxide.

It is known that in CD4^+ T cells, RyR1 is involved in NAADP-induced Ca^{2+} signaling (Dammermann et al., 2009; Diercks et al., 2018; Roggenkamp et al., 2021; Wolf et al., 2015), and the formation of Ca^{2+} microdomains within 15 s after bead stimulation are highly reduced in the absence of RyR1 (Diercks et al., 2018). Millimolar concentrations of H_2O_2 have been reported to affect the gating mechanism of the Ca^{2+} release channel in the sheep cardiac sarcoplasmic reticulum (SR) (Boraso and Williams, 1994). Further, a reversible sulfhydryl modification at RyR1 by H_2O_2 in the millimolar range has been reported in the SR of rabbit skeletal muscle (Han et al., 2006). In this study, i) TCR/CD3 ligation-induced H_2O_2 production

was less than 300 nM within seconds post-stimulation, as indicated by HyPer7 (Fig. 16); ii) 80 nM exogenous H₂O₂ did not affect the initial Ca²⁺ signals within 15 s post-stimulation; iii) ROS scavengers, i.e., catalase and BHA, and blocking H₂O₂ uptake had no effect on Ca²⁺ microdomain formation after bead stimulation; iv) a significant phenotype in Ca²⁺ microdomain formation was already shown in the first second after TCR stimulation in the DUOX2-deficient T cells. All the results above demonstrate that the phenotype of Ca²⁺ microdomain formation observed in this study is most likely not due to the modification of RyR1 by H₂O₂. However, whether H₂O₂ at physiological concentrations regulates the Ca²⁺ release via ryanodine receptors in the later phase of T cell activation requires further investigation.

The peak of global Ca²⁺ signals at around 3 min after TCR/CD3 stimulation in *Duox1*^{-/-} T cells was further diminished by BZ194, suggesting a different signaling pathway involved. Kwon and coworkers reported a similar phenotype of global Ca²⁺ kinetics after TCR stimulation in DUOX1 knockdown Jurkat T cells. However, the underlying mechanism was identified as phosphorylation of a cytosolic phosphatase, Src-homology 2 domain (SH2)-containing protein tyrosine phosphatase (PTP) 2 (SHP-2), by DUOX1-generated H₂O₂, which then phosphorylates ζ chain-associated protein kinase of 70 kD (ZAP-70) and influences phospholipase C- γ 1 (PLC- γ 1), and therefore, the InsP₃/Ca²⁺ signaling pathway (Kwon et al., 2010). Actually, ROS production has been considered to be the primary function of the NADPH oxidase family, and ROS further affect signaling molecules, e.g., by inhibiting phosphatases, activating kinases, and directly affecting Ca²⁺ signaling pathways (reviewed in Bedard and Krause, 2007). Having found NAADP synthesis by DUOX isozymes in this study, it is worth considering whether the NAADP/Ca²⁺ signaling pathway is also involved in the phenotype published previously. More likely, these DUOX isozymes influence Ca²⁺ signaling and T cell activation via both NAADP and H₂O₂ production. In line with this, except for the role of DUOX isozymes in Ca²⁺ microdomain formation within the first 15 s observed in this study, the oxidation of DCFDA at 10 min after TCR stimulation is highly reduced in the absence of InsP₃R1 and PLC- γ 1, suggesting that H₂O₂ is also produced downstream of the InsP₃/Ca²⁺ signaling pathway and requires InsP₃-induced Ca²⁺ release. Moreover, the oxidation of DCFDA from 15 to 60 min after TCR stimulation is significantly reduced in DUOX1 knockdown Jurkat T cells (Kwon et al., 2010). These results suggest that DUOX1 is also active from 10 to 60 min

after T cell activation. Whether DUOX2 also plays a role in H₂O₂ (and NAADP) production during this period needs to be further investigated.

5.4. Outlook

5.4.1. Usage of different substrates

As mentioned above, strong oxidation of DCFDA has been observed within 10 min after TCR stimulation (Jackson et al., 2004; Kwon et al., 2010, 2003), and endogenous concentrations of NAADP are known to be in the low nanomolar range upon T cell activation (Gasser et al., 2006), as indicated in Fig. 17. Therefore, DUOX1 (and maybe also DUOX2) also oxidizes NADPH to produce H₂O₂. To date, in the studies of DUOX1 and DUOX2, H₂O₂ production is generally used to indicate their enzyme activity. However, in cell-based experiments, it is not possible to distinguish which substrate is consumed. It is the first time, in this study, that their enzyme activity was compared for NADPH and NAADPH as substrates: DUOX1 significantly preferred NADPH over NAADPH, while DUOX2 showed comparable activity for both substrates. From previous observations, we know that i) DUOX1 and DUOX2 produce more H₂O₂ when intracellular Ca²⁺ concentration elevates (Rigutto et al., 2009), ii) and DUOX1 exhibits a conformational change at different Ca²⁺ concentrations (Wu et al., 2021), iii) and that, in addition, cAMP-dependent PKA and PKC further increase H₂O₂ generation by DUOX1 and DUOX2, respectively, in Cos-7 cells (Rigutto et al., 2009). Whether their enzyme activity for NADPH and NAADPH alters at different Ca²⁺ concentrations or in the presence of protein kinases will be very meaningful to be further investigated.

Although DUOX1 and DUOX2 share 83% similarity at the sequence level (De Deken et al., 2000), they appear to play distinct biological roles, for example, in congenital hypothyroidism (reviewed in Buvelot et al., 2019), and in the Ca²⁺ signaling in CD4⁺ T cells, as shown in this study. So far, only the cryo-EM structure of the DUOX1/DUOXA1 complex has been elucidated (Sun, 2020; Wu et al., 2021). It is unclear whether DUOX1 and DUOX2 have different activation mechanisms upon T cell activation, e.g., phosphorylation by protein kinases, or different structures, or both, such that they have different substrate preferences and affect Ca²⁺ signaling differently.

5.4.2. Endogenous NAADPH pool in T cells

The generation of NAADP by DUOX isozymes points out an endogenous NAADPH pool in T cells. NADP and its reduced form are critical for cellular redox metabolism. The cytosolic NADPH/NADP ratio was determined to be approximately 20 in *Saccharomyces cerevisiae*, a species of yeast (Zhang et al., 2015) and this ratio was calculated to be 85 to 100 in the cytoplasm of rat liver (Veech et al., 1969). If NAADPH and NAADP have the same ratio, the cytosolic NAADPH should be in the nanomolar range, given that the basal concentration of NAADP in Jurkat T cells is 4.4 ± 1.5 nM (Gasser et al., 2006). Therefore, a sensitive method will be required to investigate the endogenous NAADPH pool. The enzymatic cycling assay has a low detection limit for measuring endogenous NAADP in the low nanomolar range (Gasser et al., 2006). In addition, NAADP and NAADPH can be separated by anion exchange column (see methods and materials section 3.11.). It is possible to detect and quantify the endogenous NAADPH pool in Jurkat T cells by using a modified enzymatic cycling assay. The modification could be, for instance, a reducing condition during the sample preparation to protect the endogenous NAADPH from spontaneous oxidation.

NAADP-induced Ca^{2+} signaling is essential for T cell activation and downstream events (reviewed in Guse and Wolf, 2016; Wolf and Guse, 2017). Moreover, NAADP also functions as a trigger to stimulate Ca^{2+} signaling in many other cells (reviewed in Guse and Lee, 2008). The cytosolic NAADPH pool has to be maintained in non-stimulated cells for the rapid NAADP synthesis upon stimulation. It is known that CD38 and alkaline phosphatase consume NAADP (Graeff et al., 2006; Schmid et al., 2012, 2011). Therefore, theoretically, there must be enzymes that provide NAADPH without the requirement for stimulation. The modified enzymatic cycling assay could also be a solution to investigate this question.

5.4.3. NOX/DUOX as NAADP forming enzyme in other cell types

The NAADP synthesis by DUOX isozymes observed in this study provides a new perspective on whether they also function as NAADP forming enzymes in other cells. So far, only NOX5, DUOX1, and DUOX2 have been investigated in the cell-free system that they can oxidize NAADPH under physiological conditions (in this study and Gu et al., 2021). Based on the highly

conserved catalytic core in this family, as shown in Fig. 3, all the isozymes are likely capable of oxidizing NAADPH.

In the absence of NOX4, decreased Ca^{2+} signaling was observed in IL-8-treated LAK cells, and researchers came to the conclusion that NOX4-derived H_2O_2 oxidizes and activates type III CD38, which subsequently generates cADPR (Park et al., 2019). The same group also reported that CD38 is responsible for the synthesis of NAADP in LAK cells (Nam et al., 2020; Rah et al., 2010). A similar phenotype, i.e., decreased cytosolic Ca^{2+} concentration in the absence of NOX4, was observed in skeletal muscle myocytes. This led to the conclusion of a similar mechanism: oxidative modification of RyR1 by NOX4-derived H_2O_2 . Furthermore, enhancement of mitochondrial ROS production and inhibition of xanthine oxidase have no effect on RyR1 activity in SR vesicles (Sun et al., 2011). Xanthine oxidase is another source of intracellular ROS (Ardan et al., 2004; McNally et al., 2003). Despite the fact that different cell types have distinct Ca^{2+} signaling networks, for instance, cADPR is produced earlier and Ca^{2+} release evoked by InsP_3 or cADPR is required for NAADP production in LAK cells (Rah et al., 2010), it would be worthwhile to investigate further whether NOX4 can directly synthesize NAADP and, as a result, its absence reduces the Ca^{2+} signals. Furthermore, pharmacological inhibitors have been used in some studies to distinguish the isozymes of this family. However, to date, there is no selective inhibitor. Moreover, many inhibitors have ROS scavenging and redox activity (reviewed in Altenhöfer et al., 2015; Reis et al., 2020). Whether DUOX isozymes also contribute to the phenotypes reported previously may be also an interesting point to be followed.

Additionally, the phenotype in global Ca^{2+} signals in the absence of NOX4 in skeletal muscle myocytes is almost abolished at 1% O_2 , which demonstrates a physiological role of NOX4 in regulating skeletal muscle cells at different O_2 concentrations, for instance, before and after exercise (Sun et al., 2011). This observation may also indicate that the NOX/DUOX family plays a critical role in T cell activation by sensing O_2 concentrations in different tissues, altering NAADP and ROS generation, and consequently regulating T cell activation at different physiological O_2 concentrations, which merits further investigation.

6. References

- Aarhus, R., Dickey, D.M., Graeff, R.M., Gee, K.R., Walseth, T.F., Lee, H.C., 1996. Activation and Inactivation of Ca Release by NAADP(*). *J. Biol. Chem.* 271, 8513–8516. <https://doi.org/10.1074/jbc.271.15.8513>
- Aarhus, R., Graeff, R.M., Dickey, D.M., Walseth, T.F., Hon, C.L., 1995. ADP-ribosyl Cyclase and CD38 Catalyze the Synthesis of a Calcium-mobilizing Metabolite from NADP+(*). *J. Biol. Chem.* 270, 30327–30333. <https://doi.org/10.1074/jbc.270.51.30327>
- Alberts, B., Johnson, A., Lewis, J., Raff, M., Roberts, K., Walter, P., 2002. *Helper T Cells and Lymphocyte Activation*. *Mol. Biol. Cell* 4th Ed.
- Al-Essa, M., Dhaunsi, G.S., Al-Qabandi, W., Khan, I., 2013. Impaired NADPH oxidase activity in peripheral blood lymphocytes of galactosemia patients. *Exp. Biol. Med.* 238, 779–786. <https://doi.org/10.1177/1535370213480692>
- Ali, R.A., Camick, C., Wiles, K., Walseth, T.F., Slama, J.T., Bhattacharya, S., Giovannucci, D.R., Wall, K.A., 2016. Nicotinic Acid Adenine Dinucleotide Phosphate Plays a Critical Role in Naive and Effector Murine T Cells but Not Natural Regulatory T Cells. *J. Biol. Chem.* 291, 4503–4522. <https://doi.org/10.1074/jbc.M115.681833>
- Altenhöfer, S., Radermacher, K.A., Kleikers, P.W.M., Wingler, K., Schmidt, H.H.H.W., 2015. Evolution of NADPH Oxidase Inhibitors: Selectivity and Mechanisms for Target Engagement. *Antioxid. Redox Signal.* 23, 406–427. <https://doi.org/10.1089/ars.2013.5814>
- Ameziane-El-Hassani, R., Morand, S., Boucher, J.-L., Frapart, Y.-M., Apostolou, D., Agnandji, D., Gnidehou, S., Ohayon, R., Noël-Hudson, M.-S., Francon, J., Lalaoui, K., Virion, A., Dupuy, C., 2005. Dual Oxidase-2 Has an Intrinsic Ca²⁺-dependent H₂O₂-generating Activity. *J. Biol. Chem.* 280, 30046–30054. <https://doi.org/10.1074/jbc.M500516200>
- Arđan, T., Kovačeva, J., Čejková, J., 2004. Comparative histochemical and immunohistochemical study on xanthine oxidoreductase/xanthine oxidase in mammalian corneal epithelium. *Acta Histochem.* 106, 69–75.

References

- <https://doi.org/10.1016/j.acthis.2003.08.001>
- Augsburger, F., Rasti, D., Cambet, Y., Jaquet, V., 2019. NOX5 Cell-Free Assay for the High-Throughput Screening of Small Molecules, in: Knaus, U.G., Leto, T.L. (Eds.), *NADPH Oxidases: Methods and Protocols*, Methods in Molecular Biology. Springer, New York, NY, pp. 103–111. https://doi.org/10.1007/978-1-4939-9424-3_6
- Avdonin, P.V., Nadeev, A.D., Tsitrin, E.B., Tsitrina, A.A., Avdonin, P.P., Mironova, G.Yu., Zharkikh, I.L., Goncharov, N.V., 2017. Involvement of two-pore channels in hydrogen peroxide-induced increase in the level of calcium ions in the cytoplasm of human umbilical vein endothelial cells. *Dokl. Biochem. Biophys.* 474, 209–212. <https://doi.org/10.1134/S1607672917030152>
- Aycan, Z., Cangul, H., Muzza, M., Bas, V.N., Fugazzola, L., Chatterjee, V.K., Persani, L., Schoenmakers, N., 2017. Digenic DUOX1 and DUOX2 Mutations in Cases With Congenital Hypothyroidism. *J. Clin. Endocrinol. Metab.* 102, 3085–3090. <https://doi.org/10.1210/jc.2017-00529>
- Bánfi, B., Clark, R.A., Steger, K., Krause, K.-H., 2003. Two Novel Proteins Activate Superoxide Generation by the NADPH Oxidase NOX1*. *J. Biol. Chem.* 278, 3510–3513. <https://doi.org/10.1074/jbc.C200613200>
- Bánfi, B., Molnár, G., Maturana, A., Steger, K., Hegedűs, B., Demaurex, N., Krause, K.-H., 2001. A Ca²⁺-activated NADPH Oxidase in Testis, Spleen, and Lymph Nodes *. *J. Biol. Chem.* 276, 37594–37601. <https://doi.org/10.1074/jbc.M103034200>
- Bánfi, B., Tirone, F., Durussel, I., Knisz, J., Moskwa, P., Molnár, G.Z., Krause, K.-H., Cox, J.A., 2004. Mechanism of Ca²⁺ Activation of the NADPH Oxidase 5 (NOX5). *J. Biol. Chem.* 279, 18583–18591. <https://doi.org/10.1074/jbc.M310268200>
- Bedard, K., Krause, K.-H., 2007. The NOX Family of ROS-Generating NADPH Oxidases: Physiology and Pathophysiology. *Physiol. Rev.* 87, 245–313. <https://doi.org/10.1152/physrev.00044.2005>
- Belarbi, K., Cuvelier, E., Destée, A., Gressier, B., Chartier-Harlin, M.-C., 2017. NADPH oxidases in Parkinson's disease: a systematic review. *Mol. Neurodegener.* 12, 84.

References

- <https://doi.org/10.1186/s13024-017-0225-5>
- Berard, M., Tough, D.F., 2002. Qualitative differences between naïve and memory T cells. *Immunology* 106, 127–138. <https://doi.org/10.1046/j.1365-2567.2002.01447.x>
- Berg, I., Potter, B.V.L., Mayr, G.W., Guse, A.H., 2000. Nicotinic Acid Adenine Dinucleotide Phosphate (Naadp+) Is an Essential Regulator of T-Lymphocyte Ca²⁺-Signaling. *J. Cell Biol.* 150, 581–588.
- Berridge, G., Cramer, R., Galione, A., Patel, S., 2002. Metabolism of the novel Ca²⁺-mobilizing messenger nicotinic acid-adenine dinucleotide phosphate via a 2'-specific Ca²⁺-dependent phosphatase. *Biochem. J.* 365, 295–301. <https://doi.org/10.1042/BJ20020180>
- Berridge, M.J., 2016. The Inositol Trisphosphate/Calcium Signaling Pathway in Health and Disease. *Physiol. Rev.* 96, 1261–1296. <https://doi.org/10.1152/physrev.00006.2016>
- Bienert, G.P., Chaumont, F., 2014. Aquaporin-facilitated transmembrane diffusion of hydrogen peroxide. *Biochim. Biophys. Acta BBA - Gen. Subj., Aquaporins* 1840, 1596–1604. <https://doi.org/10.1016/j.bbagen.2013.09.017>
- Billington, R.A., Thuring, J.W., Conway, S.J., Packman, L., Holmes, A.B., Genazzani, A.A., 2004. Production and characterization of reduced NAADP (nicotinic acid-adenine dinucleotide phosphate). *Biochem. J.* 378, 275–280. <https://doi.org/10.1042/BJ20031284>
- Boraso, A., Williams, A.J., 1994. Modification of the gating of the cardiac sarcoplasmic reticulum Ca(2+)-release channel by H₂O₂ and dithiothreitol. *Am. J. Physiol.-Heart Circ. Physiol.* 267, H1010–H1016. <https://doi.org/10.1152/ajpheart.1994.267.3.H1010>
- Brock, V.J., Wolf, I.M.A., Er-Lukowiak, M., Lory, N., Stähler, T., Woelk, L.-M., Mittrücker, H.-W., Müller, C.E., Koch-Nolte, F., Rissiek, B., Werner, R., Guse, A.H., Diercks, B.-P., 2022. P2X₄ and P2X₇ are essential players in basal T cell activity and Ca²⁺ signaling milliseconds after T cell activation. *Sci. Adv.* 8, eabl9770. <https://doi.org/10.1126/sciadv.abl9770>

References

- Buvelot, H., Jaquet, V., Krause, K.-H., 2019. Mammalian NADPH Oxidases, in: Knaus, U.G., Leto, T.L. (Eds.), *NADPH Oxidases, Methods in Molecular Biology*. Springer New York, New York, NY, pp. 17–36. https://doi.org/10.1007/978-1-4939-9424-3_2
- Bylund, J., Goldblatt, D., Speert, D.P., 2005. Chronic Granulomatous Disease: From Genetic Defect to Clinical Presentation, in: Pollard, A.J., Finn, A. (Eds.), *Hot Topics in Infection and Immunity in Children II, Advances in Experimental Medicine and Biology*. Springer US, Boston, MA, pp. 67–87. https://doi.org/10.1007/0-387-25342-4_5
- Cancela, J.M., Churchill, G.C., Galione, A., 1999. Coordination of agonist-induced Ca²⁺-signalling patterns by NAADP in pancreatic acinar cells. *Nature* 398, 74–76. <https://doi.org/10.1038/18032>
- Charles A Janeway, J., Travers, P., Walport, M., Shlomchik, M.J., 2001. *T Cell-Mediated Immunity. Immunobiol. Immune Syst. Health Dis.* 5th Ed.
- Chen, F., Yu, Y., Haigh, S., Johnson, J., Lucas, R., Stepp, D.W., Fulton, D.J.R., 2014. Regulation of NADPH Oxidase 5 by Protein Kinase C Isoforms. *PLoS ONE* 9. <https://doi.org/10.1371/journal.pone.0088405>
- Chen, J., Guan, L., Tang, L., Liu, S., Zhou, Y., Chen, C., He, Z., Xu, L., 2019. T Helper 9 Cells: A New Player in Immune-Related Diseases. *DNA Cell Biol.* 38, 1040–1047. <https://doi.org/10.1089/dna.2019.4729>
- Cheng, G., Cao, Z., Xu, X., Meir, E.G.V., Lambeth, J.D., 2001. Homologs of gp91phox: cloning and tissue expression of Nox3, Nox4, and Nox5. *Gene* 269, 131–140. [https://doi.org/10.1016/S0378-1119\(01\)00449-8](https://doi.org/10.1016/S0378-1119(01)00449-8)
- Clark, R.A., Leidal, K.G., Pearson, D.W., Nauseef, W.M., 1987. NADPH oxidase of human neutrophils. Subcellular localization and characterization of an arachidonate-activatable superoxide-generating system. *J. Biol. Chem.* 262, 4065–4074. [https://doi.org/10.1016/S0021-9258\(18\)61312-2](https://doi.org/10.1016/S0021-9258(18)61312-2)
- Cockayne, D.A., Muchamuel, T., Grimaldi, J.C., Muller-Steffner, H., Randall, T.D., Lund, F.E., Murray, R., Schuber, F., Howard, M.C., 1998. Mice Deficient for the Ecto-Nicotinamide Adenine Dinucleotide Glycohydrolase CD38 Exhibit Altered Humoral Immune

References

- Responses. *Blood* 92, 1324–1333. <https://doi.org/10.1182/blood.V92.4.1324>
- Cordiglieri, C., Odoardi, F., Zhang, B., Nebel, M., Kawakami, N., Klinkert, W.E.F., Lodygin, D., Lühder, F., Breunig, E., Schild, D., Ulaganathan, V.K., Dornmair, K., Dammermann, W., Potter, B.V.L., Guse, A.H., Flügel, A., 2010. Nicotinic acid adenine dinucleotide phosphate-mediated calcium signalling in effector T cells regulates autoimmunity of the central nervous system. *Brain* 133, 1930–1943. <https://doi.org/10.1093/brain/awq135>
- Cosker, F., Cheviron, N., Yamasaki, M., Menteyne, A., Lund, F.E., Moutin, M.-J., Galione, A., Cancela, J.-M., 2010. The Ecto-enzyme CD38 Is a Nicotinic Acid Adenine Dinucleotide Phosphate (NAADP) Synthase That Couples Receptor Activation to Ca²⁺ Mobilization from Lysosomes in Pancreatic Acinar Cells. *J. Biol. Chem.* 285, 38251–38259. <https://doi.org/10.1074/jbc.M110.125864>
- Croft, M., 1994. Activation of naive, memory and effector T cells. *Curr. Opin. Immunol.* 6, 431–437. [https://doi.org/10.1016/0952-7915\(94\)90123-6](https://doi.org/10.1016/0952-7915(94)90123-6)
- Dammermann, W., Zhang, B., Nebel, M., Cordiglieri, C., Odoardi, F., Kirchberger, T., Kawakami, N., Dowden, J., Schmid, F., Dornmair, K., Hohenegger, M., Flügel, A., Guse, A.H., Potter, B.V.L., 2009. NAADP-mediated Ca²⁺ signaling via type 1 ryanodine receptor in T cells revealed by a synthetic NAADP antagonist. *Proc. Natl. Acad. Sci.* 106, 10678–10683. <https://doi.org/10.1073/pnas.0809997106>
- De Deken, X., Wang, D., Many, M.-C., Costagliola, S., Libert, F., Vassart, G., Dumont, J.E., Miot, F., 2000. Cloning of Two Human Thyroid cDNAs Encoding New Members of the NADPH Oxidase Family*. *J. Biol. Chem.* 275, 23227–23233. <https://doi.org/10.1074/jbc.M000916200>
- Di Marzo, N., Chisci, E., Giovannoni, R., 2018. The Role of Hydrogen Peroxide in Redox-Dependent Signaling: Homeostatic and Pathological Responses in Mammalian Cells. *Cells* 7, 156. <https://doi.org/10.3390/cells7100156>
- Diercks, B.-P., Werner, R., Schetelig, D., Wolf, I.M.A., Guse, A.H., 2019. High-Resolution Calcium Imaging Method for Local Calcium Signaling, in: Heizmann, C.W. (Ed.), *Calcium-Binding Proteins of the EF-Hand Superfamily: From Basics to Medical*

References

- Applications, *Methods in Molecular Biology*. Springer, New York, NY, pp. 27–39.
https://doi.org/10.1007/978-1-4939-9030-6_3
- Diercks, B.-P., Werner, R., Weidemüller, P., Czarniak, F., Hernandez, L., Lehmann, C., Rosche, A., Krüger, A., Kaufmann, U., Vaeth, M., Failla, A.V., Zobiak, B., Kandil, F.I., Schetelig, D., Ruthenbeck, A., Meier, C., Lodygin, D., Flügel, A., Ren, D., Wolf, I.M.A., Feske, S., Guse, A.H., 2018. ORAI1, STIM1/2, and RYR1 shape subsecond Ca²⁺ microdomains upon T cell activation. *Sci. Signal.* 11. <https://doi.org/10.1126/scisignal.aat0358>
- Eagar, T.N., Miller, S.D., 2019. 16 - Helper T-Cell Subsets and Control of the Inflammatory Response, in: Rich, R.R., Fleisher, T.A., Shearer, W.T., Schroeder, H.W., Frew, A.J., Weyand, C.M. (Eds.), *Clinical Immunology (Fifth Edition)*. Elsevier, London, pp. 235-245.e1. <https://doi.org/10.1016/B978-0-7020-6896-6.00016-8>
- Fang, C., Li, T., Li, Y., Xu, G.J., Deng, Q.W., Chen, Y.J., Hou, Y.N., Lee, H.C., Zhao, Y.J., 2018. CD38 produces nicotinic acid adenosine dinucleotide phosphate in the lysosome. *J. Biol. Chem.* 293, 8151–8160. <https://doi.org/10.1074/jbc.RA118.002113>
- Fazilleau, N., Mark, L., McHeyzer-Williams, L.J., McHeyzer-Williams, M.G., 2009. FOLLICULAR HELPER T CELLS: LINEAGE AND LOCATION. *Immunity* 30, 324–335. <https://doi.org/10.1016/j.immuni.2009.03.003>
- Feske, S., 2013. Ca²⁺ Influx in T Cells: How Many Ca²⁺ Channels? *Front. Immunol.* 0. <https://doi.org/10.3389/fimmu.2013.00099>
- Feske, S., 2007. Calcium signalling in lymphocyte activation and disease. *Nat. Rev. Immunol.* 7, 690–702. <https://doi.org/10.1038/nri2152>
- Fliegert, R., Bauche, A., Wolf Pérez, A.-M., Watt, J.M., Rozewitz, M.D., Winzer, R., Janus, M., Gu, F., Rosche, A., Harneit, A., Flato, M., Moreau, C., Kirchberger, T., Wolters, V., Potter, B.V.L., Guse, A.H., 2017. 2'-Deoxyadenosine 5'-diphosphoribose is an endogenous TRPM2 superagonist. *Nat. Chem. Biol.* 13, 1036–1044. <https://doi.org/10.1038/nchembio.2415>
- Flügel, A., Willem, M., Berkowicz, T., Wekerle, H., 1999. Gene transfer into CD4⁺ T lymphocytes: Green fluorescent protein-engineered, encephalitogenic T cells illuminate

References

- brain autoimmune responses. *Nat. Med.* 5, 843–847. <https://doi.org/10.1038/10567>
- Gasser, A., Bruhn, S., Guse, A.H., 2006. Second Messenger Function of Nicotinic Acid Adenine Dinucleotide Phosphate Revealed by an Improved Enzymatic Cycling Assay. *J. Biol. Chem.* 281, 16906–16913. <https://doi.org/10.1074/jbc.M601347200>
- Gavazzi, G., Banfi, B., Deffert, C., Fiette, L., Schappi, M., Herrmann, F., Krause, K.-H., 2006. Decreased blood pressure in NOX1-deficient mice. *FEBS Lett.* 580, 497–504. <https://doi.org/10.1016/j.febslet.2005.12.049>
- Geiszt, M., Lekstrom, K., Witta, J., Leto, T.L., 2003. Proteins Homologous to p47phox and p67phox Support Superoxide Production by NAD(P)H Oxidase 1 in Colon Epithelial Cells *. *J. Biol. Chem.* 278, 20006–20012. <https://doi.org/10.1074/jbc.M301289200>
- Genazzani, A.A., Empson, R.M., Galione, A., 1996. Unique Inactivation Properties of NAADP-sensitive Ca²⁺ Release (*). *J. Biol. Chem.* 271, 11599–11602. <https://doi.org/10.1074/jbc.271.20.11599>
- Graeff, R., Lee, H.C., 2002. A novel cycling assay for nicotinic acid-adenine dinucleotide phosphate with nanomolar sensitivity. *Biochem. J.* 367, 163–168. <https://doi.org/10.1042/BJ20020644>
- Graeff, R., Liu, Q., Kriksunov, I.A., Hao, Q., Lee, H.C., 2006. Acidic Residues at the Active Sites of CD38 and ADP-ribosyl Cyclase Determine Nicotinic Acid Adenine Dinucleotide Phosphate (NAADP) Synthesis and Hydrolysis Activities. *J. Biol. Chem.* 281, 28951–28957. <https://doi.org/10.1074/jbc.M604370200>
- Grasberger, H., De Deken, X., Mayo, O.B., Raad, H., Weiss, M., Liao, X.-H., Refetoff, S., 2012. Mice Deficient in Dual Oxidase Maturation Factors Are Severely Hypothyroid. *Mol. Endocrinol.* 26, 481–492. <https://doi.org/10.1210/me.2011-1320>
- Grasberger, H., El-Zaatari, M., Merchant, J.L., 2013. Dual Oxidases Control Release of Hydrogen Peroxide by the Gastric Epithelium to Prevent *Helicobacter felis* Infection and Inflammation in Mice. *Gastroenterology* 145, 1045–1054. <https://doi.org/10.1053/j.gastro.2013.07.011>

References

- Grasberger, H., Refetoff, S., 2006. Identification of the Maturation Factor for Dual Oxidase: EVOLUTION OF AN EUKARYOTIC OPERON EQUIVALENT*,. *J. Biol. Chem.* 281, 18269–18272. <https://doi.org/10.1074/jbc.C600095200>
- Grynkiewicz, G., Poenie, M., Tsien, R.Y., 1985. A new generation of Ca²⁺ indicators with greatly improved fluorescence properties. *J. Biol. Chem.* 260, 3440–3450. [https://doi.org/10.1016/S0021-9258\(19\)83641-4](https://doi.org/10.1016/S0021-9258(19)83641-4)
- Gu, F., Krüger, A., Roggenkamp, H.G., Alpers, R., Lodygin, D., Jaquet, V., Möckl, F., Hernandez C., L.C., Winterberg, K., Bauche, A., Rosche, A., Grasberger, H., Kao, J.Y., Schetelig, D., Werner, R., Schröder, K., Carty, M., Bowie, A.G., Huber, S., Meier, C., Mittrücker, H.-W., Heeren, J., Krause, K.-H., Flügel, A., Diercks, B.-P., Guse, A.H., 2021. Dual NADPH oxidases DUOX1 and DUOX2 synthesize NAADP and are necessary for Ca²⁺ signaling during T cell activation. *Sci. Signal.* 14, eabe3800. <https://doi.org/10.1126/scisignal.abe3800>
- Gunaratne, G.S., Brailoiu, E., He, S., Unterwald, E.M., Patel, S., Slama, J.T., Walseth, T.F., Marchant, J.S., 2021. Essential requirement for JPT2 in NAADP-evoked Ca²⁺ signaling. *Sci. Signal.* 14. <https://doi.org/10.1126/scisignal.abd5605>
- Guse, A.H., da Silva, C.P., Berg, I., Skapenko, A.L., Weber, K., Heyer, P., Hohenegger, M., Ashamu, G.A., Schulze-Koops, H., Potter, B.V.L., Mayr, G.W., 1999. Regulation of calcium signalling in T lymphocytes by the second messenger cyclic ADP-ribose. *Nature* 398, 70–73. <https://doi.org/10.1038/18024>
- Guse, A.H., da Silva, C.P., Potter, B.V., Mayr, G.W., 1997. Ca(2+)-signalling in human T-lymphocytes. Potential roles for cyclic ADP-ribose and 2'-phospho-cyclic ADP-ribose. *Adv. Exp. Med. Biol.* 419, 431–436.
- Guse, A.H., Diercks, B., 2018. Integration of nicotinic acid adenine dinucleotide phosphate (NAADP)-dependent calcium signalling. *J. Physiol.* 596, 2735–2743. <https://doi.org/10.1113/JP275974>
- Guse, A.H., Ernst, I.M.A., Fliegert, R., 2013. NAADP Signaling Revisited. *Curr. Top. Med. Chem.* 13, 2978–2990.

References

- Guse, A.H., Lee, H.C., 2008. NAADP: A Universal Ca²⁺ Trigger. *Sci Signal* 1, re10–re10. <https://doi.org/10.1126/scisignal.144re10>
- Guse, A.H., Roth, E., Emmrich, F., 1993. Intracellular Ca²⁺ pools in Jurkat T-lymphocytes. *Biochem. J.* 291, 447–451.
- Guse, A.H., Wolf, I.M.A., 2016. Ca²⁺ microdomains, NAADP and type 1 ryanodine receptor in cell activation. *Biochim. Biophys. Acta BBA - Mol. Cell Res., Calcium and Cell Fate* 1863, 1379–1384. <https://doi.org/10.1016/j.bbamcr.2016.01.014>
- Han, H., Wei, R., Lai, A.F., Yin, C., 2006. Molecular nature of sulfhydryl modification by hydrogen peroxide on type 1 ryanodine receptor1. *Acta Pharmacol. Sin.* 27, 888–894. <https://doi.org/10.1111/j.1745-7254.2006.00386.x>
- Hara-Chikuma, M., Chikuma, S., Sugiyama, Y., Kabashima, K., Verkman, A.S., Inoue, S., Miyachi, Y., 2012. Chemokine-dependent T cell migration requires aquaporin-3-mediated hydrogen peroxide uptake. *J. Exp. Med.* 209, 1743–1752. <https://doi.org/10.1084/jem.20112398>
- Hofstetter, A.R., Cruz, J.A.D.L., Cao, W., Patel, J., Belser, J.A., McCoy, J., Liepkalns, J.S., Amoah, S., Cheng, G., Ranjan, P., Diebold, B.A., Shieh, W.-J., Zaki, S., Katz, J.M., Sambhara, S., Lambeth, J.D., Gangappa, S., 2016. NADPH Oxidase 1 Is Associated with Altered Host Survival and T Cell Phenotypes after Influenza A Virus Infection in Mice. *PLOS ONE* 11, e0149864. <https://doi.org/10.1371/journal.pone.0149864>
- Howard, M., Grimaldi, J.C., Bazan, J.F., Lund, F.E., Santos-Argumedo, L., Parkhouse, R.M.E., Walseth, T.F., Lee, H.C., 1993. Formation and Hydrolysis of Cyclic ADP-Ribose Catalyzed by Lymphocyte Antigen CD38. *Science* 262, 1056–1059.
- Hwang, J.-R., Byeon, Y., Kim, D., Park, S.-G., 2020. Recent insights of T cell receptor-mediated signaling pathways for T cell activation and development. *Exp. Mol. Med.* 52, 750–761. <https://doi.org/10.1038/s12276-020-0435-8>
- Jackson, D.G., Bell, J.I., 1990. Isolation of a cDNA encoding the human CD38 (T10) molecule, a cell surface glycoprotein with an unusual discontinuous pattern of expression during lymphocyte differentiation. *J. Immunol.* 144, 2811–2815.

References

- Jackson, S.H., Devadas, S., Kwon, J., Pinto, L.A., Williams, M.S., 2004. T cells express a phagocyte-type NADPH oxidase that is activated after T cell receptor stimulation. *Nat. Immunol.* 5, 818–827. <https://doi.org/10.1038/ni1096>
- Jagnandan, D., Church, J.E., Banfi, B., Stuehr, D.J., Marrero, M.B., Fulton, D.J.R., 2007. Novel Mechanism of Activation of NADPH Oxidase 5: CALCIUM SENSITIZATION VIA PHOSPHORYLATION *. *J. Biol. Chem.* 282, 6494–6507. <https://doi.org/10.1074/jbc.M608966200>
- Kawahara, T., Quinn, M.T., Lambeth, J.D., 2007. Molecular evolution of the reactive oxygen-generating NADPH oxidase (Nox/Duox) family of enzymes. *BMC Evol. Biol.* 7, 109. <https://doi.org/10.1186/1471-2148-7-109>
- Kesarwani, P., Murali, A.K., Al-Khami, A.A., Mehrotra, S., 2013. Redox Regulation of T-Cell Function: From Molecular Mechanisms to Significance in Human Health and Disease. *Antioxid. Redox Signal.* 18, 1497–1534. <https://doi.org/10.1089/ars.2011.4073>
- Komiyama, Y., Nakae, S., Matsuki, T., Nambu, A., Ishigame, H., Kakuta, S., Sudo, K., Iwakura, Y., 2006. IL-17 Plays an Important Role in the Development of Experimental Autoimmune Encephalomyelitis. *J. Immunol.* 177, 566–573. <https://doi.org/10.4049/jimmunol.177.1.566>
- Kunerth, S., Langhorst, M.F., Schwarzmann, N., Gu, X., Huang, L., Yang, Z., Zhang, Liangren, Mills, S.J., Zhang, Li-he, Potter, B.V.L., Guse, A.H., 2004. Amplification and propagation of pacemaker Ca²⁺ signals by cyclic ADP-ribose and the type 3 ryanodine receptor in T cells. *J. Cell Sci.* 117, 2141–2149. <https://doi.org/10.1242/jcs.01063>
- Kwon, J., Devadas, S., Williams, M.S., 2003. T cell receptor-stimulated generation of hydrogen peroxide inhibits MEK-ERK activation and Ick serine phosphorylation. *Free Radic. Biol. Med.* 35, 406–417. [https://doi.org/10.1016/S0891-5849\(03\)00318-6](https://doi.org/10.1016/S0891-5849(03)00318-6)
- Kwon, J., Shatynski, K.E., Chen, H., Morand, S., de Deken, X., Miot, F., Leto, T.L., Williams, M.S., 2010. The Nonphagocytic NADPH Oxidase Duox1 Mediates a Positive Feedback Loop During T Cell Receptor Signaling. *Sci. Signal.* 3, ra59. <https://doi.org/10.1126/scisignal.2000976>

References

- Lambeth, J.D., Kawahara, T., Diebold, B., 2007. Regulation of Nox and Duox Enzymatic Activity and Expression. *Free Radic. Biol. Med.* 43, 319–331. <https://doi.org/10.1016/j.freeradbiomed.2007.03.028>
- Langhorst, M.F., Schwarzmann, N., Guse, A.H., 2004. Ca²⁺ release via ryanodine receptors and Ca²⁺ entry: major mechanisms in NAADP-mediated Ca²⁺ signaling in T-lymphocytes. *Cell. Signal.* 16, 1283–1289. <https://doi.org/10.1016/j.cellsig.2004.03.013>
- Lee, H.C., Aarhus, R., 1995. A Derivative of NADP Mobilizes Calcium Stores Insensitive to Inositol Trisphosphate and Cyclic ADP-ribose (*). *J. Biol. Chem.* 270, 2152–2157. <https://doi.org/10.1074/jbc.270.5.2152>
- Lee, H.C., Zhao, Y.J., 2019. Resolving the topological enigma in Ca²⁺ signaling by cyclic ADP-ribose and NAADP. *J. Biol. Chem.* 294, 19831–19843. <https://doi.org/10.1074/jbc.REV119.009635>
- Lerner, F., Niere, M., Ludwig, A., Ziegler, M., 2001. Structural and Functional Characterization of Human NAD Kinase. *Biochem. Biophys. Res. Commun.* 288, 69–74. <https://doi.org/10.1006/bbrc.2001.5735>
- Lu, W.J., Li, J.Y., Chen, R.J., Huang, L.T., Lee, T.Y., Lin, K.H., 2019. VAS2870 and VAS3947 attenuate platelet activation and thrombus formation via a NOX-independent pathway downstream of PKC. *Sci. Rep.* 9, 18852. <https://doi.org/10.1038/s41598-019-55189-5>
- Mándi, M., Tóth, B., Timár, G., Bak, J., 2006. Ca²⁺ release triggered by NAADP in hepatocyte microsomes. *Biochem. J.* 395, 233–238. <https://doi.org/10.1042/BJ20051002>
- Masgrau, R., Churchill, G.C., Morgan, A.J., Ashcroft, S.J.H., Galione, A., 2003. NAADP: A New Second Messenger for Glucose-Induced Ca²⁺ Responses in Clonal Pancreatic β Cells. *Curr. Biol.* 13, 247–251. [https://doi.org/10.1016/S0960-9822\(03\)00041-1](https://doi.org/10.1016/S0960-9822(03)00041-1)
- McKinstry, K.K., Strutt, T.M., Swain, S.L., 2010. Regulation of CD4⁺ T-cell contraction during pathogen challenge. *Immunol. Rev.* 236, 110–124. <https://doi.org/10.1111/j.1600-065X.2010.00921.x>
- McLennan, H.R., Esposti, M.D., 2000. The Contribution of Mitochondrial Respiratory

References

- Complexes to the Production of Reactive Oxygen Species 10.
- McNally, J.S., Davis, M.E., Giddens, D.P., Saha, A., Hwang, J., Dikalov, S., Jo, H., Harrison, D.G., 2003. Role of xanthine oxidoreductase and NAD(P)H oxidase in endothelial superoxide production in response to oscillatory shear stress. *Am. J. Physiol.-Heart Circ. Physiol.* 285, H2290–H2297. <https://doi.org/10.1152/ajpheart.00515.2003>
- Moon, C., Rousseau, R., Soria, J.-C., Hoque, M.O., Lee, J., Jang, S.J., Trink, B., Sidransky, D., Mao, L., 2004. Aquaporin expression in human lymphocytes and dendritic cells. *Am. J. Hematol.* 75, 128–133. <https://doi.org/10.1002/ajh.10476>
- Morand, S., Ueyama, T., Tsujibe, S., Saito, N., Korzeniowska, A., Leto, T.L., 2009. Duox maturation factors form cell surface complexes with Duox affecting the specificity of reactive oxygen species generation. *FASEB J.* 23, 1205–1218. <https://doi.org/10.1096/fj.08-120006>
- Moreschi, I., Bruzzone, S., Melone, L., De Flora, A., Zocchi, E., 2006. NAADP⁺ synthesis from cADPRP and nicotinic acid by ADP-ribosyl cyclases. *Biochem. Biophys. Res. Commun.* 345, 573–580. <https://doi.org/10.1016/j.bbrc.2006.04.096>
- Nam, T.-S., Park, D.-R., Rah, S.-Y., Woo, T.-G., Chung, H.T., Brenner, C., Kim, U.-H., 2020. Interleukin-8 drives CD38 to form NAADP from NADP⁺ and NAAD in the endolysosomes to mobilize Ca²⁺ and effect cell migration. *FASEB J.* 34, 12565–12576. <https://doi.org/10.1096/fj.202001249R>
- Nawrocki, M., Lory, N., Bedke, T., Stumme, F., Diercks, B.-P., Guse, A.H., Meier, C., Gagliani, N., Mittrücker, H.-W., Huber, S., 2021. Trans-Ned 19-Mediated Antagonism of Nicotinic Acid Adenine Nucleotide—Mediated Calcium Signaling Regulates Th17 Cell Plasticity in Mice. *Cells* 10, 3039. <https://doi.org/10.3390/cells10113039>
- Naylor, E., Arredouani, A., Vasudevan, S.R., Lewis, A.M., Parkesh, R., Mizote, A., Rosen, D., Thomas, J.M., Izumi, M., Ganesan, A., Galione, A., Churchill, G.C., 2009. Identification of a chemical probe for NAADP by virtual screening. *Nat. Chem. Biol.* 5, 220–226. <https://doi.org/10.1038/nchembio.150>
- Nebel, M., Schwoerer, A.P., Warszta, D., Siebrands, C.C., Limbrock, A.-C., Swarbrick, J.M.,

References

- Fliegert, R., Weber, K., Bruhn, S., Hohenegger, M., Geisler, A., Herich, L., Schlegel, S., Carrier, L., Eschenhagen, T., Potter, B.V.L., Ehmke, H., Guse, A.H., 2013. Nicotinic Acid Adenine Dinucleotide Phosphate (NAADP)-mediated Calcium Signaling and Arrhythmias in the Heart Evoked by β -Adrenergic Stimulation. *J. Biol. Chem.* 288, 16017–16030. <https://doi.org/10.1074/jbc.M112.441246>
- Niacin [WWW Document], 2014. Linus Pauling Inst. URL <https://lpi.oregonstate.edu/mic/vitamins/niacin>
- Nisimoto, Y., Diebold, B.A., Constantino-Gomes, D., Lambeth, J.D., 2014. Nox4: A Hydrogen Peroxide-Generating Oxygen Sensor. *Biochemistry* 53, 5111–5120. <https://doi.org/10.1021/bi500331y>
- O'Donnell, B.V., Tew, D.G., Jones, O.T., England, P.J., 1993. Studies on the inhibitory mechanism of iodonium compounds with special reference to neutrophil NADPH oxidase. *Biochem. J.* 290, 41–49.
- Ouyang, W., Kolls, J.K., Zheng, Y., 2008. The Biological Functions of T Helper 17 Cell Effector Cytokines in Inflammation. *Immunity* 28, 454–467. <https://doi.org/10.1016/j.immuni.2008.03.004>
- Pak, V.V., Ezeriņa, D., Lyublinskaya, O.G., Pedre, B., Tyurin-Kuzmin, P.A., Mishina, N.M., Thauvin, M., Young, D., Wahni, K., Gache, S.A.M., Demidovich, A.D., Ermakova, Y.G., Maslova, Y.D., Shokhina, A.G., Eroglu, E., Bilan, D.S., Bogeski, I., Michel, T., Vríz, S., Messens, J., Belousov, V.V., 2020. Ultrasensitive genetically encoded indicator for hydrogen peroxide identifies roles for the oxidant in cell migration and mitochondrial function. *Cell Metab.* 31, 642-653.e6. <https://doi.org/10.1016/j.cmet.2020.02.003>
- Pandey, D., Gratton, J.-P., Rafikov, R., Black, S.M., Fulton, D.J.R., 2011. Calcium/calmodulin-dependent kinase II mediates the phosphorylation and activation of NADPH oxidase 5. *Mol. Pharmacol.* 80, 407–415. <https://doi.org/10.1124/mol.110.070193>
- Park, D.-R., Nam, T.-S., Kim, Y.-W., Bae, Y.S., Kim, U.-H., 2019. Oxidative activation of type III CD38 by NADPH oxidase-derived hydrogen peroxide in Ca²⁺ signaling. *FASEB J.* 33, 3404–3419. <https://doi.org/10.1096/fj.201800235R>

References

- Preston, T.J., Muller, W.J., Singh, G., 2001. Scavenging of Extracellular H₂O₂ by Catalase Inhibits the Proliferation of HER-2/Neu-transformed Rat-1 Fibroblasts through the Induction of a Stress Response*. *J. Biol. Chem.* 276, 9558–9564. <https://doi.org/10.1074/jbc.M004617200>
- Raad, H., Paclet, M.-H., Boussetta, T., Kroviarski, Y., Morel, F., Quinn, M.T., Gougerot-Pocidallo, M.-A., Dang, P.M.-C., El-Benna, J., 2009. Regulation of the phagocyte NADPH oxidase activity: phosphorylation of gp91phox/NOX2 by protein kinase C enhances its diaphorase activity and binding to Rac2, p67phox, and p47phox. *FASEB J.* 23, 1011–1022. <https://doi.org/10.1096/fj.08-114553>
- Rah, S.-Y., Mushtaq, M., Nam, T.-S., Kim, S.H., Kim, U.-H., 2010. Generation of Cyclic ADP-ribose and Nicotinic Acid Adenine Dinucleotide Phosphate by CD38 for Ca²⁺ Signaling in Interleukin-8-treated Lymphokine-activated Killer Cells *. *J. Biol. Chem.* 285, 21877–21887. <https://doi.org/10.1074/jbc.M109.066290>
- Regier, D.S., Waite, K.A., Wallin, R., McPhail, L.C., 1999. A Phosphatidic Acid-activated Protein Kinase and Conventional Protein Kinase C Isoforms Phosphorylate p22 phox , an NADPH Oxidase Component. *J. Biol. Chem.* 274, 36601–36608. <https://doi.org/10.1074/jbc.274.51.36601>
- Reinherz, E.L., Kung, P.C., Goldstein, G., Levey, R.H., Schlossman, S.F., 1980. Discrete stages of human intrathymic differentiation: Analysis of normal thymocytes and leukemic lymphoblasts of T-cell lineage. *Proc. Natl. Acad. Sci. U. S. A.* 77, 1588–1592.
- Reis, J., Massari, M., Marchese, S., Ceccon, M., Aalbers, F.S., Corana, F., Valente, S., Mai, A., Magnani, F., Mattevi, A., 2020. A closer look into NADPH oxidase inhibitors: Validation and insight into their mechanism of action. *Redox Biol.* 32, 101466. <https://doi.org/10.1016/j.redox.2020.101466>
- Rigutto, S., Hoste, C., Grasberger, H., Milenkovic, M., Communi, D., Dumont, J.E., Corvilain, B., Miot, F., De Deken, X., 2009. Activation of Dual Oxidases Duox1 and Duox2. *J. Biol. Chem.* 284, 6725–6734. <https://doi.org/10.1074/jbc.M806893200>
- Roggenkamp, H.G., Khansahib, I., C, L.C.H., Zhang, Y., Lodygin, D., Krüger, A., Gu, F., Möckl,

References

- F., Löhndorf, A., Wolters, V., Woike, D., Rosche, A., Bauche, A., Schetelig, D., Werner, R., Schlüter, H., Failla, A.V., Meier, C., Fliegert, R., Walseth, T.F., Flügel, A., Diercks, B.-P., Guse, A.H., 2021. HN1L/JPT2: A signaling protein that connects NAADP generation to Ca²⁺ microdomain formation. *Sci. Signal.* 14. <https://doi.org/10.1126/scisignal.abd5647>
- Schmid, F., Bruhn, S., Weber, K., Mittrücker, H.-W., Guse, A.H., 2011. CD38: A NAADP degrading enzyme. *FEBS Lett.* 585, 3544–3548. <https://doi.org/10.1016/j.febslet.2011.10.017>
- Schmid, F., Fliegert, R., Westphal, T., Bauche, A., Guse, A.H., 2012. Nicotinic Acid Adenine Dinucleotide Phosphate (NAADP) Degradation by Alkaline Phosphatase. *J. Biol. Chem.* 287, 32525–32534. <https://doi.org/10.1074/jbc.M112.362715>
- Seredenina, T., Nayernia, Z., Sorce, S., Maghzal, G.J., Filippova, A., Ling, S.-C., Basset, O., Plastre, O., Daali, Y., Rushing, E.J., Giordana, M.T., Cleveland, D.W., Aguzzi, A., Stocker, R., Krause, K.-H., Jaquet, V., 2016. Evaluation of NADPH oxidases as drug targets in a mouse model of familial amyotrophic lateral sclerosis. *Free Radic. Biol. Med.* 97, 95–108. <https://doi.org/10.1016/j.freeradbiomed.2016.05.016>
- Serrander, L., Jaquet, V., Bedard, K., Plastre, O., Hartley, O., Arnaudeau, S., Demaurex, N., Schlegel, W., Krause, K.-H., 2007. NOX5 is expressed at the plasma membrane and generates superoxide in response to protein kinase C activation. *Biochimie, Transport and redox reactions from mitochondria to NADPH oxidase* 89, 1159–1167. <https://doi.org/10.1016/j.biochi.2007.05.004>
- Singh, D.K., Kumar, D., Siddiqui, Z., Basu, S.K., Kumar, V., Rao, K.V.S., 2005. The Strength of Receptor Signaling Is Centrally Controlled through a Cooperative Loop between Ca²⁺ and an Oxidant Signal. *Cell* 121, 281–293. <https://doi.org/10.1016/j.cell.2005.02.036>
- Soares, S., Thompson, M., White, T., Isbell, A., Yamasaki, M., Prakash, Y., Lund, F.E., Galione, A., Chini, E.N., 2007. NAADP as a second messenger: neither CD38 nor base-exchange reaction are necessary for in vivo generation of NAADP in myometrial cells.

References

-
- Am. J. Physiol.-Cell Physiol. 292, C227–C239.
<https://doi.org/10.1152/ajpcell.00638.2005>
- Sonntag, Y., Gena, P., Maggio, A., Singh, T., Artner, I., Oklinski, M.K., Johanson, U., Kjellbom, P., Nieland, J.D., Nielsen, S., Calamita, G., Rützler, M., 2019. Identification and characterization of potent and selective aquaporin-3 and aquaporin-7 inhibitors. *J. Biol. Chem.* 294, 7377–7387. <https://doi.org/10.1074/jbc.RA118.006083>
- Sorce, S., Stocker, R., Seredenina, T., Holmdahl, R., Aguzzi, A., Chio, A., Depaulis, A., Heitz, F., Olofsson, P., Olsson, T., Duvéau, V., Sanoudou, D., Skosgater, S., Vlahou, A., Wasquel, D., Krause, K.-H., Jaquet, V., 2017. NADPH oxidases as drug targets and biomarkers in neurodegenerative diseases: What is the evidence? *Free Radic. Biol. Med.* 112, 387–396. <https://doi.org/10.1016/j.freeradbiomed.2017.08.006>
- Sumimoto, H., 2008. Structure, regulation and evolution of Nox-family NADPH oxidases that produce reactive oxygen species. *FEBS J.* 275, 3249–3277. <https://doi.org/10.1111/j.1742-4658.2008.06488.x>
- Summerhill, R.J., Jackson, D.G., Galione, A., 1993. Human lymphocyte antigen CD38 catalyzes the production of cyclic ADP-ribose. *FEBS Lett.* 335, 231–233. [https://doi.org/10.1016/0014-5793\(93\)80735-D](https://doi.org/10.1016/0014-5793(93)80735-D)
- Sun, J., 2020. Structures of mouse DUOX1–DUOX1 provide mechanistic insights into enzyme activation and regulation. *Nat. Struct. Mol. Biol.* 27, 1086–1093. <https://doi.org/10.1038/s41594-020-0501-x>
- Sun, Q.-A., Hess, D.T., Nogueira, L., Yong, S., Bowles, D.E., Eu, J., Laurita, K.R., Meissner, G., Stamler, J.S., 2011. Oxygen-coupled redox regulation of the skeletal muscle ryanodine receptor-Ca²⁺ release channel by NADPH oxidase 4. *Proc. Natl. Acad. Sci. U. S. A.* 108, 16098–16103. <https://doi.org/10.1073/pnas.1109546108>
- Sun, Q.-A., Hess, D.T., Wang, B., Miyagi, M., Stamler, J.S., 2012. Off-target thiol alkylation by the NADPH oxidase inhibitor 3-benzyl-7-(2-benzoxazolyl)thio-1,2,3-triazolo[4,5-d]pyrimidine (VAS2870). *Free Radic. Biol. Med.* 52, 1897–1902. <https://doi.org/10.1016/j.freeradbiomed.2012.02.046>

References

- Takac, I., Schröder, K., Zhang, L., Lardy, B., Anilkumar, N., Lambeth, J.D., Shah, A.M., Morel, F., Brandes, R.P., 2011. The E-loop Is Involved in Hydrogen Peroxide Formation by the NADPH Oxidase Nox4. *J. Biol. Chem.* 286, 13304–13313. <https://doi.org/10.1074/jbc.M110.192138>
- Takasawa, S., Tohgo, A., Noguchi, N., Koguma, T., Nata, K., Sugimoto, T., Yonekura, H., Okamoto, H., 1993. Synthesis and hydrolysis of cyclic ADP-ribose by human leukocyte antigen CD38 and inhibition of the hydrolysis by ATP. *J. Biol. Chem.* 268, 26052–26054. [https://doi.org/10.1016/S0021-9258\(19\)74275-6](https://doi.org/10.1016/S0021-9258(19)74275-6)
- Takeya, R., Ueno, N., Kami, K., Taura, M., Kohjima, M., Izaki, T., Nunoi, H., Sumimoto, H., 2003. Novel Human Homologues of p47phox and p67phox Participate in Activation of Superoxide-producing NADPH Oxidases *. *J. Biol. Chem.* 278, 25234–25246. <https://doi.org/10.1074/jbc.M212856200>
- Tazzeo, T., Worek, F., Janssen, L.J., 2009. The NADPH oxidase inhibitor diphenyleneiodonium is also a potent inhibitor of cholinesterases and the internal Ca²⁺ pump. *Br. J. Pharmacol.* 158, 790–796. <https://doi.org/10.1111/j.1476-5381.2009.00394.x>
- Tirone, F., Cox, J.A., 2007. NADPH oxidase 5 (NOX5) interacts with and is regulated by calmodulin. *FEBS Lett.* 581, 1202–1208. <https://doi.org/10.1016/j.febslet.2007.02.047>
- Trebak, M., Kinet, J.-P., 2019. Calcium signalling in T cells. *Nat. Rev. Immunol.*
- Veech, R.L., Eggleston, L.V., Krebs, H.A., 1969. The redox state of free nicotinamide–adenine dinucleotide phosphate in the cytoplasm of rat liver. *Biochem. J.* 115, 609–619.
- Veldhoen, M., Uyttenhove, C., van Snick, J., Helmby, H., Westendorf, A., Buer, J., Martin, B., Wilhelm, C., Stockinger, B., 2008. Transforming growth factor- β “reprograms” the differentiation of T helper 2 cells and promotes an interleukin 9–producing subset. *Nat. Immunol.* 9, 1341–1346. <https://doi.org/10.1038/ni.1659>
- Vu, C.Q., Lu, P.-J., Chen, C.-S., Jacobson, M.K., 1996. 2'-Phospho-Cyclic ADP-ribose, a Calcium-mobilizing Agent Derived from NADP (*). *J. Biol. Chem.* 271, 4747–4754. <https://doi.org/10.1074/jbc.271.9.4747>

References

- Wolf, I.M.A., Diercks, B.-P., Gattkowsky, E., Czarniak, F., Kempinski, J., Werner, R., Schetelig, D., Mittrücker, H.-W., Schumacher, V., Osten, M. von, Lodygin, D., Flügel, A., Fliegert, R., Guse, A.H., 2015. Frontrunners of T cell activation: Initial, localized Ca²⁺ signals mediated by NAADP and the type 1 ryanodine receptor. *Sci. Signal.* 8, ra102–ra102. <https://doi.org/10.1126/scisignal.aab0863>
- Wolf, I.M.A., Guse, A.H., 2017. Ca²⁺ Microdomains in T-Lymphocytes. *Front. Oncol.* 7. <https://doi.org/10.3389/fonc.2017.00073>
- Wu, J.-X., Liu, R., Song, K., Chen, L., 2021. Structures of human dual oxidase 1 complex in low-calcium and high-calcium states. *Nat. Commun.* 12, 155. <https://doi.org/10.1038/s41467-020-20466-9>
- Yamasaki, M., Churchill, G.C., Galione, A., 2005. Calcium signalling by nicotinic acid adenine dinucleotide phosphate (NAADP). *FEBS J.* 272, 4598–4606. <https://doi.org/10.1111/j.1742-4658.2005.04860.x>
- Yang, C., Jiang, L., Zhang, H., Shimoda, L.A., DeBerardinis, R.J., Semenza, G.L., 2014. Chapter Twenty-Two - Analysis of Hypoxia-Induced Metabolic Reprogramming, in: Galluzzi, L., Kroemer, G. (Eds.), *Methods in Enzymology, Conceptual Background and Bioenergetic/Mitochondrial Aspects of Oncometabolism*. Academic Press, pp. 425–455. <https://doi.org/10.1016/B978-0-12-416618-9.00022-4>
- Yoshida, L.S., Nishida, S., Shimoyama, T., Kawahara, T., Kondo-Teshima, S., Rokutan, K., Kobayashi, T., Tsunawaki, S., 2004. Superoxide Generation by Nox1 in Guinea Pig Gastric Mucosal Cells Involves a Component with p67^{phox}-Ability. *Biol. Pharm. Bull.* 27, 147–155. <https://doi.org/10.1248/bpb.27.147>
- Zamzami, N., Marchetti, P., Castedo, M., Decaudin, D., Macho, A., Hirsch, T., Susin, S.A., Petit, P.X., Mignotte, B., Kroemer, G., 1995. Sequential reduction of mitochondrial transmembrane potential and generation of reactive oxygen species in early programmed cell death. *J. Exp. Med.* 182, 367–377. <https://doi.org/10.1084/jem.182.2.367>
- Zhang, B., Watt, J.M., Cordiglieri, C., Dammermann, W., Mahon, M.F., Flügel, A., Guse, A.H.,

References

- Potter, B.V.L., 2018. Small Molecule Antagonists of NAADP-Induced Ca²⁺ Release in T-Lymphocytes Suggest Potential Therapeutic Agents for Autoimmune Disease. *Sci. Rep.* 8, 16775. <https://doi.org/10.1038/s41598-018-34917-3>
- Zhang, J., Guan, X., Shah, K., Yan, J., 2021. Lsm12 is an NAADP receptor and a two-pore channel regulatory protein required for calcium mobilization from acidic organelles. *Nat. Commun.* 12, 4739. <https://doi.org/10.1038/s41467-021-24735-z>
- Zhang, J., Pierick, A. ten, van Rossum, H.M., Maleki Seifar, R., Ras, C., Daran, J.-M., Heijnen, J.J., Aljoscha Wahl, S., 2015. Determination of the Cytosolic NADPH/NADP Ratio in *Saccharomyces cerevisiae* using Shikimate Dehydrogenase as Sensor Reaction. *Sci. Rep.* 5, 12846. <https://doi.org/10.1038/srep12846>
- Zhao, Y.J., He, W.M., Zhao, Z.Y., Li, W.H., Wang, Q.W., Hou, Y.N., Tan, Y., Zhang, D., n.d. Acidic pH irreversibly activates the signaling enzyme SARM1. *FEBS J.* n/a. <https://doi.org/10.1111/febs.16104>
- Zhao, Z.Y., Xie, X.J., Li, W.H., Liu, J., Chen, Z., Zhang, B., Li, T., Li, S.L., Lu, J.G., Zhang, Liangren, Zhang, Li-he, Xu, Z., Lee, H.C., Zhao, Y.J., 2019. A Cell-Permeant Mimetic of NMN Activates SARM1 to Produce Cyclic ADP-Ribose and Induce Non-apoptotic Cell Death. *iScience* 15, 452–466. <https://doi.org/10.1016/j.isci.2019.05.001>
- Zhu, J., Paul, W.E., 2008. CD4 T cells: fates, functions, and faults. *Blood* 112, 1557–1569. <https://doi.org/10.1182/blood-2008-05-078154>
- Zocchi, E., Franco, L., Guida, L., Benatti, U., Bargellesi, A., Malavasi, F., Lee, H.C., Deflora, A., 1993. A Single Protein Immunologically Identified as CD38 Displays NAD⁺ Glycohydrolase, ADP-Ribosyl Cyclase and Cyclic ADP-Ribose Hydrolase Activities at the Outer Surface of Human Erythrocytes. *Biochem. Biophys. Res. Commun.* 196, 1459–1465. <https://doi.org/10.1006/bbrc.1993.2416>

Eidesstattliche Versicherung

Name: Gu

Vorname: Feng

Hiermit erkläre ich an Eides statt, dass ich die vorliegende Dissertationsschrift selbst verfasst und keine anderen als die angegebenen Quellen und Hilfsmittel benutzt habe.

Hamburg, 10.04.2022

Ort, Datum

Unterschrift

Acknowledgements

I have gotten a tremendous lot of help and support during my Ph.D. journey.

I would first like to thank my supervisor, Prof. Andreas H. Guse, for allowing me, as a Ph.D. student within SFB1328, to see the overall picture of Ca^{2+} signaling in inflammation and infection. During my work, your invaluable supervision, guidance, and comments drove me to polish my thinking and incorporate the data into a fantastic story.

I would like to express my gratitude to Prof. Christian Lohr for evaluating my thesis.

I would like to thank our collaborators, Prof. Alexander Flügel, Prof. Hans-Willi Mitrücker, Prof. Katrin Schröder, and Prof. Karl-Heinz Krause, for supplying me with the resources I needed to effectively finish this story.

Furthermore, I would like to thank my colleagues in the Calcium Signaling Group. Special thanks to Dr. Björn-Phillip Diercks for your patient support and guidance. I thank Dr. Ralf Fliegert for the insightful discussion and Dr. Sukanya Arcot Kannabiran for the advice on my thesis. I would like to thank Aileen Krüger and Franziska Möckl for helping with measurements. I would want to express my gratitude to Dr. Anke Löhndorf, Lola C. Hernandez C., Valerie J. Brock, Anette Rosche, and Andreas Bauche for your unending willingness to help. Last but not least, I would want to thank the whole team for the great and very inspiring working environment that made my stay in Germany so meaningful and colorful.

In addition, I would like to express my heartfelt gratitude to my parents. I could never have done it without your support. You're always there for me, with a sympathetic ear to help me get through the problems and pressures of life. Finally, a heartfelt thanks to Wenbo Wang. Your love strengthens me and makes the distance invisible.

Publications and presentations

Publications:

1. Dual NADPH oxidases DUOX1 and DUOX2 synthesize NAADP and are necessary for Ca²⁺ signaling during T cell activation. **Gu, F.***, Krüger, A.*, Roggenkamp, H.G.*, Alpers, R., Lodygin, D., Jaquet, V., Möckl, F., Hernandez C., L.C., Winterberg, K., Bauche, A., Rosche, A., Grasberger, H., Kao, J.Y., Schetelig, D., Werner, R., Schröder, K., Carty, M., Bowie, A.G., Huber, S., Meier, C., Mittrücker, H.-W., Heeren, J., Krause, K.-H., Flügel, A., Diercks, B.-P., Guse, A.H. *Science Signaling*. 2021. 14, eabe3800.
<https://doi.org/10.1126/scisignal.abe3800>
*equal contribution
2. HN1L/JPT2: A signaling protein that connects NAADP generation to Ca²⁺ microdomain formation. Roggenkamp, H.G.*, Khansahib, I.*, C, L.C.H.*, Zhang, Y.*, Lodygin, D., Krüger, A., **Gu, F.**, Möckl, F., Löhndorf, A., Wolters, V., Woike, D., Rosche, A., Bauche, A., Schetelig, D., Werner, R., Schlüter, H., Failla, A.V., Meier, C., Fliegert, R., Walseth, T.F., Flügel, A., Diercks, B.-P., Guse, A.H. *Science Signaling*. 2021. 14, eabe5647.
<https://doi.org/10.1126/scisignal.abd5647>
*equal contribution
3. 2'-Deoxyadenosine 5'-diphosphoribose is an endogenous TRPM2 superagonist. Fliegert, R., Bauche, A., Wolf Pérez, A.-M., Watt, J.M., Rozewitz, M.D., Winzer, R., Janus, M., **Gu, F.**, Rosche, A., Harneit, A., Flato, M., Moreau, C., Kirchberger, T., Wolters, V., Potter, B.V.L., Guse, A.H., *Nature Chemical Biology*. 2017. 13, 1036–1044.
<https://doi.org/10.1038/nchembio.2415>
4. The 2021 FASEB science research conference on NAD metabolism and signaling. Gorbunova, V., Buschbeck, M., Cambronne, X.A., Chellappa, K., Corda, D., Du, J., Freichel, M., Gigas, J., Green, A.E., **Gu, F.**, Guberovic, I., Jayabalan, A., Khansahib, I., Mukherjee, S., Seluanov, A., Simon, M.A., Sverkel, L.J., Kory, N., Levine, D.C., Matic, I., Nikiforov, A., Rack, J.G.M., Imai, S.-I., Sinclair, D.A., Toiber, D., Zhao, Y., Mostoslavsky, R., Kraus, L., Guse, A.H. *Aging*. 2021.13. <https://doi.org/10.18632/aging.203766>

Oral and poster presentations:

2nd International Online Meeting of the Junior European Calcium Society, 23-24 November 2021. **Poster:** DUOX2 (dual NADPH oxidase 2) synthesizes NAADP in the early phase of T activation.

Feng Gu¹, Aileen Krüger¹, Hannes G.Roggenkamp¹, Björn-Philipp Diercks¹, Rick Alpers¹, Dmitri Lodygin², Vincent Jaquet³, Franziska Möckl¹, Lola C. Hernandez C.¹, Kai Winterberg¹, Andreas Bauche¹, Anette Rosche¹, Helmut Grasberger⁴, John Y. Kao⁴, Daniel Schetelig⁵, René Werner⁵, Katrin Schröder⁶, Michael Carty⁷, Andrew G Bowie⁷, Samuel Huber⁸, Chris Meier⁹, Hans-Willi

Mittrücker¹⁰, Joerg Heeren¹, Karl-Heinz Krause³, Alexander Flügel², and Andreas H. Guse¹

SFB1328 4th retreat at Maritim Seehotel Timmendorfer Strand, 18-20 October 2021. **Talk and poster:** NAADP forming enzyme in T cells

Feng Gu¹, Aileen Krüger¹, Hannes G. Roggenkamp¹, Björn-Philipp Diercks¹, Rick Alpers¹, Dmitri Lodygin², Vincent Jaquet³, Franziska Möckl¹, Lola C. Hernandez C.¹, Kai Winterberg¹, Andreas Bauche¹, Anette Rosche¹, Helmut Grasberger⁴, John Y. Kao⁴, Daniel Schetelig⁵, René Werner⁵, Katrin Schröder⁶, Michael Carty⁷, Andrew G Bowie⁷, Samuel Huber⁸, Chris Meier⁹, Hans-Willi Mittrücker¹⁰, Joerg Heeren¹, Karl-Heinz Krause³, Alexander Flügel², and Andreas H. Guse¹

74th Annual Meeting and Symposium of the Society of General Physiologists: Ion Channels & Transporters in Immunity, Inflammation and Antitumor Immunity, 22-26 September 2021.

Talk and poster: NAADP forming enzyme in T cells

Feng Gu¹, Aileen Krüger¹, Hannes G. Roggenkamp¹, Björn-Philipp Diercks¹, Rick Alpers¹, Dmitri Lodygin², Vincent Jaquet³, Franziska Möckl¹, Lola C. Hernandez C.¹, Kai Winterberg¹, Andreas Bauche¹, Anette Rosche¹, Helmut Grasberger⁴, John Y. Kao⁴, Daniel Schetelig⁵, René Werner⁵, Katrin Schröder⁶, Michael Carty⁷, Andrew G Bowie⁷, Samuel Huber⁸, Chris Meier⁹, Hans-Willi Mittrücker¹⁰, Joerg Heeren¹, Karl-Heinz Krause³, Alexander Flügel², and Andreas H. Guse¹

FASEB Science Research Conference: The NAD⁺ Metabolism and Signaling Conference, 15-16 June 2021. **Talk and poster:** NAADP forming enzyme in T cells

Feng Gu¹, Aileen Krüger¹, Hannes G. Roggenkamp¹, Björn-Philipp Diercks¹, Rick Alpers¹, Dmitri Lodygin², Vincent Jaquet³, Franziska Möckl¹, Lola C. Hernandez C.¹, Kai Winterberg¹, Andreas Bauche¹, Anette Rosche¹, Helmut Grasberger⁴, John Y. Kao⁴, Daniel Schetelig⁵, René Werner⁵, Katrin Schröder⁶, Michael Carty⁷, Andrew G Bowie⁷, Samuel Huber⁸, Chris Meier⁹, Hans-Willi Mittrücker¹⁰, Joerg Heeren¹, Karl-Heinz Krause³, Alexander Flügel², and Andreas H. Guse¹

SFB1328 2nd retreat online, 28-29 January 2021. **Talk and poster:** NAADP forming enzyme in T cells

Feng Gu¹, Aileen Krüger¹, Hannes G. Roggenkamp¹, Björn-Philipp Diercks¹, Rick Alpers¹, Dmitri Lodygin², Vincent Jaquet³, Franziska Möckl¹, Lola C. Hernandez C.¹, Andreas Bauche¹, Anette Rosche¹, Helmut Grasberger⁴, John Y. Kao⁴, Daniel Schetelig⁵, René Werner⁵, Katrin Schröder⁶, Michael Carty⁷, Andrew G Bowie⁷, Samuel Huber⁸, Chris Meier⁹, Hans-Willi Mittrücker¹⁰, Joerg Heeren¹, Karl-Heinz Krause³, Alexander Flügel², and Andreas H. Guse¹

1st International Online Meeting of the Junior European Calcium Society, 20-21 October

2020. **Talk:** NAADP forming enzymes in T cell activation

Feng Gu¹, Aileen Krüger¹, Hannes G. Roggenkamp¹, Björn-Philipp Diercks¹, Andreas Bauche¹, Anette Rosche¹, Daniel Schetelig², René Werner³, Hans-Willi Mittrücker⁴, Joerg Heeren¹, and Andreas H. Guse¹

EMBO Symposium India: Calcium signaling: Molecular mechanisms to role in health and diseases, 26-29 January 2020. **Poster:** The NAADP-forming enzyme in T cells and its role in Ca²⁺ signaling

Feng Gu¹, Aileen Krüger¹, Hannes G. Roggenkamp¹, Björn-Philipp Diercks¹, Andreas Bauche¹, Anette Rosche¹, Daniel Schetelig², René Werner³, Hans-Willi Mittrücker⁴, Joerg Heeren¹, and Andreas H. Guse¹

SFB1328 1st retreat at Tagunszentrum Jesteburg, 22-23 March 2019. **Talk and poster:** NAADP forming enzyme in T cells

Feng Gu¹, Aileen Krüger¹, Björn-Philipp Diercks¹, Hannes G. Roggenkamp¹, Andreas Bauche¹, Vincent Jaquet², and Andreas H. Guse¹

XV International Meeting of the European Calcium Society Hamburg Germany, 09-13 September 2018. **Poster:** Development of a HPLC Method for the Identification and Quantification of 2'-deoxy-ADPR and 2'-deoxy-NAD

Feng Gu¹, Andreas Bauche¹, Ralf Fliegert¹, and Andreas H. Guse¹